AD-A180 594 DEVELOPMENT OF A HIGH SPEED INGAAS/INP SCHOTTKY BARRIER 1/2
PHOTODETECTOR FOR..(U) FLORIDA UNIV GAINESVILLE S S LI
JUL 87 RADC-TR-87-83 F30602-81-C-0202

UNCLASSIFIED F/G 20/6.1 NL

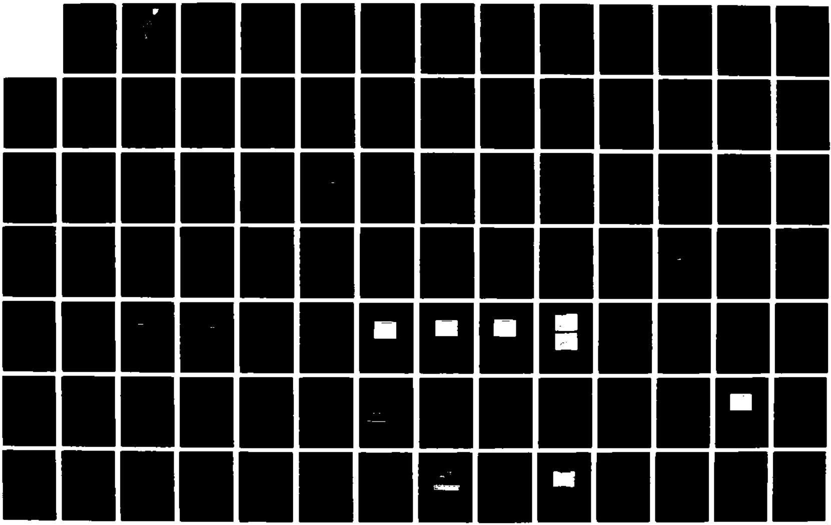

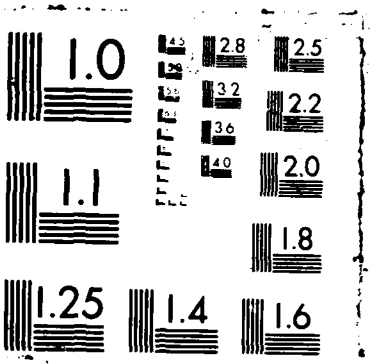
1.0
4.5
5.0
5.6
6.3
2.8
2.5
3.2
2.2
3.6
4.0
2.0
1.1
1.8
1.25
1.4
1.6

TIC FILE COPY

②

RADC-TR-87-83
Final Technical Report
July 1987

AD-A188 594

DEVELOPMENT OF A HIGH SPEED InGaAs/InP SCHOTTKY BARRIER PHOTODETECTOR FOR MILLIMETER-WAVE FIBER OPTICAL LINKS

University of Florida

DTIC
S ELECTE D
DEC 1 5 1987
D

Dr. Sheng S. Li

APPROVED FOR PUBLIC RELEASE; DISTRIBUTION UNLIMITED

ROME AIR DEVELOPMENT CENTER
Air Force Systems Command
Griffiss Air Force Base, NY 13441-5700

87 12 9 101

This report has been reviewed by the RADC Public Affairs Office (PA) and is releasable to the National Technical Information Service (NTIS). At NTIS it will be releasable to the general public, including foreign nations.

RADC TR-87-83 has been reviewed and is approved for publication.

APPROVED:

Paul Sierak

PAUL SIERAK
Project Engineer

APPROVED:

R. L. Rhame

ROBERT L. RHAME, Colonel, USAF
Director of Communications

FOR THE COMMANDER:

Richard W. Pouliot

RICHARD W. POULIOT
Directorate of Plans and Programs

If your address has changed or if you wish to be removed from the RADC mailing list, or if the addressee is no longer employed by your organization, please notify RADC (DCLW) Griffiss AFB NY 13441-5700. This will assist us in maintaining a current mailing list.

Do not return copies of this report unless contractual obligations or notices on a specific document requires that it be returned.

UNCLASSIFIED
SECURITY CLASSIFICATION OF THIS PAGE

REPORT DOCUMENTATION PAGE A188594

Form Approved
OMB No. 0704-0188

1a. REPORT SECURITY CLASSIFICATION UNCLASSIFIED

1b. RESTRICTIVE MARKINGS N/A

2a. SECURITY CLASSIFICATION AUTHORITY N/A

2b. DECLASSIFICATION / DOWNGRADING SCHEDULE N/A

3. DISTRIBUTION / AVAILABILITY OF REPORT
Approved for public release;
Distribution unlimited.

4. PERFORMING ORGANIZATION REPORT NUMBER(S) N/A

5. MONITORING ORGANIZATION REPORT NUMBER(S) RADC-TR-87-83

6a. NAME OF PERFORMING ORGANIZATION University of Florida

6b. OFFICE SYMBOL *(If applicable)*

7a. NAME OF MONITORING ORGANIZATION Rome Air Development Center (DCLW)

6c. ADDRESS *(City, State, and ZIP Code)*
Gainesville FL 32611

7b. ADDRESS *(City, State, and ZIP Code)*
Griffiss AFB NY 13441-5700

8a. NAME OF FUNDING / SPONSORING ORGANIZATION Rome Air Development Center

8b. OFFICE SYMBOL *(If applicable)* DCLW

9. PROCUREMENT INSTRUMENT IDENTIFICATION NUMBER F30602-81-C-0202

8c. ADDRESS *(City, State, and ZIP Code)*
Griffiss AFB NY 13441-5700

10. SOURCE OF FUNDING NUMBERS

PROGRAM ELEMENT NO.	PROJECT NO.	TASK NO	WORK UNIT ACCESSION NO.
62702F	4519	21	P2

11. TITLE *(Include Security Classification)*
DEVELOPMENT OF A HIGH SPEED InGaAs/InP SCHOTTKY BARRIER PHOTODETECTOR FOR MILLIMETER-WAVE FIBER OPTICAL LINKS

12. PERSONAL AUTHOR(S) Dr. Sheng S. Li

13a. TYPE OF REPORT Final

13b. TIME COVERED FROM Dec 85 TO Dec 86

14. DATE OF REPORT *(Year, Month, Day)* July 1987

15. PAGE COUNT 132

16. SUPPLEMENTARY NOTATION
N/A

17. COSATI CODES

FIELD	GROUP	SUB-GROUP
20	06	

18. SUBJECT TERMS *(Continue on reverse if necessary and identify by block number)*
Detectors, Optical, Fiber Optics, Long Wavelength, Schottky Barrier

19. ABSTRACT *(Continue on reverse if necessary and identify by block number)*

This report describes the development of long wavelength (1.3 to 1.65 micrometer) Schottky barrier photodetectors in InGaAs/InP. Two material overlays were investigated. These are the Au/P$^+$-n-InGaAs/n$^+$-InP and the Au/P-InGaAs/P$^+$-InP structures. The P$^+$-InP detector exhibited a responsivity of 0.43A/W and a quantum efficiency of 40.5% at 1.3 μm without an antireflection coating. The impulse response gave a risetime of 85 ps and a FWHM of 490 ps. The RC time constant measured was 34.7 ps which corresponds to a cutoff frequency of 28.8 GHz. The n$^+$-InP Schottky barrier requires more work to obtain good reproducibility of the barrier height enhancement technique employed.

The work performed indicates that long wavelength, high frequency response, Schottky barrier for use as fiber optic compatible detectors are viable. Processing techniques are described along with supportive device modeling and experimental data on the initial devices.

20. DISTRIBUTION / AVAILABILITY OF ABSTRACT
☐ UNCLASSIFIED/UNLIMITED ☒ SAME AS RPT ☐ DTIC USERS

21. ABSTRACT SECURITY CLASSIFICATION UNCLASSIFIED

22a. NAME OF RESPONSIBLE INDIVIDUAL PAUL SIERAK

22b. TELEPHONE *(Include Area Code)* (315) 330-4092

22c. OFFICE SYMBOL RADC (DCLW)

DD Form 1473, JUN 86 *Previous editions are obsolete.* SECURITY CLASSIFICATION OF THIS PAGE

UNCLASSIFIED

TABLE OF CONTENTS

PAGE

ABSTRACT iii

CHAPTER

ONE INTRODUCTION 1

- 1.1. Development of A High-Speed Photodetector 1
- 1.2. Synopsis of Chapters 3

TWO THEORETICAL ANALYSIS OF PHOTODETECTOR PARAMETERS 6

- 2.1. General Requirements for A Photodetector 6
- 2.2. Spectral Response 6
- 2.3. Response Speed 7
  - 2.3.1. Drift Time 8
  - 2.3.2. Diffusion Time 9
  - 2.3.3. RC Time Constant 9
- 2.4. Dark Current 10
  - 2.4.1. Thermionic-emission Current 10
  - 2.4.2. Generation-Recombination Current 10
  - 2.4.3. Tunneling Current 11
- 2.5. D.C. Parameters 12
  - 2.5.1. Junction Capacitance 12
  - 2.5.2. Overlay Capacitance 13
  - 2.5.3. Series Resistance 13
- 2.6. Noise-Equivalent Power (NEP) 15
- 2.7. Device Packaging 17
  - 2.7.1. Microstrip Line Parameters 19
  - 2.7.2. Microstrip Line Design 24
- 2.8. Response Speed Measurement 24
  - 2.8.1. Impulse Response 26
  - 2.8.2. Sampling/Cross-Correlation 26
  - 2.8.3. Electro-Optical Sampling 31
  - 2.8.4. Optical Heterodyning 31

THREE FORMATION OF SCHOTTKY BARRIER AND OHMIC CONTACT ON III-V COMPOUND SEMICONDUCTORS 35

- 3.1. Introduction 35
- 3.2. Schottky Barrier Height Enhancement 36
- 3.3. Ohmic Contact Formation 42
- 3.4. Device Fabrication 44
  - 3.4.1. Schottky Gate Formation 44
  - 3.4.2. Ohmic Contact Formation 46
- 3.5. Experimental Results and Discussion 53
- 3.6. Summary and Conclusions 60

FOUR DEVELOPMENT OF A HIGH-SPEED Au/p$^+$-n-In$_{0.53}$Ga$_{0.47}$As/n$^+$-InP SCHOTTKY BARRIER PHOTODETECTOR FOR 1.30-1.65 um PHOTODETECTION... 61

- 4.1. Introduction 61
- 4.2. Theoretical Analysis 61

DTIC COPY INSPECTED 6

A-1

4.2.1. Quantum Efficiency.................................. 62
4.2.2. Response Speed...................................... 63
4.2.3. Dark Current.. 65
4.3. Device Fabrication.................................... 67
4.4. Experimental Results and Discussion................... 69
4.4.1. Current-Voltage (I-V) Measurement................... 69
4.4.2. Capacitance-Voltage (C-V) Measurement............... 69
4.4.3. A.C. Admittance Measurement......................... 69
4.4.4. Spectral Response Measurement....................... 70
4.4.5. Response Speed Measurement.......................... 70
4.5. Summary and Conclusions............................... 76

FIVE DEVELOPMENT OF A HIGH-SPEED Au/p-$In_{0.53}Ga_{0.47}As/P^+$-InP SCHOTTKY BARRIER PHOTODETECTOR FOR 1.30-1.65 um PHOTODETECTION.... 77

5.1. Introduction.. 77
5.2. Theoretical Analysis.................................. 78
5.2.1. Quantum Efficiency.................................. 78
5.2.2. Response Speed...................................... 79
5.2.3. Dark Current.. 80
5.3. Device Fabrication.................................... 81
5.4. Experimental Results and Discussion................... 84
5.4.1. Current-Voltage (I-V) Measurement................... 84
5.4.2. Capacitance-Voltage (C-V) Measurement............... 84
5.4.3. A.C. Admittance (Y-V) Measurement................... 84
5.4.4. Spectral Response Measurement....................... 89
5.4.5. Response Speed Measurement.......................... 89
5.5. Summary and Conclusions............................... 96

SIX SUMMARY, CONCLUSIONS, AND RECOMMENDATIONS.................. 97

6.1. Summary and Conclusions............................... 97
6.2. Recommendations for Follow-up Research................ 98
6.2.1. Packaging Optimization.............................. 98
6.2.2. Development of High-Speed $In_{0.53}Ga_{0.47}As$ Schottky Barrier Photodetector on Semi-insulating InP Substrate for Monolithic Integration........................... 98
6.2.3. Monolithic Integration of An Optical Receiver Module.................................. 99

SEVEN REFERENCES... 100

EIGHT LIST OF PUBLICATIONS................................... 106

APPENDIX.. 107

A Fabrication Procedures of InGaAs Schottky Barrier Photodiode...... 107
B Circuit Simulation for Determining Response Speed................ 110
C General Model for Schottky Barrier Height....................... 113
D Schottky Barrier Height Enhancement.............................. 115
E Schottky Barrier and Ohmic Contact Formation..................... 118
F Lift-Off Photolithography.. 120
G Chemical Etch.. 120
H Surface Passivation.. 121

ABSTRACT

This final technical report describes the development of a new high-speed $In_{0.53}Ga_{0.47}As/InP$ Schottky barrier photodetector operating in the infrared regime for millimeter-wave optical fiber communications supported by US Air Force RADC under contract No. F30602-81-C-0202 subcontracted through the University of South Florida.

The objective of this research program is to develop a high-speed long wavelength (1.30-1.55 um) $In_{0.53}Ga_{0.47}As/InP$ Schottky barrier photodetector capable of detecting the optical signals up to 20 GHz for millimeter-wave fiber optical links. For this purpose we have developed a novel high-speed $In_{0.53}Ga_{0.47}As/InP$ Schottky barrier photodiode using Au/p^+-n-InGaAs/n^+-InP and Au/p-InGaAs/p^+-InP structure. The results show that Au/p-InGaAs/p^+-InP Schottky barrier photodiode is a promising candidate for high frequency and high-speed photodetector applications, while Au/p^+-n-InGaAs/n^+-InP Schottky barrier photodiode needs more study to obtain a good reproducibility of the barrier height enhancement in spite of its promising potential.

The Au/p-InGaAs/p^+-InP Schottky barrier photodiode has a responsivity of 0.43 A/W and a quantum efficiency of 40.5 % at 1.3 um without antireflection coating. The impulse response measurement on this photodiode yields a risetime of 85 ps and an FWHM of 490 ps. However, the measured RC time constant is 34.7 ps, which corresponds to a cutoff frequency of 28.8 GHz. Therefore, it is obvious that the response speed of our photodiodes can be further improved by optimizing the device parameters and minimizing the packaging parasitics. The response speed can also be increased by fabricating our photodetectors on the semi-insulating substrate. Packaging optimization and fabrication of new InGaAs Schottky barrier photodiodes on semi-insulating InP substrates are the two main tasks to be carried out in the renewal contract for the coming year.

CHAPTER ONE
INTRODUCTION

1.1. Development of A High-Speed Photodetector

The main objective of this research project is to develop a high-speed photodetector capable of demodulating the optical signals greater than 20 GHz for millimeter-wave optical fiber links. The high bit-rate fiber optic systems for long distance lightwave communication require the development of high-speed, high efficiency, and low noise photodetectors operating in the infrared regime, especially close to the dispersion minimum of the optical fibers [1-5]. The high-speed photodiodes have been fabricated mainly on GaAs using a Schottky barrier structure for 0.80-0.90 um and on $In_{0.53}Ga_{0.47}As$ using a p-i-n structure for 1.30-1.65 um. The Schottky barrier photodiodes have many advantages such as simplicity of fabrication, reliability, absence of high-temperature diffusion processes which can degrade the carrier lifetime, and high response speed. For this purpose a high-speed $In_{0.53}Ga_{0.47}As$ Schottky barrier photodiode for 1.30 - 1.65 um detection has been developed in this research project.

Figure 1.1. shows the block diagram of the millimeter-wave optical fiber links using an electro-optic modulator (EOM). The promising candidates are GaAs Schottky barrier [6-9], AlGaAs/GaAs or GaAs p-i-n [10,11], $In_xGa_{1-x}As$ p-i-n [12-17], $In_xGa_{1-x}As$ Schottky barrier [18-21], avalanche photodiode [22-25], and photoconductive detector [26-33]. The InGaAs/InP material systems have shown a great potential for use as high-speed optoelectronic device materials because of their extremely high electron mobility, high saturation velocity, and good lattice-match with InP [34-36]. The $In_{0.53}Ga_{0.47}As$ is one of the most promising materials for the long wavelength photodetector applications because its bandgap can be tailored to the wavelength of 0.95-1.65 um. To take advantage of these excellent physical properties, the parasitic RC components and the high power

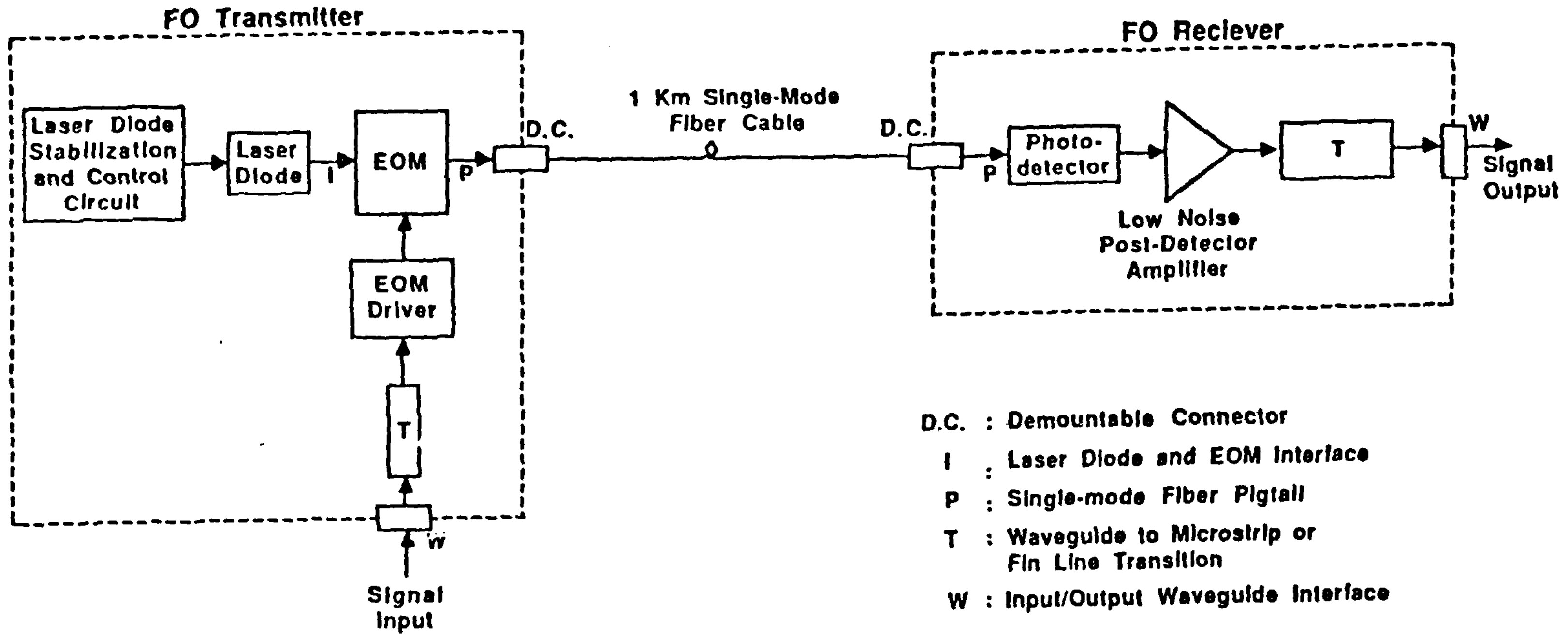
FO Transmitter
Laser Diode Stabilization and Control Circuit
Laser Diode
I
EOM
P
EOM Driver
T
W
Signal Input
D.C.
1 Km Single-Mode Fiber Cable
D.C.
FO Reciever
P
Photo-detector
Low Noise Post-Detector Amplifier
T
W
Signal Output
D.C. : Demountable Connector
I : Laser Diode and EOM Interface
P : Single-mode Fiber Pigtail
T : Waveguide to Microstrip or Fin Line Transition
W : Input/Output Waveguide Interface

Fig. 1.1. Block Diagram for Millimeter-wave Fiber Optical Links

consumption in parasitic resistances should be reduced and hence a low specific contact resistance is required for the photodiode applications. To develop a high-speed photodetector for millimeter-wave optical fiber communications, the Schottky barrier structure has been chosen.

Unfortunately, the Schottky barrier contacts on n-$In_{0.53}Ga_{0.47}As$ yield low barrier height (Φ_{Bn} = 0.2-0.3 eV) [37,38], which makes Schottky contacts too leaky to be useful for photodetector applications. Therefore, the effective barrier height needs to be increased to overcome the problem associated with the low Schottky barrier height. In order to reduce the dark current of the photodetector the barrier height enhancement is needed for such applications. Schottky barrier contacts on a moderately doped p-$In_{0.53}Ga_{0.47}As$ epilayer are expected to yield a good barrier height (Φ_{Bp} = 0.55 eV) when a suitable metal and good surface preparation are obtained [39,40].

In this research program, high-speed Au/p^+-n-$In_{0.53}Ga_{0.47}As$/n^+-InP and Au/p-$In_{0.53}Ga_{0.47}As$/p^+-InP Schottky barrier photodiodes have been developed. The design goal of the high-speed photodetectors is shown in Table 1.1. The test results of our photodetectors have shown that a Au/p-InGaAs/p^+-InP Schottky barrier photodiode can be a very promising candidate for high frequency and high-speed detector applications. In order to familiarize with the state of the art in photodetector development, a summary of the literature survey on the high-speed photodetectors is given in Table 1.2.

1.2. Synopsis of Chapters

This final technical report covers research activities on the development of a novel high-speed $In_xGa_{1-x}As$/InP Schottky barrier photodiode fabricated on InP conductive substrate for millimeter wave optical fiber links. In chapter 2, a theoretical analysis of the photodiode parameters relating to the general requirements of photodetectors is reviewed. For device characterization the microstrip transmission line, on which the photodetector is mounted, has been designed and fabricated on a Cr-Au metalized alumina substrate.

In Chapter 3, Schottky barrier and ohmic contact formation on III-V compound semiconductors such as GaAs, $In_xGa_{1-x}As$, and InP is discussed. In Chapter 4, Au/p^+-n-$In_{0.53}Ga_{1-x}As/n^+$-InP Schottky barrier photodiode operating in the infrared regime is depicted. In Chapter 5, a picosecond response Au/p-$In_{0.53}Ga_{1-x}As/p^+$-InP Schottky barrier photodiode for the infrared detection is described. Summary and conclusions are presented in Chapter 6. In addition, subjects for further study are recommended, which include (1) packaging optimization, (2) fabrication of photodiode on semi-insulating substrate, (3) photoreceiver module for monolithic optoelectronic integration, and (4) high gain and low noise avalanche photodiode with a quantum-well structure. In the appendixes, the device fabrication, Schottky barrier and ohmic contact formation, lift-off photolithography, and chemical etching procedures including mesa etch and metal etch are depicted.

Table 1.1 DESIGN REQUIREMENTS FOR A HIGH-SPEED PHOTODETECTOR

Millimeter-Wave Frequency	20-27 GHz
Modulation Bandwidth	10 % of Center Frequency
Input/Output Power Level	0 dBm
Input/Output Impedance	50 ohm
Input Signal Type	Analog Signal
Optical Source	Laser Diode
Quantum Efficiency	50 %
Optical Fiber Type	Single-mode

Table 1.2. Development of High-Speed Photodetectors

Device Type	Speed/Efficiency	Characteristics	Institute	References
GaAs Schottky Barrier Photodiode	f = 20 GHz(16 ps FWHM) n = 30 % at 0.60 um n = 25 % at 0.85 um R = 0.15 A/W at 0.60 um R = 0.17 A/W at 0.85 um I_D= 6x10^{-7} A/cm^2 at V_R=5 V	High-Speed Low Efficiency Vertical Mesa Low Dark Current	Hewlett Packard Lab.	APL 42(2) pp. 190 Jan. 1983 IEEE IEDM pp. 712 Dec. 1984
GaAs Schottky Barrier Photodiode	f =100 GHz (5.4 ps FWHM)	Ultra High-Speed Minimum Parasitic Capacitance Planar Mesa	Hewlett Packard Lab.	Elec.Lett. 19(14) pp. 554 1983
GaAs Schottky Barrier Photodiode	f = 18 GHz n = 70 % at 0.63 um n = 35 % at 0.83 um	High-Speed Low Efficiency	Hughes Research Lab.	APL 45(3) pp. 195 Aug. 1984
InGaAs/InP PIN Photodiode	35 ps Risetime n = 90 % at 1.30 um n = 83 % at 1.55 um	High-Speed High Efficiency Low Dark Current	TRW/Electro Optic Research Center	Elec.Lett. 20(5) pp. 198 Mar. 1984
InGaAs/InP PIN	n = 78 % at 1.0-1.6 um R = 0.82 A/W at 1.3 um	High Efficiency Low Dark Current	Japan	Conf.Solid State D&M pp. 579 1984
InGaAs PIN Photodiode	60 ps Risetime n = 35 % at 1.30 um n = 25 % at 1.55 um I_D= 2x10^{-9} A	Low Dark Current Low Capacitance	AT & T Bell Lab.	IEEE JQE 17(2) pp. 227 Feb. 1981
InGaAs/InP PIN Photodiode	f = 22 GHz	Back-Illuminated Structure	AT & T Bell Lab.	Tech. Dig. TMPEO ThA3 Mar. 1985
GaAs PIN Photodiode	f = 20 GHz (19 ps FWHM)	High-Speed Planar Structure	MIT Lincoln Lab.	APL 46(2) pp. 191 Jan. 1985
AlGaAs/GaAs PIN Photodiode	f = 2.5 to 20 GHz n = 65 % at 0.84 um R = 0.45 A/W 0.84 um	High-Speed High Efficiency	Ortel Corp. & CALTEC	APL 43(3) pp. 261 Aug. 1983
GaInAs Schottky Photodiode	15 ps Risetime n = 19 % at 1.27 um	High-Speed	TUA GERMANY	Elec. Lett. 21(5) pp. 180 1985

CHAPTER TWO
THEORETICAL ANALYSIS OF PHOTODETECTOR PARAMETERS

2.1. General Requirements for A Photodetector

The general requirements for a high-speed photodetector include (1) high quantum efficiency, (2) low dark current, (3) low capacitance and resistance (for high-speed and low noise), and (4) low excess noise (especially for avalanche photodiode). These requirements for photodetectors are tied to the particular material requirements which include [12]:

(1) Energy bandgap, preferably a direct bandgap with a high absorption coefficient, should be smaller than the photon energy to be detected.

(2) Direct energy bandgap material must be used so that optical radiation can be absorbed in a short distance to minimize transit time effects for high response speed.

(3) High-quality low-defect density and high-purity (especially for long wavelength photodetector) material must be used so that Zener-tunneling and dark current can be minimized.

(4) The material must be doped properly so that the depletion layer width, which is a trade-off between high-speed and high quantum efficiency, can be optimized.

(5) The epilayer material should be lattice-matched to the substrate material for a long wavelength photodetector.

2.2. Spectral Response

For short wavelength (0.50-0.85 um) detection, photons are absorbed near the semiconductor surface. The photogenerated excess carriers are separated in the depletion region close to the surface of a photodiode. It is advantageous to use a metal-semiconductor Schottky barrier structure with a thin semi-transparent metal film. In this detection mode an extremely high response speed and high quantum efficiency can be obtained, if the depletion region is small and comparable to the light penetration depth. For long wavelength (0.95-1.65 um) detection, light penetrates deeply into the material. Therefore, a high quantum efficiency requires the material with a wide depletion layer width. For these photodiodes a trade-off exists between a quantum efficiency and a response speed.

The external quantum efficiency of a Schottky barrier photodiode is determined mainly by the transmission loss in the metal film and the reflection loss at the metal-semiconductor interface as well as the recombination loss in the diode. To reduce the reflection loss an AR coating is usually incorporated in the photodiode fabrication. This can be achieved by depositing a thin dielectric film such as Ta_2O_5,SiO_2 or Si_3N_4 with its thickness equal to the quarter wavelength of the incident radiation at the selected wavelength. The thickness of a single layer AR coating film is given by [41]:

$$d_1=(\lambda_o/4\, n_1)\tan^{-1}[2n_1k_s/(n_1^2-n_s^2-k_s^2)] \qquad (2.1)$$

where λ_o is the wavelength of a selected incident light, n_1 the index of refraction of the dielectric film, and n_s the complex index of refraction of the semiconductor. In the case of a weakly or nonabsorbing substrate, Eq.(2.1) can be reduced to the well-known quarter wavelength design formula, i.e., $d_1 = \lambda_o/4n_1$.

2.3. Response Speed

The response speed of a photodetector can be determined primarily by three parameters: the drift time in the depletion region, the diffusion time in the quasi-neutral region, and the RC time constant required to discharge the junction capacitance (C_d) through a combination of internal and external resistances. The total risetime of a photodiode, which is defined as the response time from 10 % to 90 % of a pulse height, is essentially equal to the largest of the three. The total risetime can be expressed by:

$$t_r = (t_{tr}^2 + t_{diff}^2 + t_{RC}^2)^{1/2} \qquad (2.2)$$

where t_{tr}, t_{diff}, and t_{RC} are transit time, diffusion time, and RC time constant, respectively. We can relate the risetime (t_r) to the cutoff frequency (f_c) by [5]:

$$t_r = 0.35/f_c \qquad (2.3)$$

where the cutoff frequency, f_c is often regarded as the bandwidth of the system. For high speed operation, the carriers are being excited within the depletion region of the junction or close to the junction so that diffusion time is shorter than or at least comparable to carrier drift time and the carriers are collected across the junction at scattering limited velocity (V_{sat}).

The optimum depletion width is a trade-off between the fast transit time requiring a narrow depletion region and the combination of quantum efficiency and low capacitance which requires a wide depletion region. The depletion region width is chosen so that the transit time is of the order of one-half the modulation period (i.e., half-power frequency roll-off due to RC time and transit time is comparable).

2.3.1. Drift time

When the carriers are injected from the highly doped contact region or generated in the depletion region, they transverse across the depletion region. The carrier drift (transit) time across the depletion region is given by $t_{tr} = W/2.8\ v_s$ [32], where v_s is the saturation drift velocity of the carriers, and W is the depletion region width. For high mobility materials, this transit time is limited by the saturated drift velocity.

2.3.2. Diffusion time

The carriers which are generated within the highly doped contact region or in the quasi-neutral region will diffuse to the drift region. This carrier diffusion will result in a time delay of the carriers reaching the drift region. The frequency response for diffusion time is given by $t_{diff} = W_p^2/(2.43\ D_n)$, if the thickness of the highly doped p+ region (W_p) is less than the carrier diffusion length (L_n) [42].

2.3.3. RC time constant

Assuming that the drift time and the diffusion time can be greatly reduced by optimizing the device configuration, the response speed is mainly determined by the depletion capacitance (C_d), the series resistance (R_s), and the load resistance (R_L). The shunt resistance (R_i) is generally very high but is included to account for the relatively low leakage resistance of the photodiode. Therefore, the response speed can be estimated from the RC time constant. The resulting RC time constant is given by :

$$t_{RC} = (R_s + R_L)C_d \tag{2.4}$$

The cutoff frequency is given by:

$$f_c = 1/[2\pi(R_s+R_L)C_d] \qquad \text{for} \quad (R_s+R_L)/R_i \ll 1 \tag{2.5}$$

It should be noted that practical detection systems usually have lower cutoff frequency because of the finite load resistance, the parasitic capacitance and the load inductance of the photodiode. For high speed operation, the series resistance should be small (usually less than 10 ohm for a well-designed diode) and the load resistance should be low (usually 50 ohm). The load resistance may be reduced in a high-speed circuit. However, it should be as high as possible for a low-noise detection circuit. Therefore, the depletion capacitance should be minimized.

2.4. Dark Current

The dark current depends strongly on the barrier height of a Schottky barrier photodiode. The dark current depends also strongly on diode material, geometry, and surface passivation. The use of $In_xGa_{1-x}As/InP$ heterostructure and surface passivation could reduce the dark current of a photodiode. The reduction of dark current is important for the improvement of the minimum detectable power.

The dark current of a Schottky barrier photodiode consists of thermionic-emission current, generation-recombination current via traps in the depletion region, tunneling current due to carriers tunneling across the bandgap, and surface leakage current or interface current due to traps at the metal-semiconductor interface. Tunneling current can be neglected for low impurity doping concentration (less than 10^{17} cm^{-3}). Surface leakage current is not a fundamental device characteristic and, in most cases, can be eliminated by careful processing and passivation techniques. The total current consists of thermionic-emission current over the Schottky barrier and the generation-recombination current in the depletion region.

2.4.1. Thermionic-emission Current

The dark current in the forward bias direction of a Schottky barrier diode is determined mainly by thermionic-emission of majority carriers from the semiconductor into the metal for doping levels less than 10^{17} cm^{-3}.

$$I_{th} = SA^{*}T^{2}\exp[-q(\Phi'_{Bn})/kT][\exp(qV/nkT) - 1] \qquad (2.6)$$

The effective barrier height, $\Phi'_{Bn} = \Phi_{Bn} - \Phi_m$ can be determined from the measured value of the saturation current.

2.4.2. Generation-Recombination Current

At zero bias, the depletion region of the Schottky barrier is in thermal equilibrium and the rate of electron-hole pair generation is balanced by the rate of recombination. In the presence of an applied voltage, there will be a net generation or recombination current depending on the polarity of the bias. The generation-recombination current through the midgap traps in the depletion region, which is dominant at low voltage, is given by:

$$I_{gr} = qn_i AW/t_{eff}[\exp(qV/2kT) - 1] \qquad (2.7)$$

where $t_{eff} = (t_n t_p)^{1/2}$ is the effective carrier lifetime in the depletion region. This current is added to the thermionic-emission current and may cause deviations from ideal behavior in a Schottky barrier diode. Note that the current is a generation current when the junction is reverse biased, and is a recombination current when the junction is forward biased. The total current can be expressed by:

$$I_{tot} = I_{ths}[\exp(qV/kT) - 1] + I_{grs}[\exp(qV/2kT) - 1] \qquad (2.8)$$

The ratio of thermionic-emission current to generation-recombination current increases with a bias voltage, energy-gap, effective carrier lifetime, and temperature and decreases with the barrier height. The recombination current is important in high barrier, in low lifetime material, at low temperature, and at low forward bias voltage [43,44].

2.4.3. Tunneling Current

Tunneling current, either band-to-band or via deep-level traps dominates the dark current at high voltage (and then low capacitance), resulting in the soft breakdown characteristics. For heavily doped semiconductors the dominant process changes from thermionic-field emission to field emission and the contact states to behave like an ohmic contact with a sufficiently small contact resistance. In addition, the exponential dependence of the current changes from qV/kT to qV/E_{oo} [45].

$$J = J_s \exp\{qV/[E_{00}\coth(E_{00}/kT)]\} \qquad (2.9)$$

$$E_{00} = (qh/2)(N_D/m^*\epsilon_s)^{1/2} \qquad (2.10)$$

$$= 1.85\text{x}10^{-14}(N_D/m_r\epsilon_r)^{1/2} \qquad (2.11)$$

where m^* ($= m_r m_o$) is the effective mass of electron and ϵ_s ($= \epsilon_o\epsilon_r$) is permittivity of the semiconductor. E_{oo} is a very useful parameter in predicting the relative importance of thermionic-emission or tunneling. For $E_{oo}/kT << 1$, the thermionic-emission process dominates and the contact behaves as a Schottky barrier. For $E_{oo}/kT >> 1$, field emission dominates and the contact exhibits ohmic characteristics. For $E_{oo}/kT = 1$, a mixed mode of transport occurs.

2.5. D.C. Parameters

The total capacitance of a packaged Schottky barrier photodiode is given by $C_T = C_j + C_o + C_p$, where C_j is the metal-semiconductor junction capacitance, C_o is the overlay capacitance across the dielectric passivation layer, and C_p is the package parasitic capacitance. The overlay and package parasitic capacitance should be minimized.

2.5.1. Junction Capacitance

The junction capacitance is simply given by the one-sided abrupt junction analysis. Measurements of junction capacitance can be used for determining the background shallow impurity profile of a Schottky barrier diode or a one-sided abrupt junction diode. The background dopant density is given by:

$$N_B = (2/q\epsilon_o\epsilon_s A^2)[d(V_R + V_D)/dC_j^{-2}) \qquad (2.12)$$

where

$$C_j = A[q\epsilon_o\epsilon_r N_D/2(V_D - V)]^{1/2} \qquad (2.13)$$

where N_B is the dopant density of the light-doped side. The diffusion potential

V_D of a Schottky barrier diode is determined from the intercept of C_j^{-2} vs. V_R curve, and the barrier height of a Schottky diode can be calculated

$$\Phi_{Bn} = V_D + (kT/q)\ln(N_C/N_D) \tag{2.14}$$

2.5.2. Overlay Capacitance

The capacitance due to the metal contact overlaying the passivating dielectric layer in a Schottky barrier diode may be important. Assuming negligible space-charge penetration (a realistic assumption for SiO_2 on the semiconductor), the overlay capacitance is given by:

$$C_o = \epsilon_o \epsilon_r A/W_o \tag{2.15}$$

where W_o is the thickness of the dielectric layer, and A [=2(R_i +)] is the area of the dielectric layer. This parasitic capacitance must be kept to a minimum particularly at X-band frequency or higher. Overlay contacts are not generally used above 40 GHz frequencies because they degrade the overall performance of a diode [45]. Figure 2.1. shows the different values of the overlay capacitance for different values of R_i, Δ, and W_o. The thick dielectric layer (e.g., 2 um) can substantially reduce the overlay capacitance of a Schottky barrier diode.

2.5.3. Series Resistance

The series resistance is due mainly to the resistance of the semiconductor substrate and the undepleted epilayer. The series resistance in the epitaxial layer and the semiconducting substrate is distributed depending on the contact geometry and frequency dependent. The resistance of an epilayer is given by:

$$R_{s1} = 2W/q\mu_n N_D A \tag{2.16}$$

where W is the thickness of the epilayer, and N_d is the donor density of the epitaxial or active layer. The resistance contributed by the substrate may be

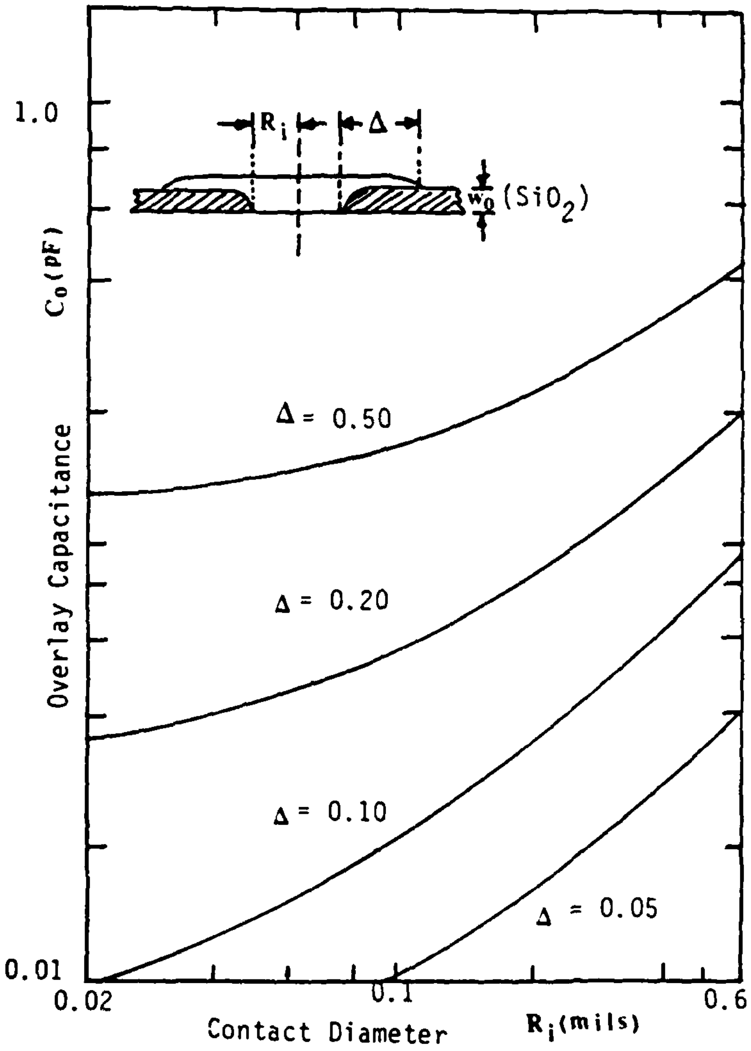

Fig. 2.1. Overlay Capacitance for SiO_2 Width of 0.1 um.

modeled by using the resistance of a contact dot on a semi-infinite semiconductor substrate.

$$R_{s2} = 2\rho_s (A/\pi)^{1/2} \qquad (2.17)$$

where ρ_s is the substrate resistivity. The total series resistance shown in Fig.2.2. consists of R_{s1} due to the epilayer and R_{s2} due to the semiconductor substrate.

2.6. Noise-Equivalent Power (NEP)

The minimum detectable optical power of a photodiode is limited by its noise performance. The noise generated in a photodiode operating under reverse bias condition is a combination of shot noise, 1/f noise (or flicker noise), and the thermal noise (or Johnson noise). The shot noise is due to the photogenerated currents of the signal, background illumination, and the reverse-bias dark current. The thermal noise arises from a random motion of the carriers within any resistive materials including semiconductors, and is always associated with a dissipative mechanism. The flicker noise (or 1/f noise) has a current-dependent power spectrum which is inversely proportional to the frequency existing in all devices when a current flows.

At low frequency 1/f noise dominates, and at intermediate frequency the generation-recombination noise dominates. At high frequency, the infrared photodetectors exhibit a white (frequency independent) noise which includes thermal, generation-recombination, and shot noise. The transition points vary with semiconductor material, doping, and processing technology. However, for infrared detectors, these transition frequencies are roughly at 1 KHz and 1 MHz, respectively. In the wavelength region of interest for optical communication, the detection is limited either by thermal or shot noise. The effect of noise on signal transmission is measured by the signal-to-noise ratio (SNR) for analog signals. The signal-to-noise ratio (SNR) is the signal power at an output of the

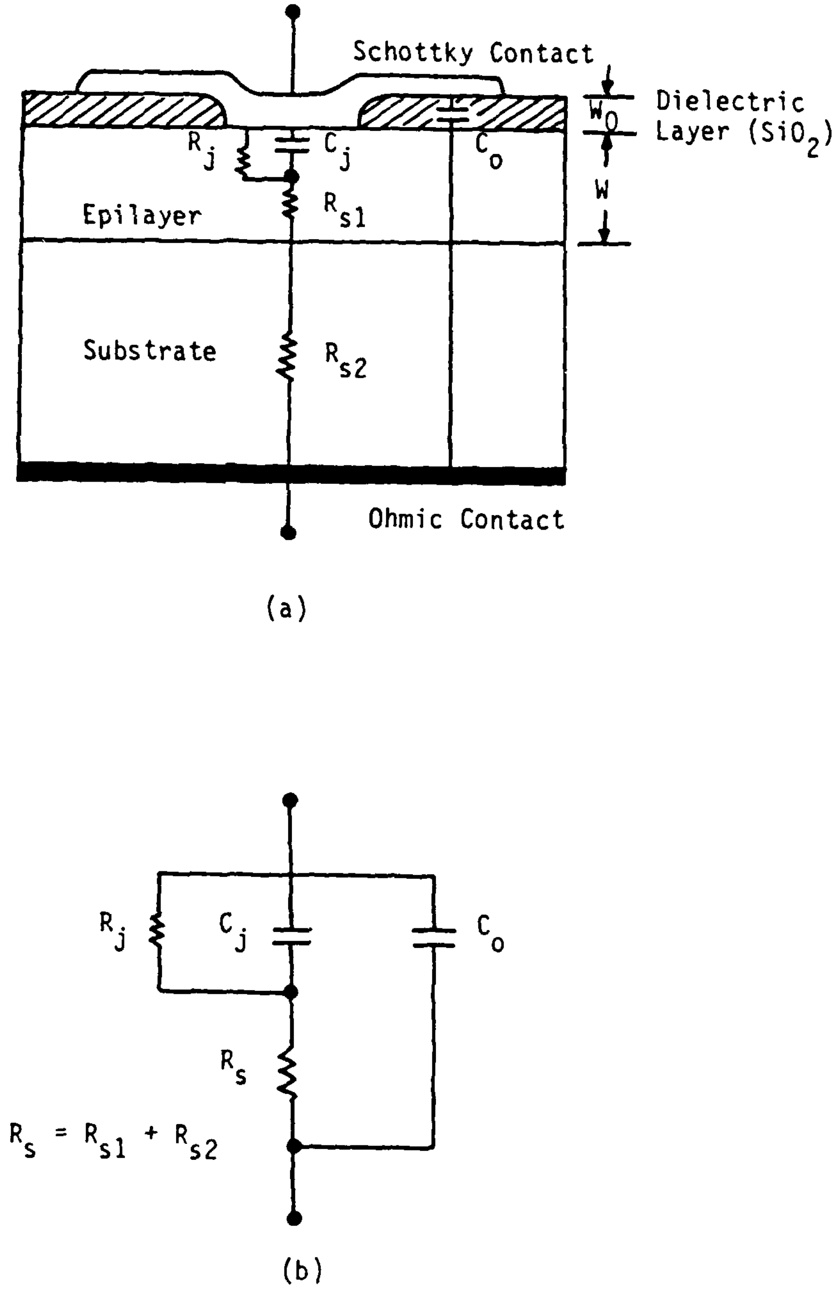
Schottky Contact
W_0
Dielectric Layer (SiO_2)
R_j
C_j
C_o
W
Epilayer
R_{s1}
Substrate
R_{s2}
Ohmic Contact
(a)
R_j
C_j
C_o
R_s
$R_s = R_{s1} + R_{s2}$
(b)

Fig. 2.2. Schottky Barrier Diode: (a) Structure
(b) Equivalent Circuit

detection circuit divided by the average noise power.

$$SNR = (1/2)\bar{i}_s{}^2 R_{eff}/i_n{}^2 R_{eff} \qquad (2.18)$$

where $\bar{i}_n{}^2$ is the sum of the square of all noise source currents.

$$\bar{i}_n{}^2 = \bar{i}_s{}^2 + \bar{i}_b{}^2 + \bar{i}_d{}^2 + \bar{i}_{th}{}^2 \qquad (2.19)$$

and $\bar{i}_s$ is the signal noise current amplitude obtained from a sinusoidally modulated optical signal, $\bar{i}_s = (\eta q \lambda P_L/h\nu)$, where P_L is the average optical signal power, which is assumed to be 100 % intensity modulated. Therefore, SNR is given by [5]:

$$SNR = \frac{(1/2)(\eta q \lambda P_L/h\nu)^2}{2q\,\Delta f(I_S+I_B+I_D)+(4kT\Delta f/R_{eff})F} \qquad (2.20)$$

The optical power P_L which generates a signal amplitude equal to the noise amplitude (i.e., SNR = 1) at the output is called the minimum detectable power P_{min}, which is given by:

$$P_{min} = (2h\nu/\lambda\eta)(\Delta f)^{1/2}((\Delta f)^{1/2}+(\Delta f+(I_B+I_D)/q+(2kTF/q^2R_{eff}))^{1/2}) \qquad (2.21)$$

The noise-equivalent power is obtained by dividing P_{min} by $(\Delta f)^{1/2}$:

$$NEP = (2h\nu/\lambda\eta)((\Delta f)^{1/2}+(\Delta f+(I_B+I_D)/q+(2kTF/q^2R_{eff}))^{1/2}) \qquad (2.22)$$

The noise due to the background illumination can be neglected because it can be made vanishingly small in optical fiber communication circuits. Figure 2.3. shows the theoretical calculation of NEP vs. effective resistance, R_{eff}, with a parameter of a dark current for the photodetectors.

2.7. Device Packaging

The photodetector should be packaged to protect them from mechanical or other possible damages and to allow their incorporation into electrical and

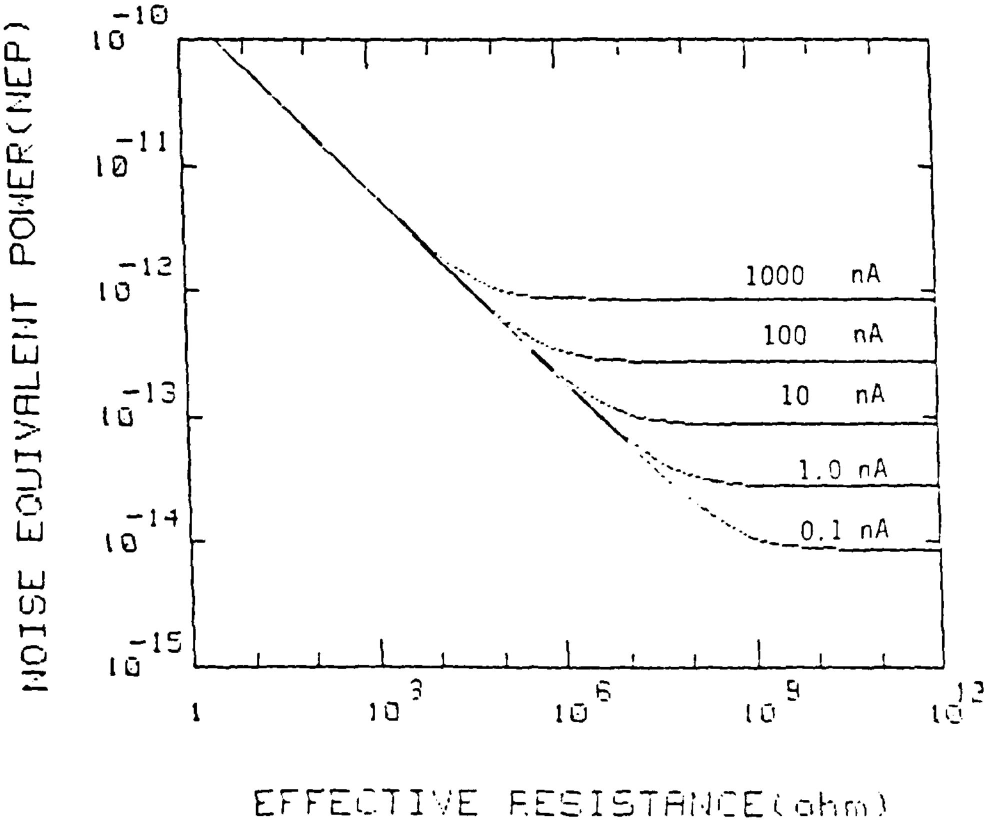

Fig. 2.3 Noise-Equivalent Power (NEP) vs Effective Resistance with a Dark Current as a Parameter. ($C_t = C_d + C_L = 0.5$ pF)

optical circuits. However, packaging introduces additional parasitic effects and may attenuate or distort both electrical and optical signals, if not properly designed. The package size determines the parasitic impedance added to the diode impedance, predominantly the lead inductance and package capacitance. For low noise and large bandwidth,the capacitance should be extremely small. Therefore, small packages are preferable for low noise-equivalent power and high modulation frequency of photodiodes for optical fiber communications.

In packaging a specially designed photodetector for optical fiber communications, a fiber with a relatively large numerical aperature and diameter is positioned close to the top contact above the illumination window of the diode. This kind of package allows the maximum quantum efficiency at minimum background illumination obtainable for a fiber-diode connection. Electrical contact to a photodiode is most easily achieved by soldering the wireleads or bonds into the electrical circuit. If a microstrip line is used, parasitic capacitance can be reduced. To allow a demountable connection to a commercial 50 ohm amplifier, the photodiode should be incorporated into a miniature coaxial cable. The latter approach may limit the system performance because of the low input impedance (thermal noise). A variety of packages for MIC applications which satisfy these requirements are shown in Fig.2.4. Their characteristics are summarized in Table 2.1.

2.7.1. Microstrip Line Parameters

Microstrip transmission lines have been extensively used for microwave and millimeter-wave hybrid integrated circuits. Microwave integrated circuits (MIC) can be made in monolithic or hybrid form. However, monolithic technology is not well suited to MIC because the processing difficulties, low yields, and poor performance have seriously limited their applications. The hybrid technology is used almost exclusively for MIC in the frequency range of 1 to 15 GHz. The passive lumped elements can be fabricated on the same substrate and chip or

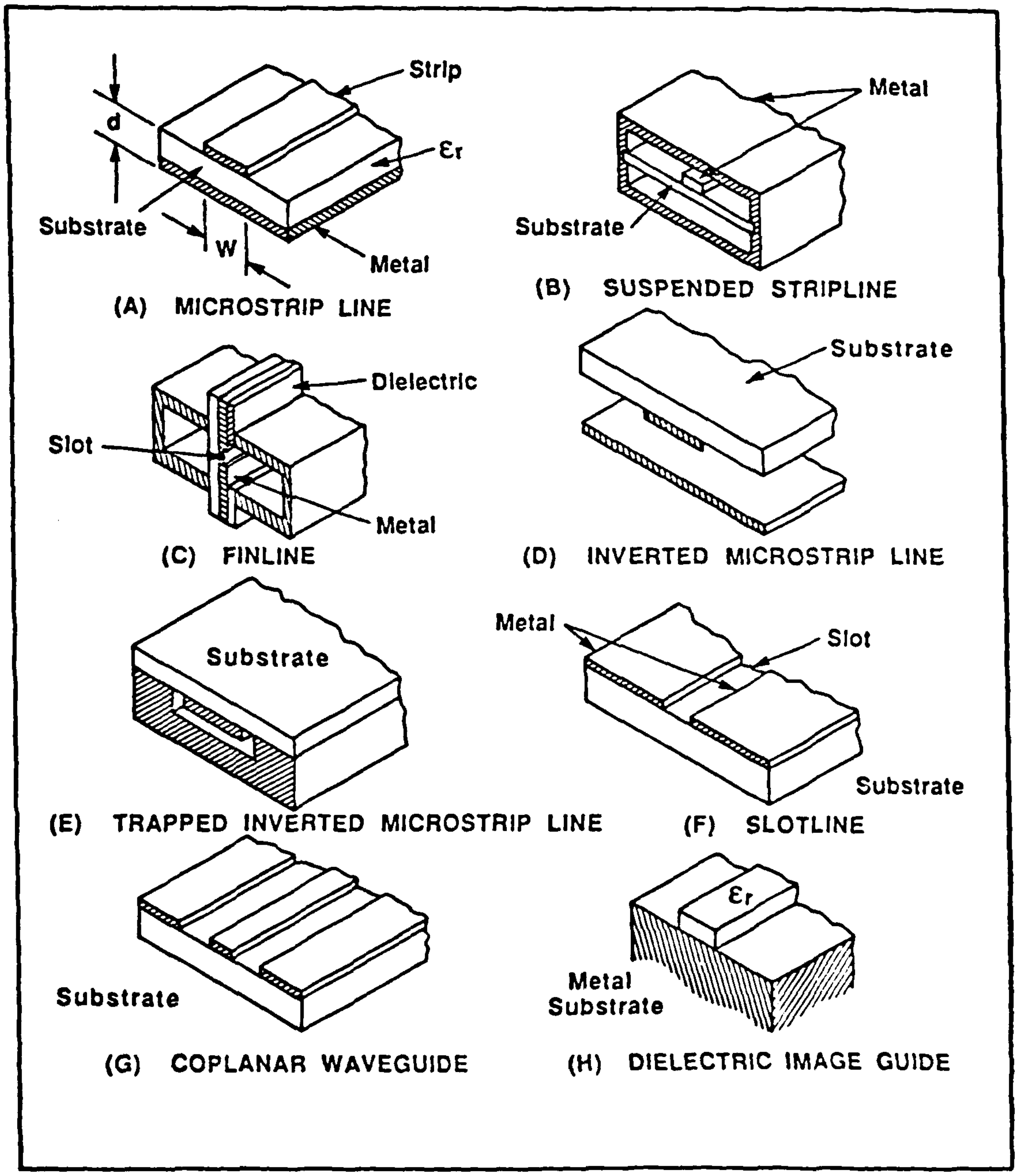
Strip
d
ε_r
Substrate
W
Metal
(A) MICROSTRIP LINE
Metal
Substrate
(B) SUSPENDED STRIPLINE
Dielectric
Slot
Metal
(C) FINLINE
Substrate
(D) INVERTED MICROSTRIP LINE
Substrate
(E) TRAPPED INVERTED MICROSTRIP LINE
Metal
Slot
Substrate
(F) SLOTLINE
Substrate
(G) COPLANAR WAVEGUIDE
ε_r
Metal
Substrate
(H) DIELECTRIC IMAGE GUIDE

Fig. 2.4. Structure of Microwave Package for MIC Applications

Table 2.1. Comparison of Different Transmission Line Structures

TRANSMISSION LINE STRUCTURES	CHARACTERISTIC IMPEDANCE (Ω)	FREQUENCY RANGE OF OPERATION (GHz)	LOSS	DISPERSION	DEVICE COMPATABILITY INTEGRATION LEVEL	
					IN SERIES	IN PARALLEL
Microstrip Line	25-125	up to 100	Medium	Low	Easy	Difficult
Coplanar Waveguide	30-150	up to 60	High	High	Easy	Easy
Slot Line	60-200	—	High	Non Tem Mode	Difficult	Easy
Suspended Stripline	40-150	>100	Low	High	Easy	Difficult
Finline	10-400	30-100	Low	Low	Easy	Easy
Inverted Microstrip Line	25-130	>100	Low	Low	Unknown	Unknown
Trapped Inverted Microstrip Line	30-140	up to 100	Low	Low	Unknown	Unknown
Dielectric Image Waveguide	20-30	>100	High	High	Difficult	Difficult

beam-lead active devices can be bonded directly to the strips.

The parameter analysis of microstrip lines can be obtained by numerical approximations such as conformal mapping method, variational method, or relaxation method if the transverse electro-magnetic (TEM) mode is assumed to be dominant. The electrical parameters are characterized by characteristic impedance, attenuation factor, and wavelength. The microstrip width can be calculated iteratively for a required line impedance using the substrate dielectric constant and thickness. The operation frequency is then used to obtain the guide wavelength and phase velocity. The conductor loss and dielectric loss [46–48] can be calculated using the substrate dissipation factor and metallization resistivity and thickness. The microstrip lines are assumed to be propagated in only quasi-TEM mode or can be approximated as such at the operating frequency. Therefore, the operating frequency must be lower than the cutoff frequency f_c of the lowest transverse electric surface wave.

$$f_c = 75/H(C_r-1)^{1/2} \quad (\mathrm{GHz}) \qquad (2.23)$$

where H is the substrate thickness (mm). The relative magnetic permeability of the substrate μ_r should equal the unity. The characteristic impedance to determine the width of microstrip lines is given by [39]: For $W/H < 1$,

$$Z_o = 1/2\pi \, (\mu_o/\epsilon_{eff}\epsilon_o)^{1/2} \ln(8H/W + W/4H) \qquad (2.24)$$

$$= 60/(\epsilon_{eff})^{1/2} \ln(8H/W + W/4H) \qquad (2.25)$$

where $\mu_o = 4 \times 10^{-7}$ H/m and $\epsilon_o = 8.854 \times 10^{-12}$ F/m and W,H are the width, thickness of microstrip lines, respectively. The effective relative dielectric constant ϵ_{eff} for a microstrip line depends on the ratio W/H, the relative dielectric constant ϵ_r, and the geometrical factors of the boundary between air and dielectric substrate material.

$$\epsilon_{eff} = (\epsilon_r+1)/2 + (\epsilon_r-1)/2\ [(1+12H/W)^{-1/2}+0.04(1-W/H)^2] \qquad (2.26)$$

The zero thickness (t=0) formulas given above can be modified to consider the thickness of the microstrip when W is replaced by an effective strip width W' as follows (t<H and t<W/2). For $W/H \leq \pi/2$

$$W' = W + (t/\pi)[1 + \ln(4\pi W/t)] \qquad (2.27)$$

The attenuation constant of the dominant microstrip mode depends on geometrical factors, electrical properties of the substrate and conductor, and the frequency. For a nonmagnetic dielectric substrate, the two sources of dissipative loss in microstrip lines are conductor loss in the strip conductor and ground plane and dielectric loss in the substrate. The sum of these two losses may be expressed as losses per unit length in terms of an attenuation factor, α. The ohmic loss α_c for $W/H < 1$ is given by:

$$\alpha_c = (20R_s/\ln 10)[1-(W'/4H)^2]/2\pi ZH[1+H/W'+H/\pi W'\{\ln(4\pi W/t)+t/W\}] \qquad (2.28)$$

where the surface resistivity R_s is given in terms of the free space permeability μ_o and the conductivity, σ of the strip metal as

$$R_s = (\pi f \mu_o/\sigma)^{1/2} \qquad (2.29)$$

The dielectric loss α_d with loss tangent, $\tan\delta$ is given by:

$$\alpha_d = (20\pi/\ln 10)(\epsilon_r/\epsilon_{eff}^{1/2})(\epsilon_{eff}-1)/(\epsilon_r-1)\tan\delta/\lambda \qquad (2.30)$$

where the loss tangent, $\tan\delta$ is the substrate dissipation factor. The microstrip wavelength and phase velocity can be determined in terms of the effective relative dielectric constant, ϵ_{eff}.

$$v_p = C(\epsilon_{eff})^{-1/2} \quad (2.31)$$

$$= 29.980/(\epsilon_{eff})^{1/2}f \text{ (cm)} \quad (2.32)$$

2.7.2. Microstrip Line Design

The width of the microstrip transmission line can be calculated iteratively for a required line impedance using the substrate dielectric constant and thickness [49]. The alumina substrate with a gold film coated on both sides is commercially available. The design parameters and the structure of a microstrip line are given in Table 2.2. and Fig.2.5., respectively.

Table 2.2. DESIGN PARAMETERS FOR MICROWAVE TRANSMISSION STRIPLINE

Alumina (Al_2O_3) Substrate	1x1x0.025 "
Dielectric Constant	$\epsilon_r = 9.8$
Substrate Thickness	H = 0.025 "
Gold Film Thickness	t = 0.0002 "
Output Impedance	Z = 50 ohm
Microstrip Line Width	W = 0.02425 "
W/H Ratio	W/H = 0.97
Effective Strip Width	W' = 0.02478 "

2.8. Response Speed Measurement

The typical response speed measurement techniques for an impulse response of the photodetector are (1) impulse response technique using a sampling scope or a microwave spectrum analyzer [50], (2) sampling and cross-correlation technique using two photodetectors [51], (3) optical heterodyne technique [52-54], and (4) electro-optical sampling technique [55]. Table 2.3. lists the test equipments used for the measurement of the photodiode parameters.

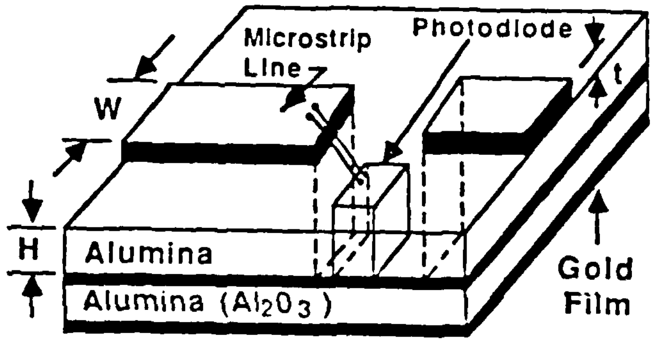
Microstrip Line
Photodiode
W
t
H
Alumina
Alumina (Al2O3)
Gold Film

(Not in Scale)

$Z_o = 50$ ohm, $W/H = 0.97$, $\varepsilon_r = 9.8$

Fig. 2.5. Structure of the Microstrip Line used in this research project.

2.8.1. Impulse Response

This method requires an optical source generating the ultrashort pulses preferably shorter than the impulse response of the device under test. For broadband characterization either a synchronously pumped mode-locked dye laser or a diode laser driven by a comb generator (or a step-recovery diode) at an operating wavelength is necessary. The schematic diagram for the impulse response measurement is shown in Fig.2.6. The impulse response is measured by either a sampling scope in a time domain or a microwave spectrum analyzer in a frequency domain. The output pulse of the photodetector and sampler to the narrow incident light pulses are shown in Fig. 2.7. Note that this response is a convolution of the photodetector and the measurement system including the sampling gate width, laser pulse width, pulse broadening due to the transmission lines, and impulse response.

2.8.2. Sampling/Cross-Correlation

This technique is to make a cross-correlation of two identical optical pulses by delaying one with respect to the other for measuring the duration of picosecond optical pulses. In this case, the two photodetectors, one acting as a sampling gate to sample the waveform of the other, are not necessary identical. The detectors are connected in order that the device under test (DUT) launches a waveform onto a transmission line by an incident short optical pulse and the second detector is a sampling gate on the transmission line that is probed by the same optical pulse with a variable delay time. The schematic diagram is shown in Fig.2.8. The signal output from the second device is given by a correlation of the signal from the first photodetector with the response of the second photodetector with a delay time as is shown in Fig.2.9. Note that each signal is a convolution of the impulse response of the device, the optical pulse width, and the circuit effects such as the transmission line.

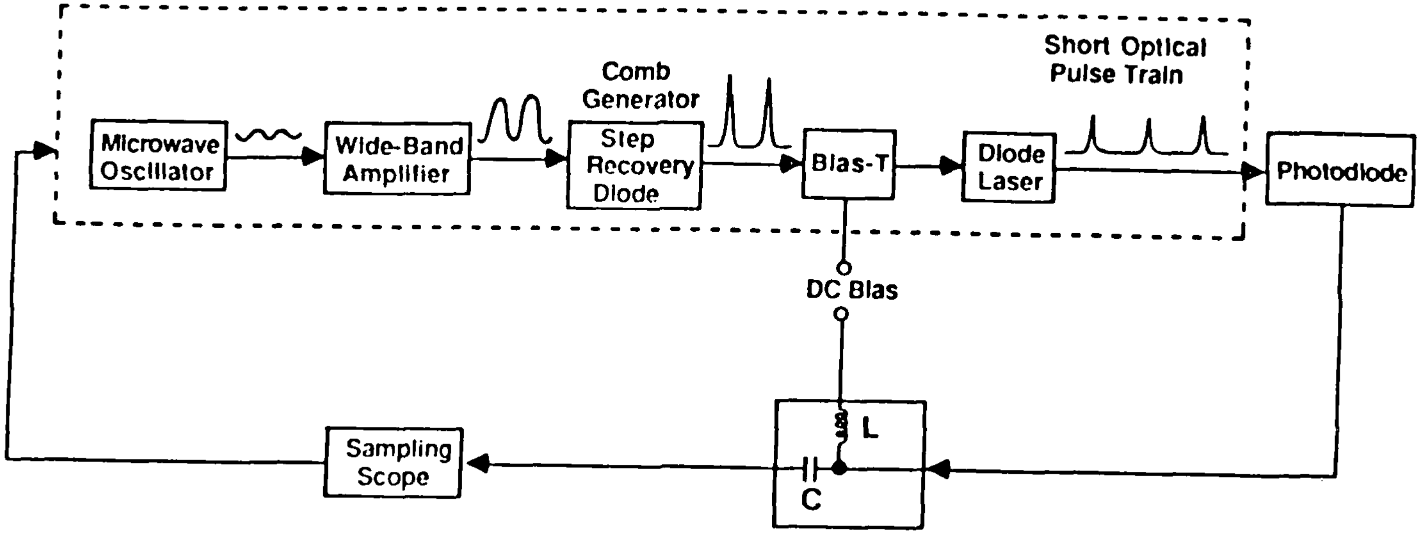
Short Optical
Pulse Train
Comb
Generator
Microwave
Oscillator
Wide-Band
Amplifier
Step
Recovery
Diode
Bias-T
Diode
Laser
Photodiode
DC Bias
L
C
Sampling
Scope

Fig. 2.6. Schematic Diagram for an Impulse Response Measurement System.

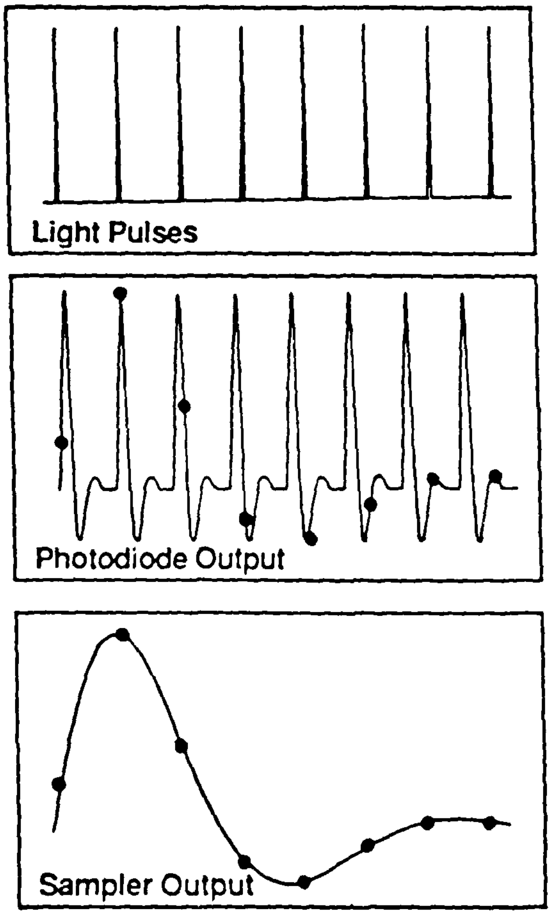
Light Pulses
Photodiode Output
Sampler Output

Fig. 2.7. Output Pulse of the Detector and Sampler.

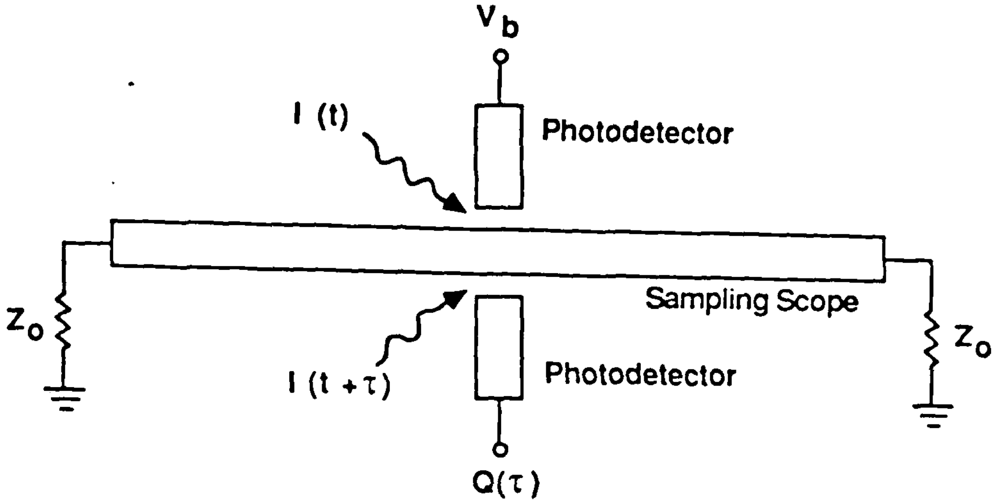
V_b
I (t)
Photodetector
Sampling Scope
Z_o
Z_o
I (t + τ)
Photodetector
Q(τ)

Fig. 2.8. Schematic Diagram for Sampling/Cross-Correlation.

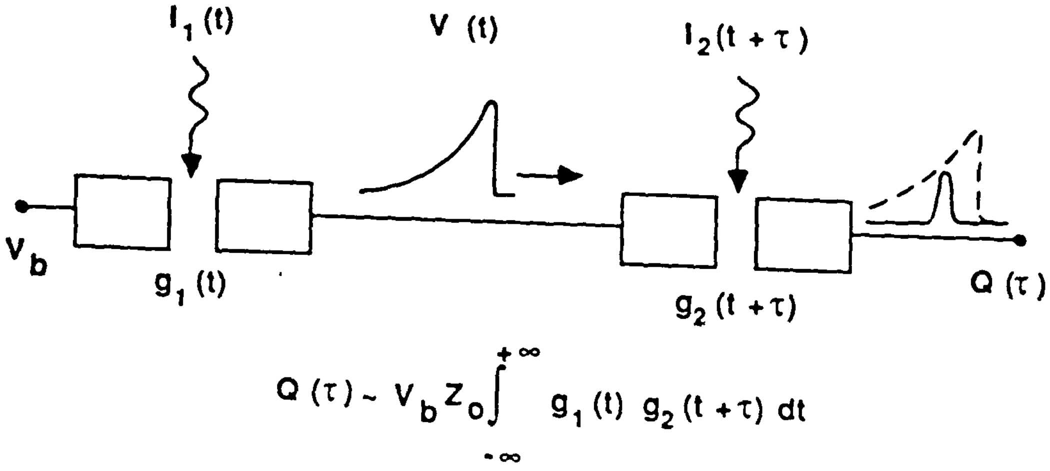

$I_1(t)$
$V(t)$
$I_2(t+\tau)$
V_b
$g_1(t)$
$g_2(t+\tau)$
$Q(\tau)$
$Q(\tau) \sim V_b Z_o \int_{-\infty}^{+\infty} g_1(t)\, g_2(t+\tau)\, dt$

Fig. 2.9. Convolution of the impulse response.

2.8.3. Electro-Optical Sampling

This technique shown in Fig.2.10 requires a microstrip transmission line deposited on a linear electro-optic crystal such as $LiTaO_3$ and used as an active element in a lithium tantalate traveling-wave Pockels cell amplitude light modulator. A train of picosecond pulses from a modelocked dye laser is split into two beams. One beam strikes the photodiode and launches a signal onto the modulator transmission line. The other beam passes transversely through the crystal and its intensity is modulated by the electric field under the transmission line sampling the signal. By varying the relative delay between the two beams, the waveform on the transmission line can be mapped out.

The voltage waveform on the transmission line is a convolution of the photodiode response, the laser pulse response, dispersion in the transmission line. The subsequent sampling is a cross-correlation of the laser pulse with the voltage waveform. The operations of convolution and correlation are associative and the sampler output is,therefore,equivalent to the convolution of the photodiode impulse response with the auto-correlation of the laser pulse. Since the auto-correlation of the laser pulse is independently measured, its contribution can be deconvolved to extract the photodiode impulse response. Then the equivalent time representation of the photodiode response is obtained. The temporal resolution is determined by several factors; the sampling light beam spot size, the optical transit time, and the laser pulse duration.

2.8.4. Optical Heterodyning

This technique can characterize the bandwidth of a photodetector accurately using two CW lasers. The limitation in the accuracy is the bandwidth of the transmission line and the microwave spectrum analyzer. The simple system shown in Fig.2.11 consists of two semiconductor diode lasers whose frequency is temperature tuned and the combined beam is incident on the photodiode. Since the photocurrent is proportional to the square of the electric field of the

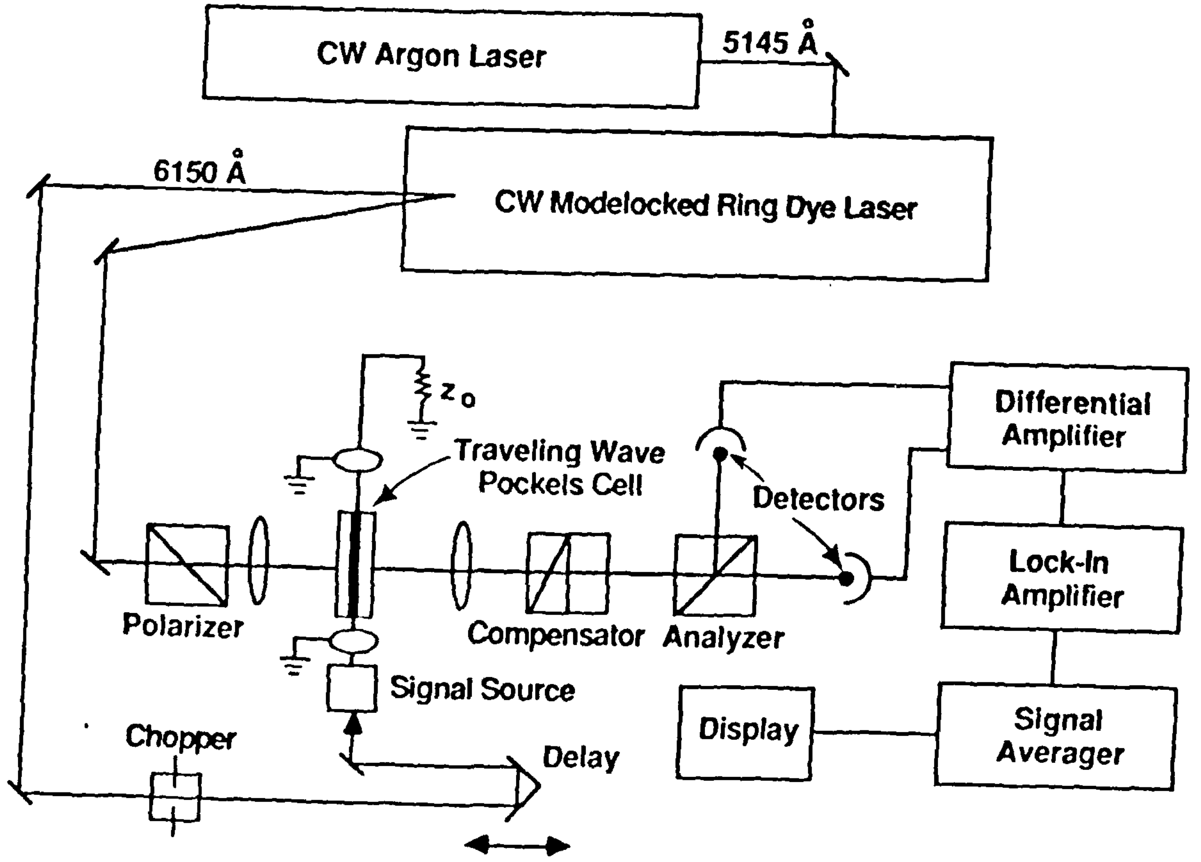
CW Argon Laser
5145 Å
6150 Å
CW Modelocked Ring Dye Laser
z_o
Traveling Wave
Pockels Cell
Detectors
Differential
Amplifier
Polarizer
Compensator
Analyzer
Lock-In
Amplifier
Signal Source
Chopper
Delay
Display
Signal
Averager

Fig. 2.10 Schematic Diagram for Electro-Optical Sampling Measurement.

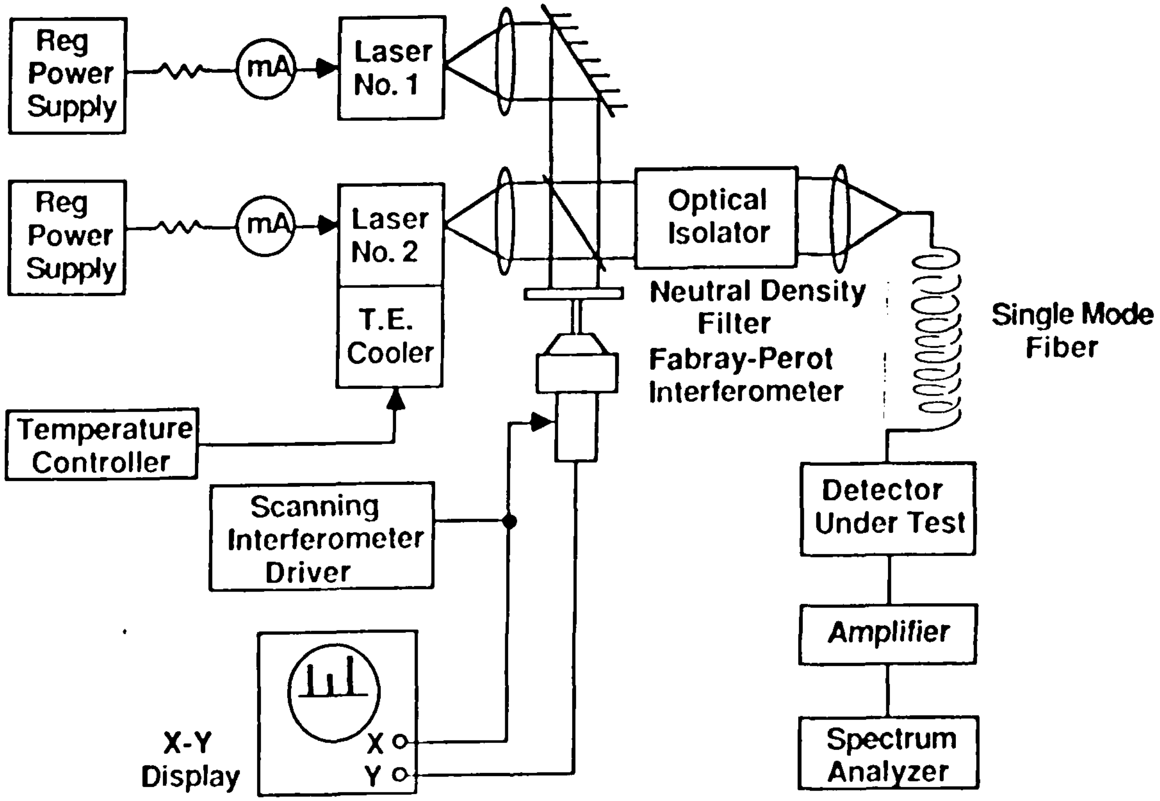
Reg
Power
Supply
mA
Laser
No. 1
Reg
Power
Supply
mA
Laser
No. 2
T.E.
Cooler
Temperature
Controller
Optical
Isolator
Neutral Density
Filter
Fabray-Perot
Interferometer
Single Mode
Fiber
Scanning
Interferometer
Driver
X
Y
X-Y
Display
Detector
Under Test
Amplifier
Spectrum
Analyzer

Fig. 2.11. Schematic Diagram for Optical Heterodyning.

laser, the product of two laser fields at a different frequency will produce a difference or beat frequency detected by a photodiode. With standard thermoelectric cooler/heater and feedback electronic circuit, the temperature of the laser diode can be controlled to within a few tenths of a millidegree.

Table 2.3. EQUIPMENTS FOR THE MEASUREMENT OF THE PHOTODIODE PARAMETERS

Parameter	Measurement Equipment	Maker/Model
Darkcurrent	Curve Tracer	Tektronix 576
	Pico Ammeter	HP 4140B
Capacitance	C-V Plotter	PAR M-410
	C Meter/C-V Plotter	HP 4280A
	Multifrequency LCR Meter	HP 4275A
	Probe Station (0.7X-3.0X)	Bausch and Lomb
A.C. Admittance	Impedance Analyzer	HP 4191A
Spectral Response	He-Ne Laser (0.63 um)	Spectra Physics 120
	Pulse Diode Laser (1.30 um)	
	Power Meter 1	Optics Tech. M-615
	Power Meter 2	LaserPrec. RL-3610
	Chopper	Laser Prec.CTX-532
	Detector Probe	Laser Prec. RKP-360
	Monochromator	Jarrell-Ash 82-410
	Pico Ammeter	Keithley M-480
Response Speed	Pulse Diode Laser (110 ps)	
	Sampling Scope (25 ps)	Tektronix 7S-12/S-4
	Spectrum Analyzer	HP 8559A/853A
	Step Recovery Diode (100 MHz)	HP 33002B
	OSSM Connector	Omni Spectra OSSM-40
	Coaxial Bias Tee	PS Pulse Lab. 5575A
		HP 8717B/HP 11612A
	MicroStrip Line	
	Microwave test Fixture	
Noise	Noise Figure Meter	HP 8970A

CHAPTER THREE

FORMATION OF SCHOTTKY BARRIER AND OHMIC CONTACT ON III-V COMPOUND SEMICONDUCTORS

3.1. Introduction

The Schottky barrier contacts are used in many high-speed III-V compound semiconductor electronic and optoelectronic devices such as MESFETs, MODFETs, photodetectors, LEDs, and lasers. $In_{0.53}Ga_{0.47}As$ is most suitable for high frequency optical fiber communications in the 1.30-1.55 um wavelength regime because of its energy bandgap (i.e., 0.75 eV), high electron mobility, high saturation velocity, and lattice-match to the InP substrate [35.36]. However, the technology of InGaAs(P)/InP material and device systems is still in need of considerable development. The main reason for this is due to the difficulty of achieving a sufficiently high Schottky barrier necessary for the development of a practical MESFET technology and the lack of a suitable dielectric insulating layer with a low interface state density required for the development of a practical MISFET technology.

Schottky barrier height enhancement is a promising compromise between the MESFET's and MISFET's technology even though more study is needed to have a good reproducibility. On the other hand, Schottky barrier contacts on a moderate doped p-type InGaAs and InP can provide good barrier heights (i.e., $\Phi_{Bp} = 0.76$ eV for InP and 0.55 eV for $In_{0.53}Ga_{0.47}As$). For III-V compound semiconductors the electrical properties of Schottky contacts depend strongly on the Fermi level pinning, which results when metal is deposited on the semiconductor surface [56]. The reproducibility and reliability for the ohmic contacts still need to be developed although low ohmic contact resistance is essential for most III-V compound semiconductor devices. New studies on the ohmic contacts have been reported recently because of the needs for good ohmic contacts on III-V compound semiconductor devices and the availability of more sophisticated high vacuum surface analytical instruments required to understand the metallurgical properties of the ohmic contacts.

In this chapter the theory and fabrication of barrier-enhanced Schottky diodes with different thicknesses of p^+-$In_{0.53}Ga_{0.47}As$ surface layer on the n-$In_{0.53}Ga_{0.47}As$ epilayers grown by MBE on n^+-InP substrates are depicted. The significance of this structure lies in its ability to increase the barrier height and hence to reduce the large dark current commonly observed in the n-$In_{0.53}Ga_{0.47}As$ Schottky barrier diodes. The metal/p-InGaAs/p^+-InP as well as metal/p-InP/P^+-InP Schottky barrier diodes also have been fabricated and characterized in this research.

3.2. Schottky Barrier Height Enhancement

The barrier height of an ideal Schottky contact is determined primarily by the difference of metal work function and electron affinity of the semiconductor. However, for a practical Schottky diode the property of metal-semiconductor interface such as interface trap density plays an importment role in determining the effective barrier height of the Schottky contact. Since there are only limited numbers of metals which are suitable for good Schottky contact, the control of the Schottky barrier height is essential for specific electronic circuit application. A low barrier height makes the Schottky contact too leaky to be useful for MESFET and photodetector applications. Thus, the effective barrier height needs to be increased in order to overcome the problem associated with low Schottky barrier height.

Barrier height enhancement can be achieved by the use of (1) a thin insulating layer (i.e., MIS Schottky diode) [57,58], (2) an oppositely doped thin surface layer to that of an active layer (i.e., Barrier height-enhanced Schottky diode) [59-62], and (3) Schottky contact on wide-bandgap materials such as InP or AlInAs (i.e., Heterojunction Schottky diode) [63-65]. Effective barrier height for a MIS Schottky barrier structure, which consists of a thin interfacial insulating layer between metal and semiconductor, can be increased and resulted in a low reverse leakage current. However, high interface state density, oxide breakdown, and charge storage effects are some of the problems that need to be overcome in III-V semiconductor Schottky contacts [57,58]. Schottky barrier enhancement is a promising technique for formation of a Schottky contact on InGaAs/InP material system, which employs a very thin p-$In_{0.53}Ga_{0.47}As$ surface layer grown on the n-InGaAs epitaxial layer.

Schottky barrier contacts on n-$In_{0.53}Ga_{0.47}As$ usually yield very low barrier height (Φ_{Bn} = 0.2-0.3 eV), which makes Schottky contacts too leaky to be useful for photodetector applications. The barrier height enhancement can be achieved by depositing a thin p^+-$In_{0.53}Ga_{0.47}As$ layer on the n-$In_{0.53}Ga_{0.47}As$ epilayer as is shown in Fig.3.1. The effective barrier height can be increased by band bending due to the space charge in the p^+-$In_{0.53}Ga_{0.47}As$ surface layer provided that the dopant density and the thickness of the surface layer are selected to an optimum value and the layer is fully depleted at thermal equilibrium. The thickness and the dopant density of p^+-$In_{0.53}Ga_{0.47}As$ layer can be related to the effective barrier height, Φ'_{Bn} by:

$$\Phi_{Bn} = qN_A x_m^2/2\epsilon_o\epsilon_r \tag{3.1}$$

The enhanced barrier potential will reach a maximum value at $x = x_m$ inside the p^+-$In_{0.53}Ga_{0.47}As$ surface layer provided that $N_A W_p >> N_D W_n$.

$$x_m = (1/N_A)(N_A W_p - N_D W_n) \quad \text{and} \quad E_m = (q/\epsilon_o\epsilon_r)(N_A W_p - N_D W_n) \tag{3.2}$$

The effective barrier height Φ'_{Bn} obtained at $x = x_m$ is given by

$$\Phi'_{Bn} = \Phi_{Bn} + E_m x_m - qN_A x_m^2/2\epsilon_o\epsilon_r \tag{3.3}$$

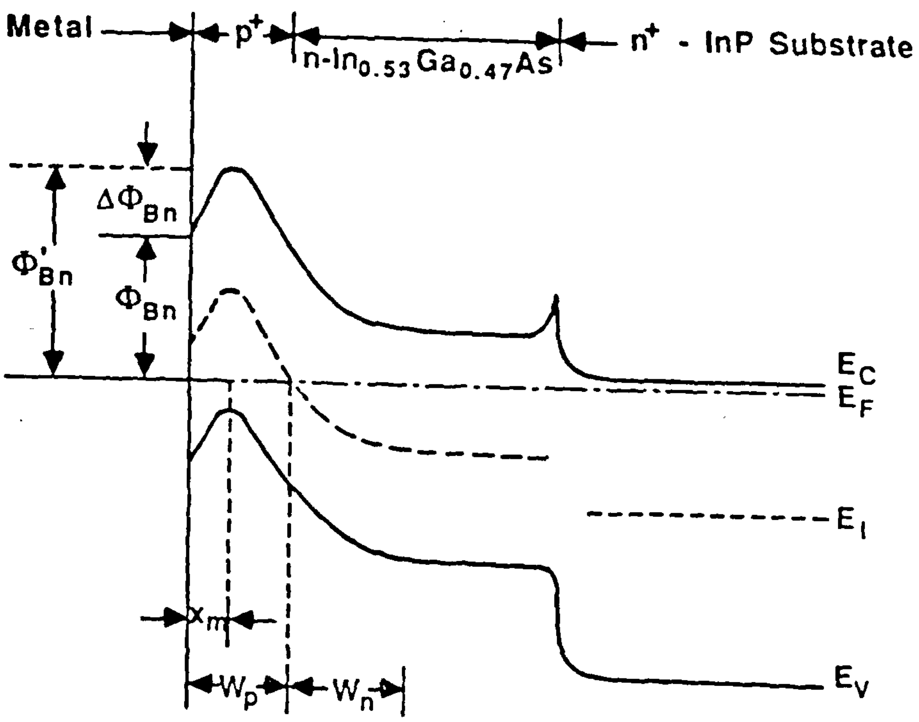
Metal
p^+
$n\text{-}In_{0.53}Ga_{0.47}As$
n^+ - InP Substrate
$\Delta\Phi_{Bn}$
Φ'_{Bn}
Φ_{Bn}
E_C
E_F
E_I
E_V
x_m
W_p
W_n

Fig. 3.1. Schottky Barrier Height Enhancement.

By substituting Eq.(3.2) into Eq.(3.3) the effective Schottky barrier height can be obtained.

$$\Phi'_{Bn} = \Phi_{Bn} + (q/2\epsilon_o\epsilon_r N_A)(N_A W_p - N_D W_n)^2 \quad (3.4)$$

For $N_A >> N_D$ and $N_A W_p >> N_D W_n$, the barrier height enhancement of a metal-p-n Schottky barrier diode, $\Delta\Phi_{Bn}$ due to the p surface layer may be simplified to

$$\Delta\Phi_{Bn} = qN_A W_p^2/2\epsilon_o\epsilon_r \quad (3.5)$$

It can be shown that Eq.(3.5) holds only for $\Delta\Phi_{Bn} >> V_D N_D/N_A$. Note that N_A and N_D denote the dopant density of the p^+- and n-$In_{0.53}Ga_{0.47}As$ layers, respectively. W_p is the thickness of the p^+-$In_{0.53}Ga_{0.47}As$ layer, and V_D is the built-in potential of the p^+-n junction. Therefore, the effective barrier height will increase as the product $N_A W_p$ increases. The thickness and dopant density of the p^+-$In_{0.53}Ga_{0.47}As$ surface layer should be determined in order to satisfy the condition of $\Delta\Phi_{Bn} >> V_D N_D/N_A$. The depletion layer width of the n-InGaAs epilayer is given by

$$W_n = - W_p + [W_p^2 + (N_A/N_D)W_p^2 + 2\epsilon_o\epsilon_r(\Phi_m - \Phi_n - V)/qN_D]^{1/2} \quad (3.6)$$

where $\Phi_n = X_s + (kT/q)\ln(N_c/N_D)$ (3.7)

The effective barrier height for the proposed photodetector can be tailored to its optimum value via properly selected thickness and dopant density of the surface layer. Theoretically the effective barrier height equal to the bandgap energy of $In_{0.53}Ga_{0.47}As$ can be achieved by the proposed structure. Figure 3.2. shows the effective barrier height vs. dopant density as a function of the thickness of p^+-$In_{0.53}Ga_{0.47}As$ surface layer. Figure 3.3. shows the theoretical saturation current density of the Schottky barrier diode on n-InGaAs. The effective barrier height Φ'_{Bn} of the Schottky barrier diode can be determined

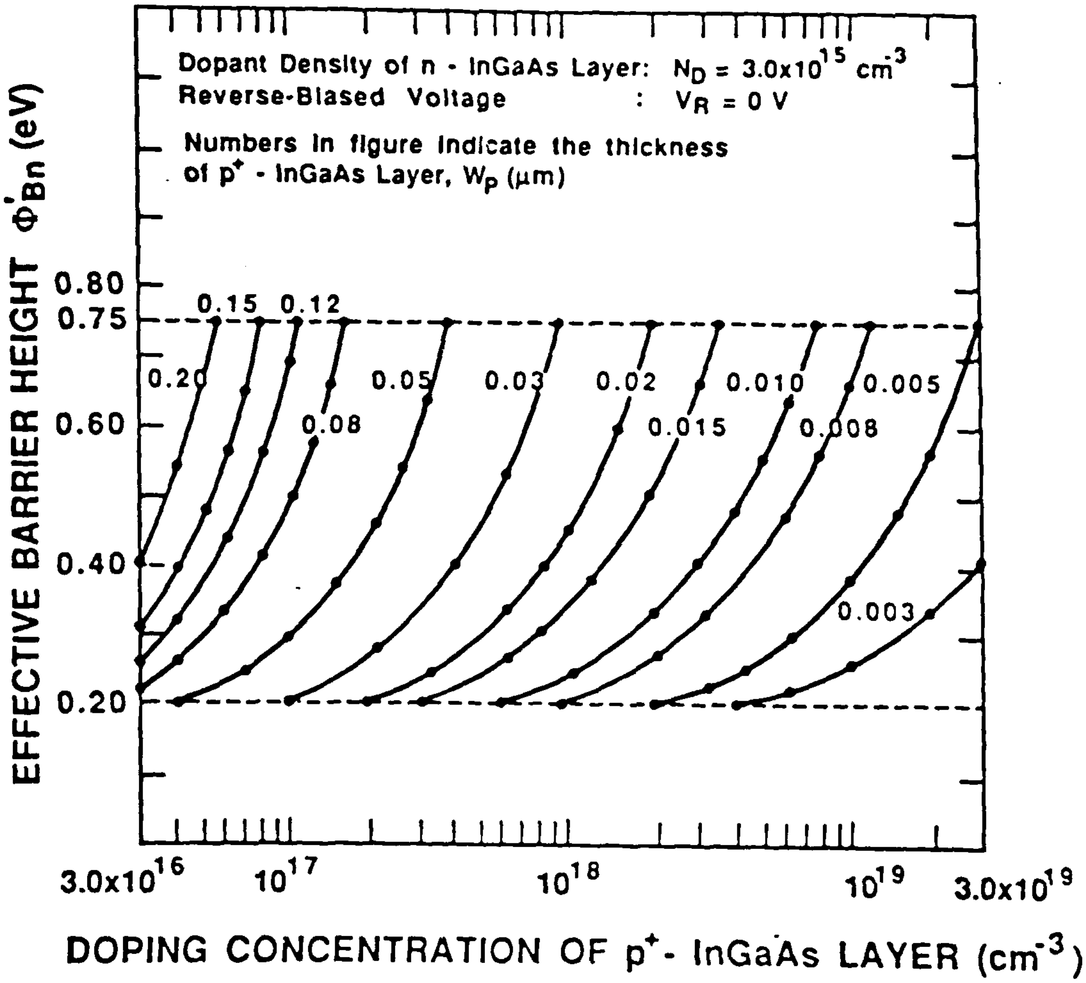

Fig. 3.2. Theoretical Effective Barrier Height vs. dopant density of the surface layer.

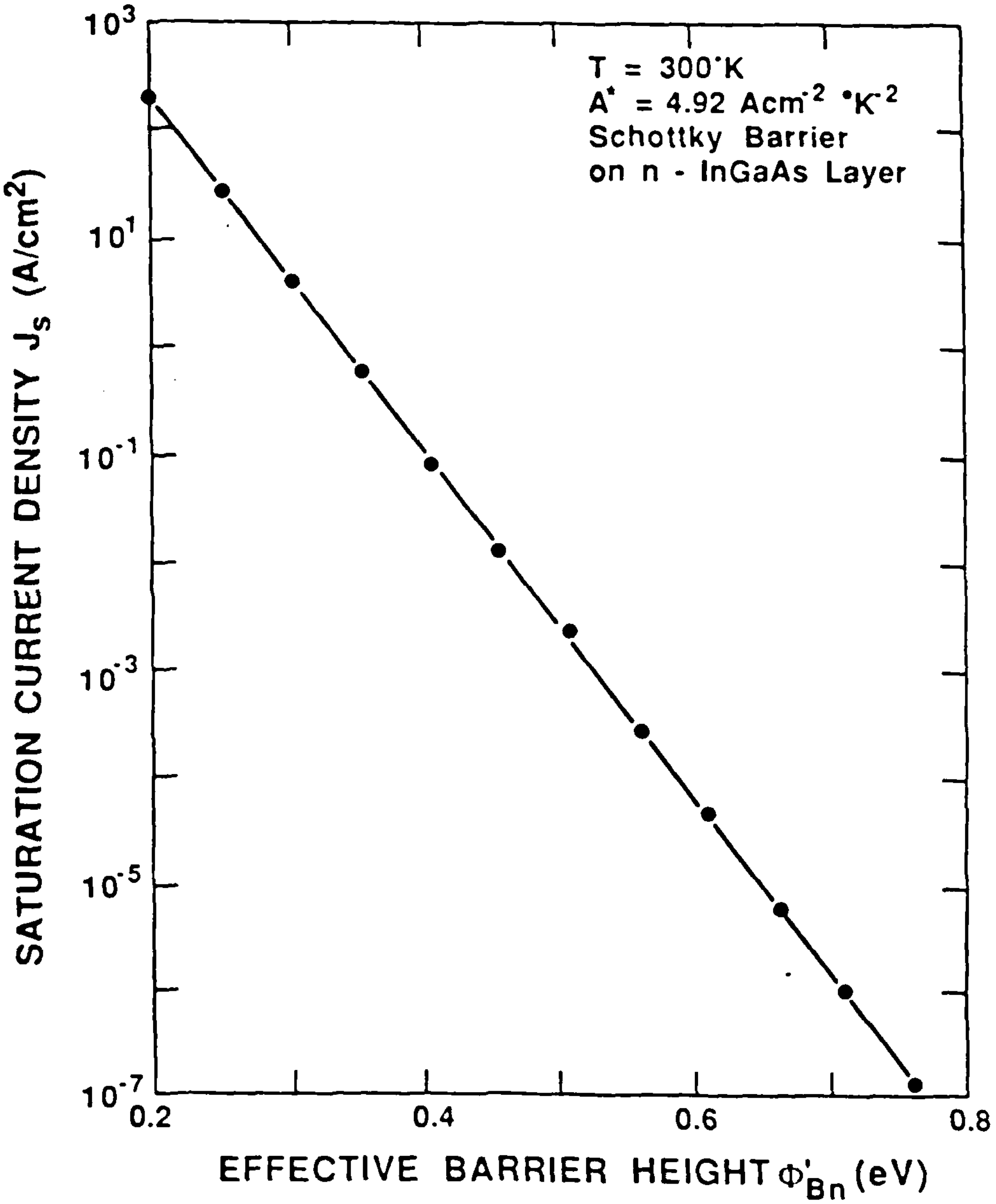

Fig. 3.3. Theoretical Saturation Current Density vs. Effective Barrier Height.

$$\Phi'_{Bn}{}^{I-V} = (kT/q)\ln(A^{*}T^{2}/J_{s}) \qquad (3.8)$$

$$\Phi'_{Bn}{}^{C-V} = V_{D} + (kT/q)\ln(N_{C}/N_{D}) \qquad (3.9)$$

$$\Phi'_{Bn}{}^{I-T} = -kT\ln(J/A^{*}T^{2}) \qquad (3.10)$$

$$\Phi'_{Bn}{}^{I-E} = hv - kT(J/A^{*}T^{2}) \qquad (3.11)$$

where A^{*} ($= 4\pi qm^{*}k^{2}/h^{3}$) is the effective Richardson constant for the thermionic-emission neglecting the effects of optical phonon scattering, quantum mechanical reflection, and tunneling of carriers at the metal-semiconductor interface, and J_s is the reverse saturation current density.

3.3. Ohmic Contact Formation

A practical way to obtain low resistance ohmic contacts [66-69] is to increase the dopant density near the metal-semiconductor interface ($N_D > 10^{19}$ cm^{-3}) so that the depletion layer caused by Schottky barrier becomes very thin and the current transport through the barrier is enhanced by tunneling. Nearly all methods of making ohmic contacts depend on depositing a thin layer of metal alloy on a relatively oxide-free clean semiconductor surface and on heat treatment during or after deposition in vacuum or in an inert atmosphere. Generally, it is preferred that the metal deposited on semiconductor should be heat treated at a temperature higher than the alloying temperature because a heavily doped contact layer is often formed between metal and semiconductor during the cooling cycle.

The selection of metals for ohmic contact to a particular III-V compound semiconductor depends on several factors [45,67]. The primary factor is that the metal used for contact should be such an element that it can be acted as a dopant to the semiconductor so that a heavily doped surface layer can be formed. For example, the possible materials are Si, Ge, Sn, Se, or Te for contacts on n-type semiconductors and Zn, Cd, Be, or Mg for contacts on p-type semiconductors. In addition to this factor, there are a number of other factors that need to be considered before selecting a particular contact metal: (1) easy deposition, (2) good adhesion, (3) low alloying temperature, (4) minimum interface reaction, (5) minimum thermal mismatch, (6) no surface tension effects during alloying, (7) good electrical and thermal behavior, and (8) adaptability to thermo-compression or ultrasonic wire bonding. The most widely used metal for ohmic contact on III-V compound semiconductors are Au, Ag, or In base alloys. The final factor for choosing a particular metal system is the eutectic temperature of the alloy metal (i.e., Au, Ag, or In) with the semiconductor and its correlation to the temperature for which the semiconductor can be safely heated. After suitable choice of contact metal, an appropriate technique has to be selected for depositing the contact metal system onto the semiconductor surface. A number of techniques, e.g., evaporation, sputtering, and electrolytic or electroless plating in a chemical solution have been reported for this purpose.

The evaporation technique is by far the most widely used for the deposition of contact metal systems on III-V compound semiconductors. Sputtering technique has rarely been used for depositing the contact metal system on III-V compound semiconductors because of low sputtering rates, surface damage, and difficulty in accurate monitoring of the metal film thickness [45,67]. The electroless plating technique has been frequently used for depositing overlayers of Au, Ni, etc., on ohmic contacts as well as Schottky contacts. Such overlayers are required for bonding thin wires with contact metal systems without any change in the properties of the contacts. The wire bonding is usually carried out by either the thermocompression or the ultrasonic bonding technique.

Finally, the requirement of a buffer layer (e.g., n^+-layer on n-type semiconductor) between the contact metal system and semiconductor in order to ensure good ohmic contact can also be satisfied by using epitaxial technique. Recently, the molecular beam epitaxial (MBE) technique has been used for growing such buffer layers. Ion implantation also promises to be a desirable alternative to the epitaxial technique for obtaining submicron layers without introducing any undesirable interface states. However, thermal annealing is usually required after ion implantation to remove damages and crystal defects. The annealing can be carried out by using thermal, laser, or electron beam annealing. Therefore, it can be predicted that ion implantation (for producing a buffer layer) followed by evaporation (for depositing the contact metal system) may be a good combination method for making good reproducible ohmic contacts on III-V compound semiconductors.

3.4. Device Fabrication

3.4.1. Schottky Gate Formation

The Au/p^+-n-$In_{0.53}Ga_{0.47}As$/n^+-InP and Au/p-$In_{0.53}Ga_{0.47}As$/p^+-InP Schottky barrier diodes have been fabricated as is shown in Fig.3.4. using a standard lift-off process [70-73] in this research project. A lift-off photolithography gives an excellent resolution available with positive photoresist and avoids incompatability problem of many metal etchants with InP in a two-metal system [45]. The p^+-n-$In_{0.53}Ga_{0.47}As$ epitaxial layers were grown on n^+-InP substrates by MBE technique. The thicknesses of the p^+-$In_{0.53}Ga_{0.47}As$ epilayer were chosen to be 0.03 um - 0.15 um with corresponding dopant densities of 5.5×10^{16} - 9.0×10^{17} cm^{-3}, and the thickness of an n-$In_{0.53}Ga_{0.47}As$ and p-$In_{0.53}Ga_{0.47}As$ epilayer with a dopant density of 3.0×10^{15} cm^{-3} is 1.5 um. A 100 Å gold film was deposited on the p^+-$In_{0.53}Ga_{0.47}As$ layer at a deposit rate of 2 Å/sec and at a pressure of 5.0×10^{-7} Torr for the transparent Schottky contact and Cr/Au (60/1,000 Å) was deposited for the bonding pad. The Cr provides contact adhesion to the semiconductor and Au reduces the contact resistance and provides

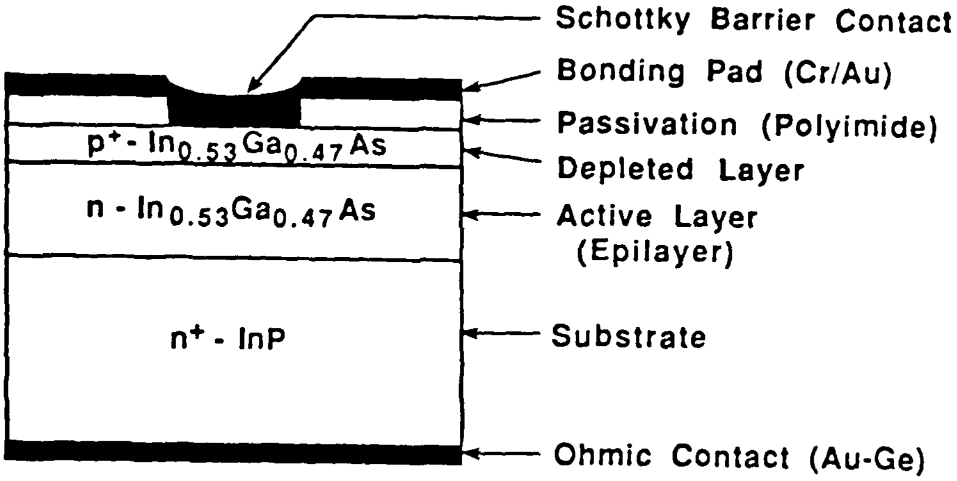
Schottky Barrier Contact
Bonding Pad (Cr/Au)
Passivation (Polyimide)
p^+ - $In_{0.53}Ga_{0.47}As$
Depleted Layer
n - $In_{0.53}Ga_{0.47}As$
Active Layer (Epilayer)
n^+ - InP
Substrate
Ohmic Contact (Au-Ge)

Fig. 3.4. Structure of p^+-n-InGaAs/n^+-InP Schottky Barrier Diode.

a surface suitable for bonding or probing. Just before evaporation, a wet chemical etching was performed to remove native oxides from surface of the contact area. Wafers are dipped in buffered HF ($HF:H_2O$ = 1:5) or etching solution ($NH_4OH:H_2O_2:H_2O$ = 20:7:100).

For p-InP/p^+-InP Schottky barrier diode shown in Fig.3.5. the (100) oriented Zn-doped InP substrates with a dopant density of $N_A = 5.0\text{x}10^{18}$ cm^{-3} were used. The p-InP epitaxial layer with doping concentration of N_A = 1.0-$2.0\text{x}10^{17}$ cm^{-3} was grown on p^+-InP substrate by Vapor Phase Epitaxy. Aluminum was used as the gate metal because of low resistivity and low work function. The contact has a circular shape with a diameter of 200-800 um, which gives a contact area of $3.0\text{x}10^{-4}$ to $5.0\text{x}10^{-3}$ cm^2.

3.4.2. Ohmic Contact Formation

We investigated the properties of the ohmic contact using several metal alloys at a different alloy temperature and alloy time to obtain the optimum ohmic contact condition. For this purpose the test ohmic contact pattern was fabricated as is shown Fig. 3.6. The optimum conditions are summarized in Table 3.1. The specific contact resistance was claculated for the vertical and the planar structure as is shown in Fig.3.7. and Fig.3.8., respectively. The specific contact resistance at a different alloy time is shown in Fig.3.9.

For the ohmic contact on n^+-InP, Au-Ge (88-12 %) alloy (1,500 Å) was deposited and alloyed at 400 °C for 30 sec in H_2-N_2 (5-95 %) forming gas ambient. Zn, Be, and Mg are usually incorporated in epitaxial InP layer as acceptors for the ohmic contact on p-InP. After cleaning wafer with TCE, acetone, methanol, and D.I. water followed by blowing dry with N_2, an ohmic contact was formed on the back surface of the p^+-InP substrate by depositing Au-Zn (84%-16%) metal alloy (1500 Å) in E-beam evaporator at a pressure of $7.0\text{x}10^{-7}$ Torr. The Au-Zn ohmic contact was annealed at 450 °C for 2 min in H_2-N_2 (10%-

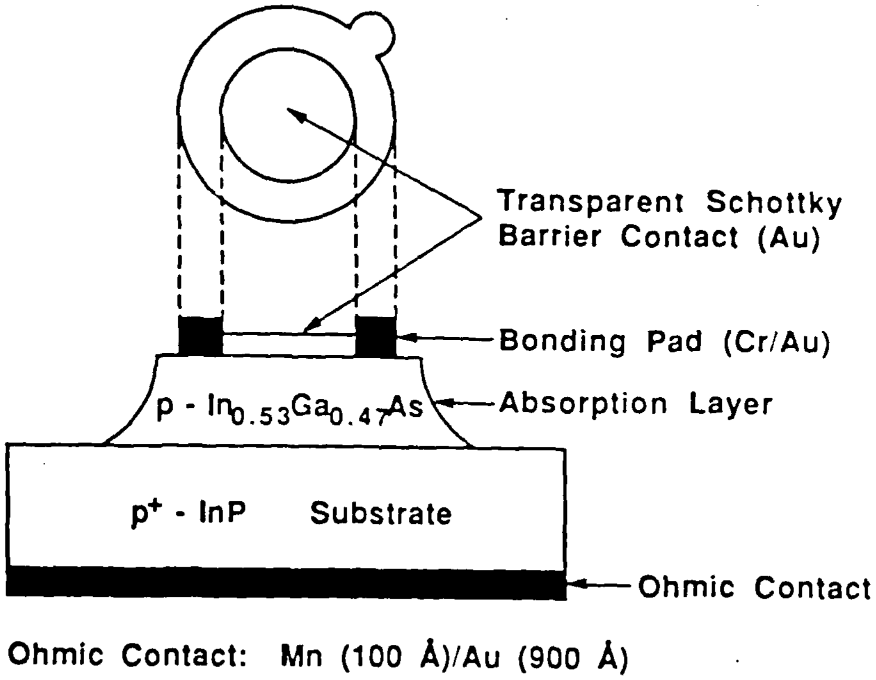
Transparent Schottky Barrier Contact (Au)
Bonding Pad (Cr/Au)
p - $In_{0.53}Ga_{0.47}As$
Absorption Layer
p^+ - InP Substrate
Ohmic Contact
Ohmic Contact: Mn (100 Å)/Au (900 Å)

Fig. 3.5. Structure of p-InGaAs/p^+-InP Schottky Barrier Diode.

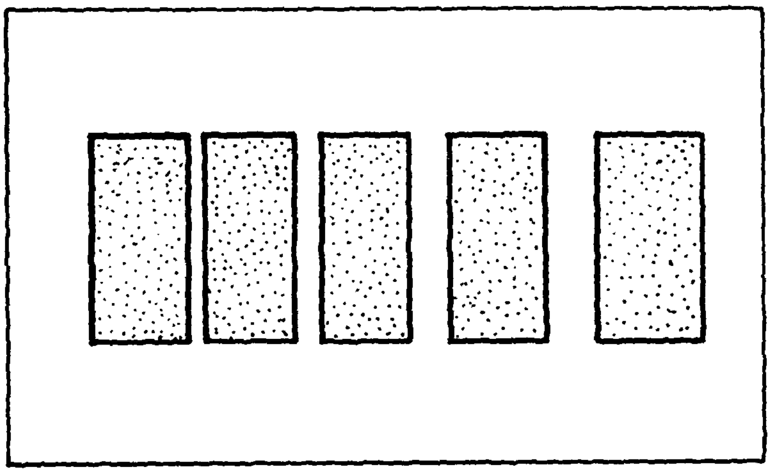

Contact Spacing : 10, 20, 30, 40 um
Contact Pad : 100 x 200 um
Ohmic Contact : Au-Ge/Ni/Au

Fig. 3.6. The pattern for the ohmic contact on n-type:
Au-Ge (1,200 Å)/Ni (300 Å)/Cr (400 Å)/Au (1,000 Å)

Table 3.1. Optimum Conditions for Ohmic Contact

Metal Alloy	Thickness (Å)	Alloy Time (sec)	Special Comment
Au-Ge	1,200	30 at 400 °C	Good Ohmic Bonding Problem
Au-Ge/Ni and/Cr/Au	1,200/350 /400/1,000	120 at 450 °C	Good Ohmic
Au-Ge/Ni/Au	1,200/500/1,000	90-120 at 450 °C	Good Ohmic
Au-Zn	1,500	30-45 at 400 °C	Contamination Adhesion Problem
Cr/Au-Zn/Au	50/500/1,500	60-90 at 450 °C	
Mn/Au	100/900	30 at 460 °C	Good Ohmic

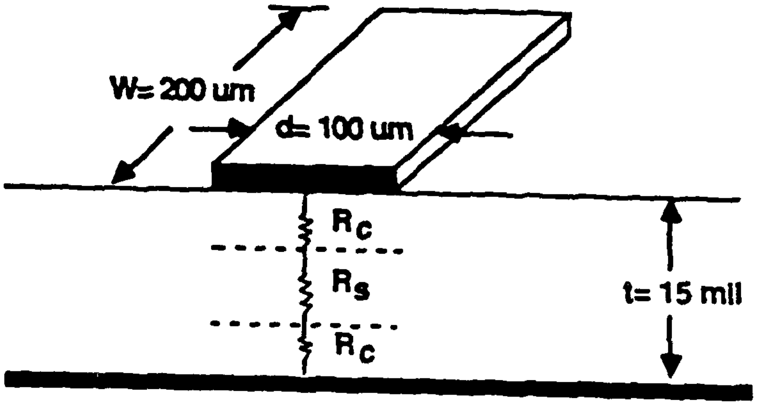
W= 200 um
d= 100 um
R_c
R_s
R_c
t= 15 mil

$R_{Test} = 2R_C + R_S = R_{Total} - R_{System} = 0.27\ [\Omega]$

$R_S = \rho t/Wd = (0.0013)\ (0.038)/(200)\ (100)\ (10^{-4}) = 0.248\ [\Omega]$

$R_C = 1/2\ (R_{Test} - R_S) = 1/2\ (0.27 - 0.248) = 0.011\ [\Omega]$

Thus,

$r_c = R_C Wd = (0.011)\ (200)\ (100)\ (10^{-8}) = 2.2 \times 10^{-6} [\Omega cm^2]$

Fig. 3.7. Specific Contact Resistance of Vertical Structure.

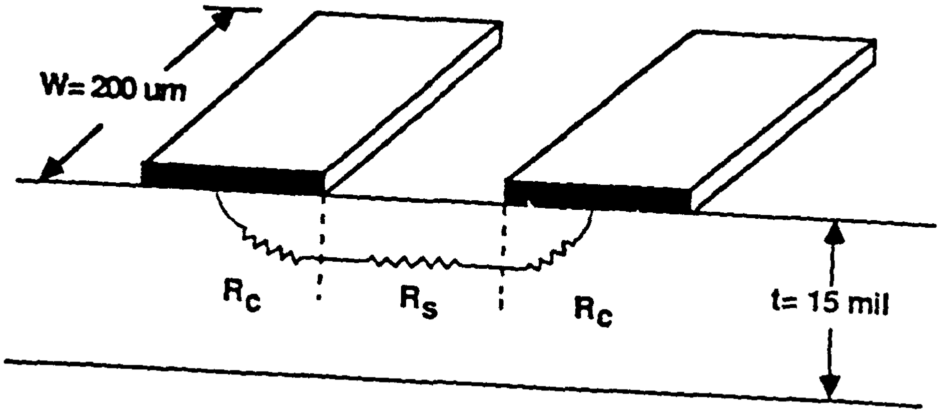
W= 200 um
R_c
R_s
R_c
t= 15 mil

$$R_c = R_{sc} L_t / W = 1/2\,(R_{Total} - R_{System}) = 1.2\ [\Omega]$$

$$R_{sc} = (1.2)\,(200)/1 = 240\ [\Omega] \text{ assuming } L_t = 1\ [\mu m]$$

Thus,

$$r_c = R_{sc} L_t^2 = (240)\,(1)^2 = 2.4 \times 10^{-6} [\Omega cm^2]$$

Fig. 3.8. Specific Contact Resistance of Planar Structure.

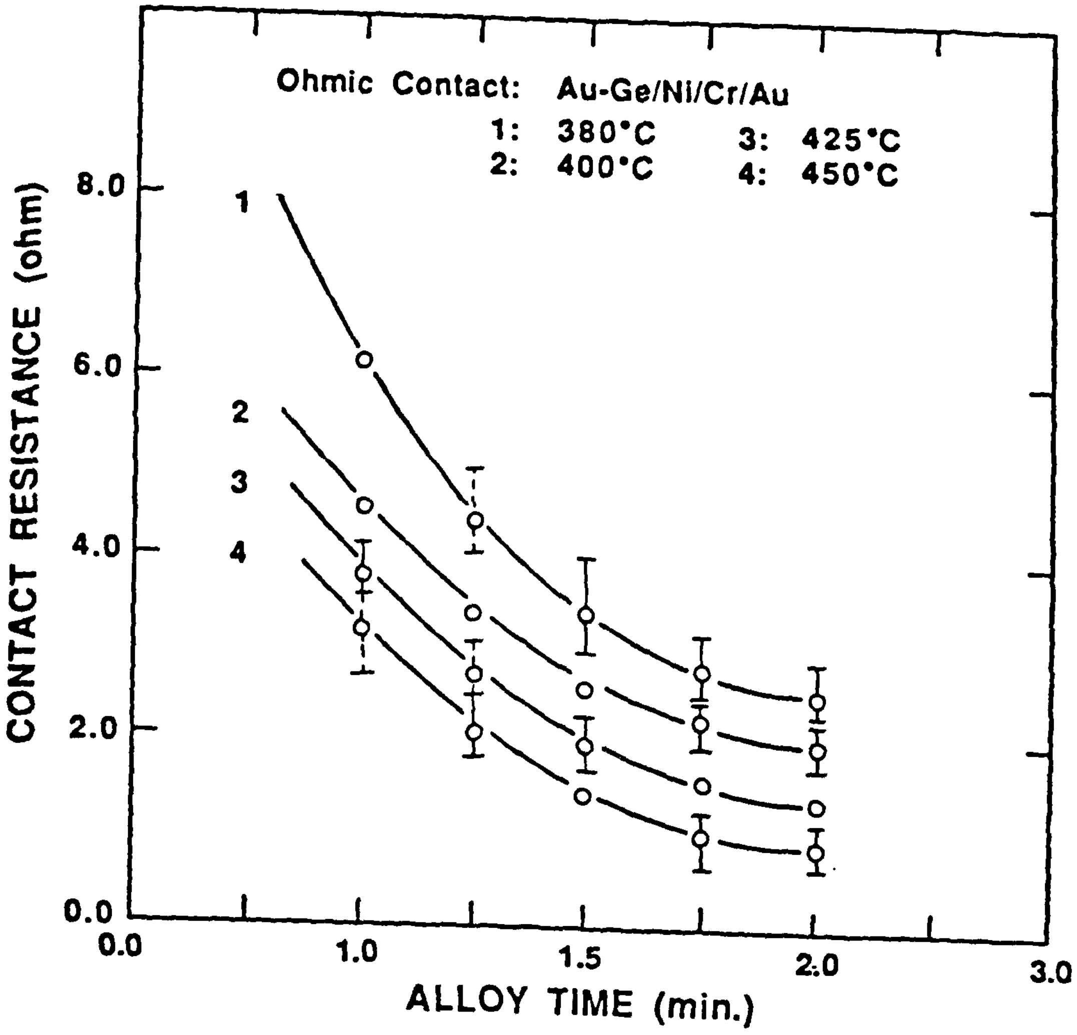

Fig. 3.9. Specific Contact Resistance at a Different Alloy Time.

90%) forming gas environment in alloy furnace. The adhesion of Zn on InP was not always good, some peeling off occured during the lift-off process [73].

3.5. Experimental Results and Discussion

The current-voltage (I-V) characteristics of Au/p^+-n-$In_{0.53}Ga_{0.47}As$/n^+-InP Schottky diode with a p-InGaAs layer of 1,500 and 500 Å thick show a large reverse leakage current as is shown in Fig. 3.10. and Fig.3.11., respectively. The reason for the large leakage current may be attributed partly to the surface leakage due to the poor surface morphology and partly to the existance of the thin neutral region between the p-Schottky barrier and the p-n junction, consisting of a Schottky barrier contact in series with a p-n junction diode due to a thick surface layer. However, the leakage current was greatly reduced in Schottky diodes with a p^+-InGaAs layer of 300 Å as is shown in Fig.3.12. The reverse leakage current depends strongly on the thickness of the p^+-$In_{0.53}Ga_{0.47}As$ surface layer. The reverse leakage current density is given by 5.0×10^{-3} A/cm^2 at $V_R = 1$ V. The effective barrier height of 0.52 eV is obtained by using $A^* = 4.92$ A/cm^2/K^2 for an electron effective mass of 0.041 m_o. The capacitance was found to be 0.3 pF at $V_R = 5$ V for Schottky barrier diode with a contact area of 2.0×10^{-5} cm^2. The effective barrier height, $\Phi'_{Bn}{}^{I-V} = 0.52$ eV and $\Phi'_{Bn}{}^{C-V} = 0.58$ eV is obtained, which indicates the barrier enhancement of approximately 0.35 eV.

Most of the p-InP/p^+-InP Schottky barrier diodes have a breakdown voltage of 15-20 V as is shown Fig. 3.13. The junction capacitance is C = 0.18 pF at $V_R = 0$ V and C = 0.16 pF at $V_R = 5$ V for an Al/p-InP/p^+-InP Schottky barrier diode with a contact area of 5.0×10^{-3} cm^2 as is shown in Fig.3.14. The background doping concentration determined from the slope of C^{-2} vs. V_R in Fig.3.15 is 1.4×10^{17} cm^{-3}. The built-in potential is obtained from the intercept of C^{-2}, i.e., $V_D = 0.65$ eV. Thus, the barrier height for metal/p-InP/p^+-InP Schottky

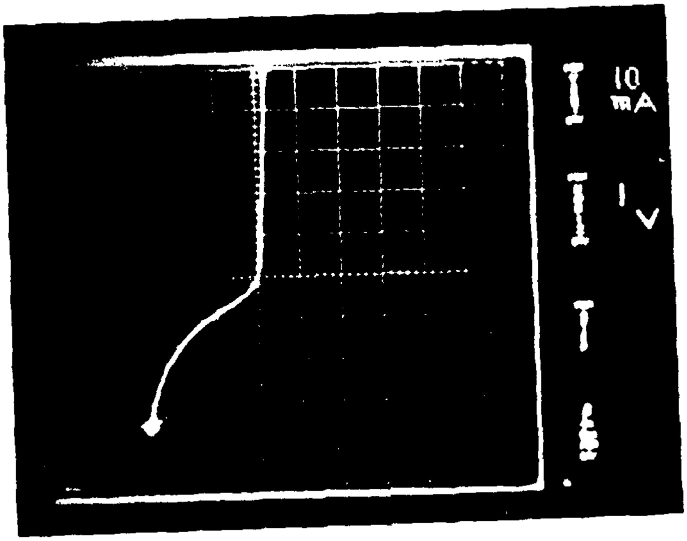

Fig. 3.10. Current-Voltage (I-V) Characteristics for Au/p^+-n-$In_{0.53}Ga_{0.47}As$/n^+-InP Schottky Barrier Photodiode.

Contact Area: 50 um diameter

p^+-$In_{0.53}Ga_{0.47}As$ layer: 1,500 Å

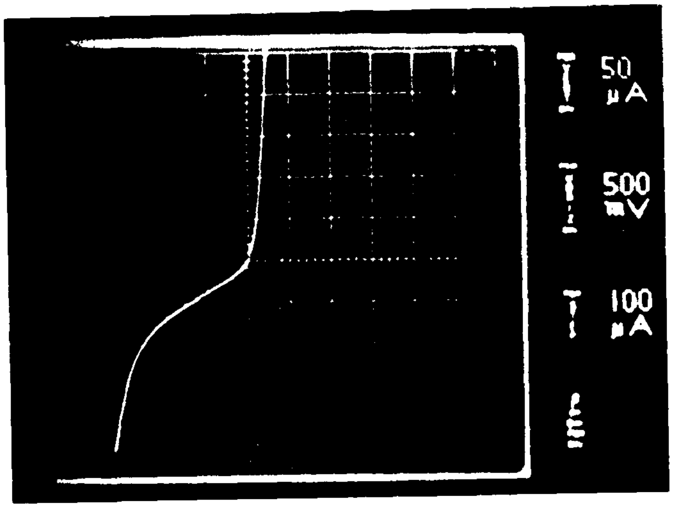

Fig. 3.11. Current-Voltage (I-V) Characteristics for Au/p$^+$-n-In$_{0.53}$Ga$_{0.47}$As/n$^+$-InP Schottky Barrier Photodiode.

Contact Area: 50 um diameter

p$^+$-In$_{0.53}$Ga$_{0.47}$As layer: 500 Å

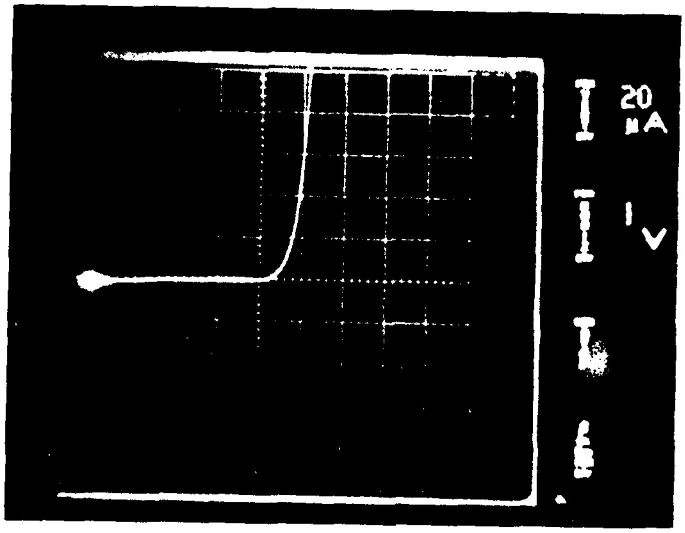

Fig.3.12. Current-Voltage (I-V) Characteristics for p^+-n-In$_{0.53}$Ga$_{0.47}$As/n$^+$-InP Schottky Barrier Photodiode.

Contact Area: 50 um diameter

p^+-In$_{0.53}$Ga$_{0.47}$As layer: 300 Å

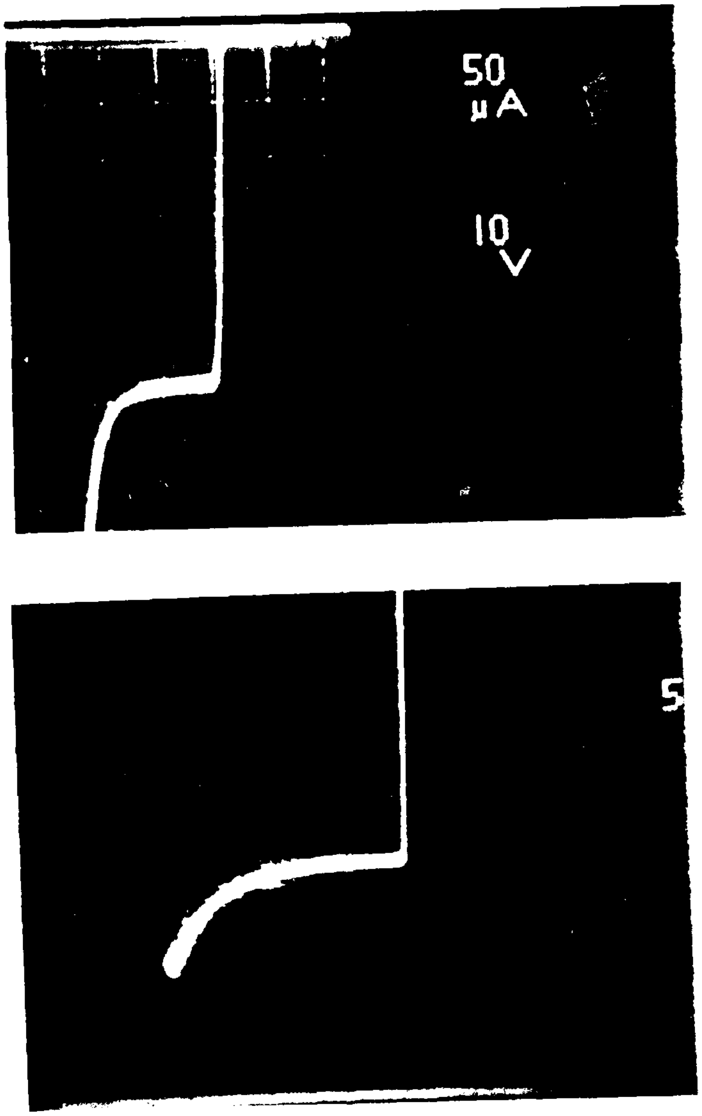

Fig. 3.13. Current vs. Voltage Characteristic Curve measured by Tektronix 576 Curve Tracer for Metal-p-InP Schottky Barrier Diode. (Breakdown Voltage V_{BR} = 15-20 V)

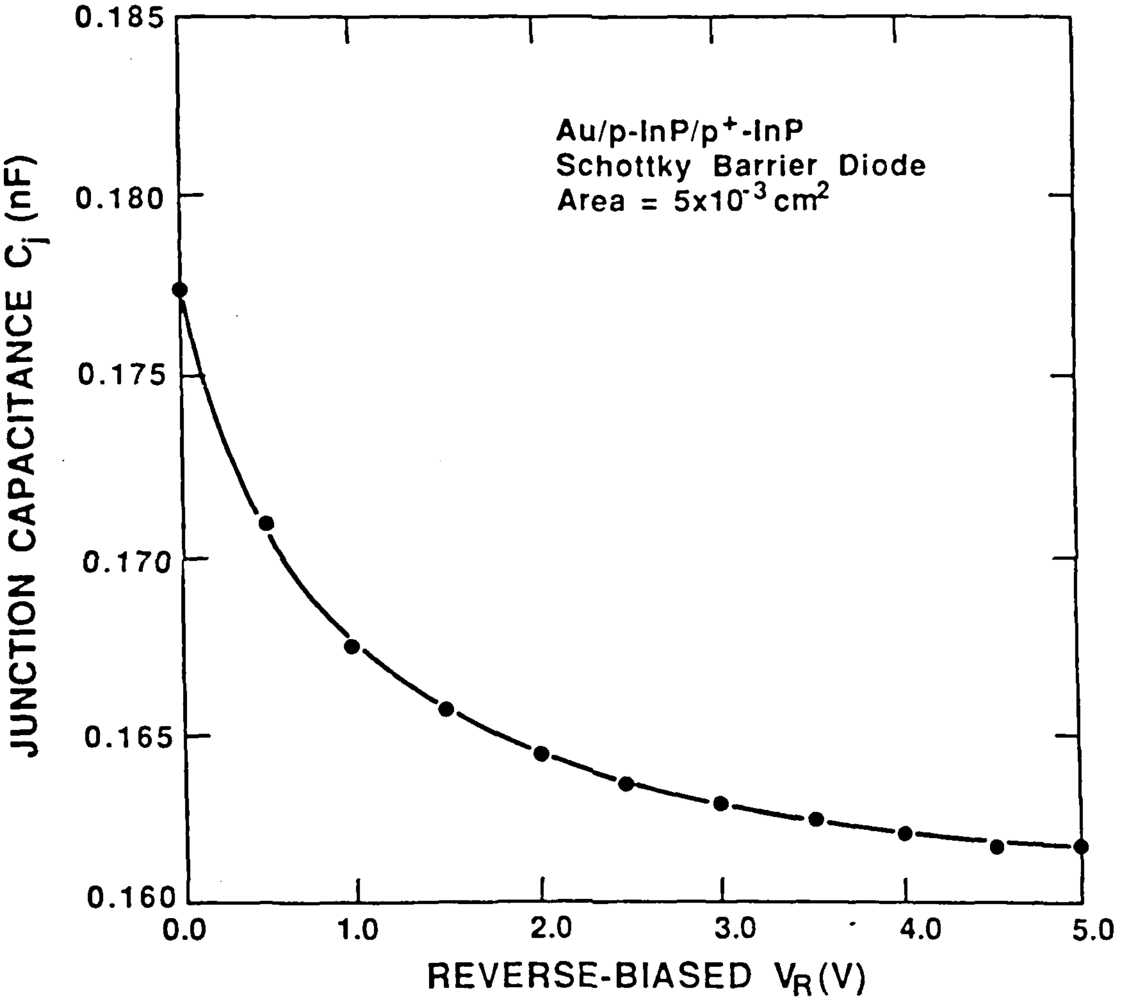

Fig. 3.14. Junction Capacitance of p-InP/p$^+$-InP Schottky Barrier Diode.

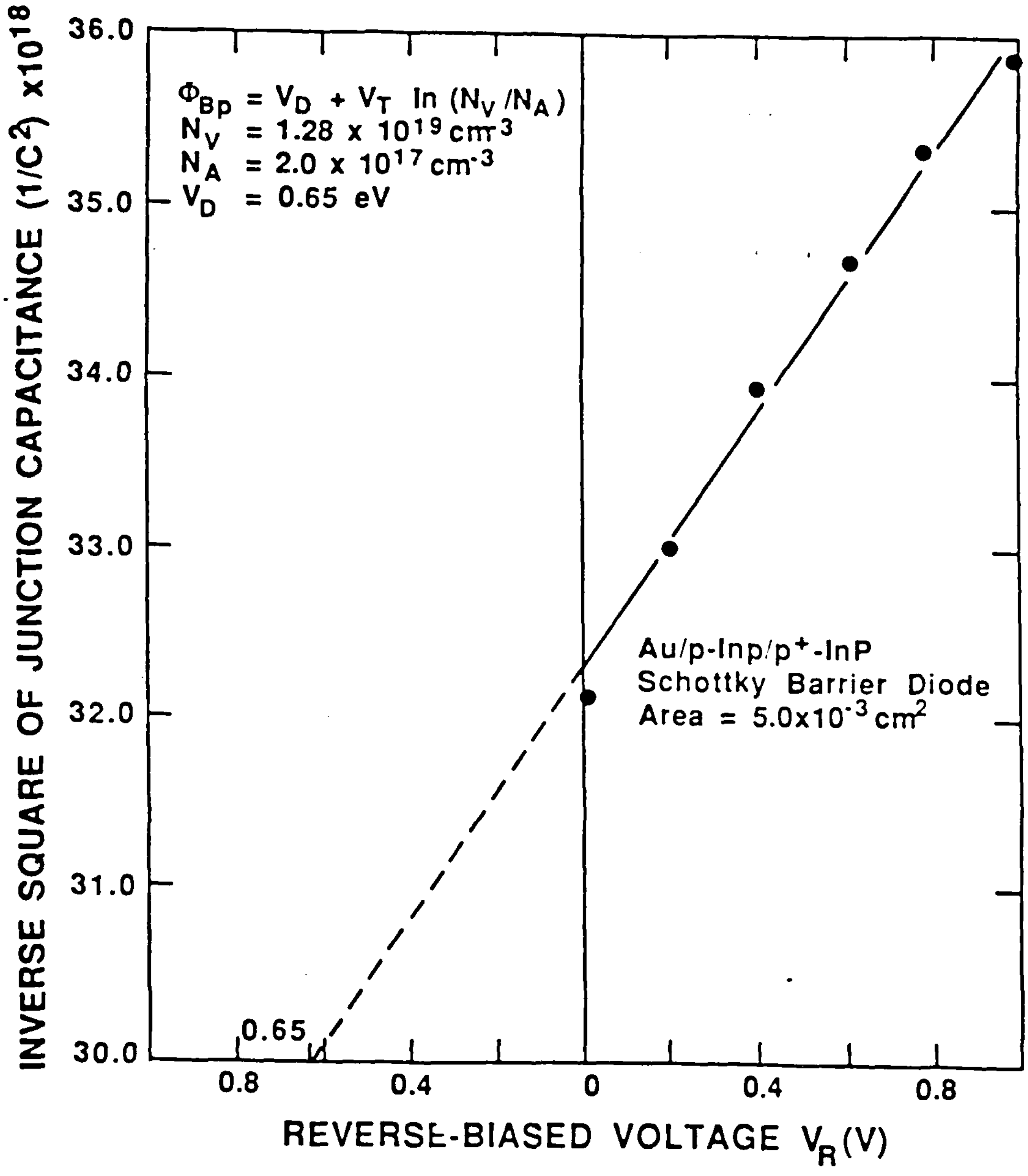

Fig. 3.15. Inverse Square of Junction Capacitance of p-InP/p$^+$-InP Schottky Barrier Diode.

barrier diode can be determined by Eq.(3.9), which shows $\Phi_{Bp} = 0.77$ eV. Recent measurement for Schottky barrier contact with Au or Al on n-InP has shown that $\Phi_{Bn} = 0.5 + 0.04$ eV independent of the metal. These results imply the barrier height for p-InP of $0.8 + 0.04$ eV.

3.6. Summary and Conclusions

The Au/p^+-n-$In_{0.53}Ga_{0.47}As$/n^+-InP Schottky barrier diodes with a different thickness of the p^+-InGaAs surface layer have been fabricated and characterized. The results show that our modified Schottky barrier diodes have the total capacitance of 0.3 pF, the series resistance of 11.8 ohm, and the effective barrier height of 0.52-0.58 eV. We have also fabricated Al/p-InP/p^+-InP Schottky barrier diode using a lift-off photolithographic process on p-InP epilayer grown by Vapor Phase Epitaxy (VPE). The direct measurement of the barrier height shows $\Phi_{Bp}{}^{C-V} = 0.77$ eV.

CHAPTER FOUR

DEVELOPMENT OF A HIGH-SPEED Au/p^+-n-$In_{0.53}Ga_{0.47}As$/n^+-InP SCHOTTKY BARRIER PHOTODETECTOR FOR 1.30-1.65 um PHOTODETECTION

4.1. Introduction

The high bit-rate fiber optic systems for long distance lightwave communication require the development of high-speed, high efficiency, and low noise photodetectors operating in the infrared regime, especially close to the dispersion minimum of the optical fibers. Most of high-speed photodetectors have been fabricated mainly on GaAs using Schottky barrier structure for 0.80 - 0.90 um and on $In_{0.53}Ga_{0.47}As$ for 1.30-1.65 um using p-i-n structure.

In this project, we have developed a novel metal/p^+-n-InGaAs/n^+-InP Schottky barrier photodetector operating in the 1.30-1.65 um infrared regime. The proposed metal/p^+-n-$In_{0.53}Ga_{0.47}As$/n^+-InP Schottky barrier photodiode structure requires the use of a very thin surface layer of p^+-$In_{0.53}Ga_{0.47}As$ on the n-$In_{0.53}Ga_{0.47}As$ epitaxial layer grown on n^+-InP substrate in order to enhance the effective barrier height. The significance of this new structure lies on its ability to increase the effective barrier height, and hence to overcome the problem of large dark current encountered in such a photodetector. This approach for barrier height enhancement has been demonstrated previously in GaAs [59] and InGaAs Schottky diodes [60-62], and is used in our Au/$In_{0.53}Ga_{0.47}As$/InP system for photodetector applications in the 1.30-1.55 infrared regime.

4.2. Theoretical Analysis

For a metal-p^+-n InGaAs Schottky barrier photodiode, there exists the region between $x = 0$ and $x = x_m$ where a retarding field tends to oppose the collection of the photogenerated carriers. For simplicity this region is assumed as a dead layer for the photogenerated carriers.

4.2.1. Quantum Efficiency

The two main components of the photocurrent come from the depletion region and the active region (i.e., the "base" of the Schottky barrier photodiode). The photogenerated excess carriers in the depletion region are swept out by the built-in electric field, resulting in a photocurrent for an incident monochromatic light.

$$J_d = q(1-R)\Phi[\exp(-aX_m)-\exp(-aW)] \qquad (4.1)$$

where a is the absorption coefficient, Φ is the incident photon flux density, R is reflection coefficient in the metal film, and W (= $W_p + W_n + X_m$) depletion region width, respectively. W_p is the thickness of p^+ region, which is fully depleted at thermal equilibrium, and W_n is the depletion layer width in the n region. Note that the reflection loss of the incident photons from metal surface is accounted for by the reflection coefficient, R.

The photocurrent due to holes collected from the n-type base region is given by

$$J_p = [qa\Phi(1-R)L_p/(a^2L_p{}^2-1)]e^{-aW}[aL_p$$

$$- \{\cosh(H'/L_p) - e^{-aH'}\}/\sinh(H'/L_p)] \qquad (4.2)$$

where H (= H' + W) is the epilayer thickness, and W is the depletion region width. The total photocurrent density is obtained from Eq.(4.1) and (4.2), which is given by

$$J_{ph} = q\Phi(1-R)[e^{-ax_m} - e^{-aW}] + [qa\Phi RL_p/(a^2L_p{}^2-1)]$$

$$e^{-aW}[aL_p - \{(\cosh(H'/L_p) - e^{-aH'}\}/\sinh(H'/L_p)] \qquad (4.3)$$

The quantum efficiency of a Schottky barrier photodiode is given by

$$\eta = (1-R)[e^{-ax_m} + e^{-aW}/(a^2L_p{}^2-1)$$

$$\{1-aL_p(\cosh(H'/L_p)- e^{-aH'})/\sinh(H'/L_p)\}] \qquad (4.4)$$

Eq.(4.4) will be reduced to Gartner's expression [74] for quantum efficiency if the device thickness is much greater than the diffusion length, i.e., $H' \gg L_p$.

$$\eta = (1-R)[e^{-ax_m} - e^{-aW}/(aL_p + 1)] \qquad (4.5)$$

The minimum reflection loss with a quarter wavelength anti-reflection (AR) coating is given by [75,76]:

$$R_{min} = (n_1{}^2-n_on_2/n_1{}^2+n_on_2)^2 \qquad (4.6)$$

where n_o, n_1, and n_2 are the index of refraction of air, AR coating film and semiconductor substrate, respectively. For example, $R_{min} = 0.0526$ at 1.3 um for $n_o = 1.00$ (air), $n_1 = 1.46$ (SiO_2), and $n_2 = 3.40$ (InGaAs). The quantum efficiency for a p^+-n-InGaAs/n^+-InP Schottky barrier photodiode is shown in Fig.4.1. as a parameter of the thickness of the p^+-InGaAs layer. For a single layer antireflection coating, the thickness of the dielectric film can be obtained from the well-known quarter wavelength formula given by:

$$d_1 = (\lambda_o/4\ n_1)\tan^{-1}[2n_1k_s/(n_1{}^2-n_s{}^2-k_s{}^2)] \qquad (4.7)$$

where λ_o is wavelength of incident light at peak intensity, n_1 is index of refraction of the dielectric film, and n_s is complex index of refraction of the semiconductor.

4.2.2. Response Speed

The response speed of a photodetector is determined primarily by the transit (drift) time in the depletion region, the diffusion time in the quasi-neutral base region, and the RC time constant required to discharge the junction

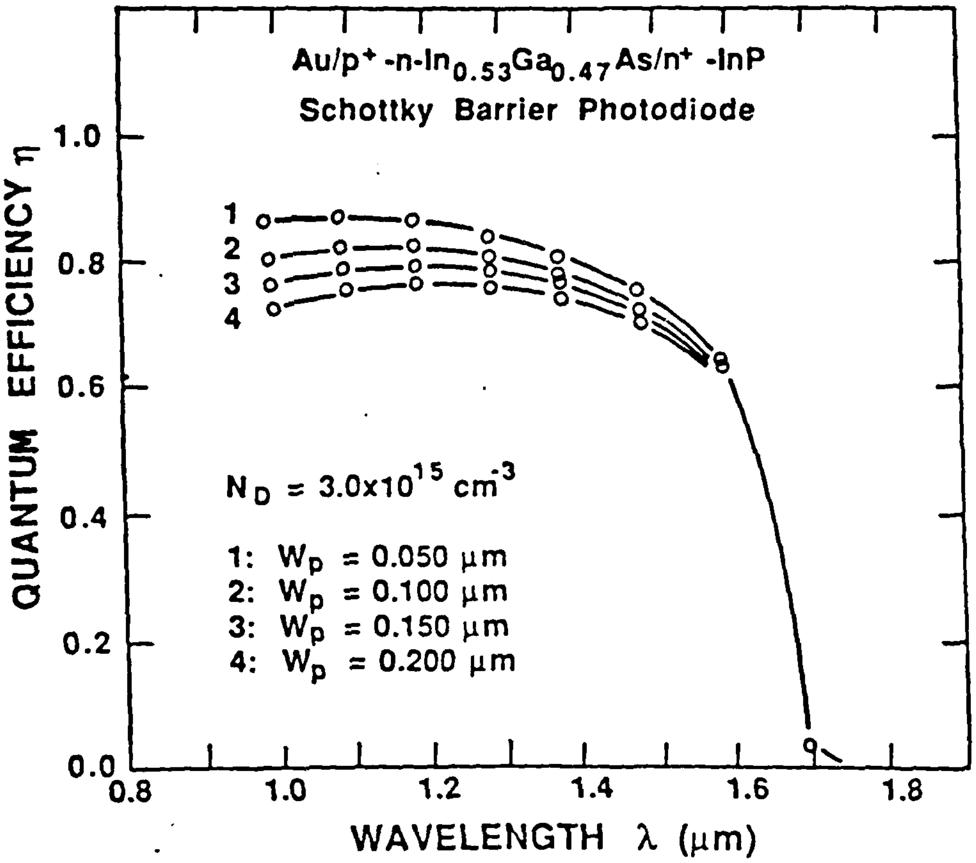

Fig. 4.1. Theoretical Quantum Efficiency of p$^+$-n-InGaAs/n$^+$-InP Schottky Barrier Photodiode.

capacitance (C_j) through a combination of internal and external resistances. The total risetime can be expressed by

$$t_r = (t_{tr}^2 + t_{diff}^2 + t_{RC}^2)^{1/2} \tag{4.8}$$

The drift time across the depletion layer is given by $t_{tr} = W/2.8\ v_s$, where v_s is the saturation drift velocity of the carriers. The diffusion time is given by $t_{diff} = W_p^2/(2.43\ D_n)$, if the thickness of the highly doped p^+-layer (W_p) is less than the carrier diffusion length (L_n). The RC time constant is given by $t_{RC} = (R_s + R_L)C_j$

The cutoff frequency is given by

$$f_c = 0.35/t_r \tag{4.9}$$

Assuming that the transit time and the diffusion time can be greatly reduced by optimizing the device configuration, the response speed is mainly determined by the junction capacitance (C_j), series resistance (R_s), and load resistance (R_L). The shunt resistance (R_i) is generally very high but is included to account for the relatively low leakage resistance of the photodiode. The series resistance (R_s) is composed of the lead resistance, the spreading resistance in the base material, and the sheet resistance of the thin epilayer. The sheet resistance term is the most important. This resistance is distributed, depending on the contact geometry, and is frequency dependent. Thus, the response speed can be estimated from RC time constant.

4.2.3. Dark Current

The dark current depends strongly on the barrier height of the photodiode while the photocurrent does not depend much on the barrier height. The total dark current for a Schottky barrier photodiode consists of: (1) thermionic-emission current, (2) recombination current via traps in the depletion region,

(3) tunneling current due to carriers tunneling across the bandgap, and (4) leakage current or interface current due to traps at the metal-semiconductor interface. Tunneling current can be neglected for low doping concentration (less than 10^{17} cm^{-3}). For a good diode with negligible surface leakage, the total current is composed of the thermionic-emission current over the Schottky barrier and the generation-recombination current in the depletion region.

For high mobility low doped (less than 10^{17} cm^{-3}) semiconductors the dark current density can be described by thermionic-emission theory.

$$J = A^{*}T^{2}\exp(-q\Phi_{Bn}/kT)[\exp(qV/nkT) - 1] \tag{4.10}$$

$$= J_{s}[\exp(qV/nkT) - 1] \tag{4.11}$$

The quantum-mechanical tunneling through the barrier may modify the ordinary thermionic-emission process. The current-voltage relation suitable for thermionic-field emission due to tunneling of excited carriers, which do not have sufficient energy for thermionic-emission, can be expressed by [69]:

$$J = J_{s}\{\exp(qV/kT) - \exp[(n^{-1} - 1)qV/kT]\} \tag{4.12}$$

When n equals unity Eq.(4.12) is reduced to Eq.(4.11). For $n > 2$, the Schottky contact conducts better under reverse bias because tunneling is the dominant mechanism. At zero bias the depletion region of the Schottky barrier is in thermal equilibrium and the rate of electron-hole pair generation is balanced by the rate of recombination. In the presence of an applied voltage, there will be a net generation or recombination of carriers depending on the polarity of the applied bias. The generation-recombination current J_{g-r} through the midgap traps in the depletion region is given by

$$J_{g-r} = J_{ro}[\exp(qV/2kT) - 1] \tag{4.13}$$

where $J_{ro} = qn_i W/2t_o$ and $t_o = (t_n t_p)^{1/2}$ is the minority carrier lifetime in the depletion region. This current is added to the thermionic-emission current and may cause deviation from ideal behavior (i.e., n = 1) in Schottky barrier diodes. The recombination current is important in high barrier, in low lifetime material, at low temperature, and at low forward bias voltage.

4.3. Device Fabrication

A high-speed Au/p^+-n-$In_{0.53}Ga_{0.47}As/n^+$-InP Schottky barrier photodiode has been fabricated using a lift-off photolithography process. The structure of the proposed InGaAs Schottky barrier photodiode is shown in Fig.4.2. The p^+-n-$In_{0.53}Ga_{0.47}As$ epitaxial layers were grown on n^+-InP substrates by MBE. The thickness of the p^+-$In_{0.53}Ga_{0.47}As$ epilayer is 0.03 - 0.15 um with a corresponding dopant density of 5.5×10^{16} - 9.0×10^{17} cm^{-3}, and the thickness of n-$In_{0.53}Ga_{0.47}As$ epilayer is 1.5-2.0 um with a dopant density of 3.0×10^{15} cm^{-3}. A 100 Å gold film was deposited on the p^+-$In_{0.53}Ga_{0.47}As$ layer at a deposit rate of 2 Å/sec and at a pressure of 5.0×10^{-7} Torr for a transparent Schottky contact and Cr/Au (60/1,000 Å) was deposited for the bonding pad. The Cr provides contact adhesion to the semiconductor, and Au reduces the contact resistance as well as providing contact area for bonding or probing.

Just prior to evaporation, a wet chemical etching was performed to remove native oxide from surface of the contact area. Wafers are dipped in buffered HF ($HF:H_2O$ = 1:5) or etching solution ($NH_4OH:H_2O_2:H_2O$ = 20:7:100). For ohmic contact on n^+-InP, Au-Ge (88-12 %) alloy (1,500 Å) was deposited and alloyed at 400 °C for 30 sec in H_2-N_2 (5-95 %) forming gas. For mesa etch, $H_2SO_4:H_2O_2:H_2$ = 3:1:1 was used for the $In_{0.53}Ga_{0.47}As$ epilayer with an etch rate of 0.1 um/sec at T = 300 K. For device characterization, the photodiodes were mounted on a 50-ohm microstrip transmission line fabricated on the Cr-Au metallized alumina (Al_2O_3) substrate [8].

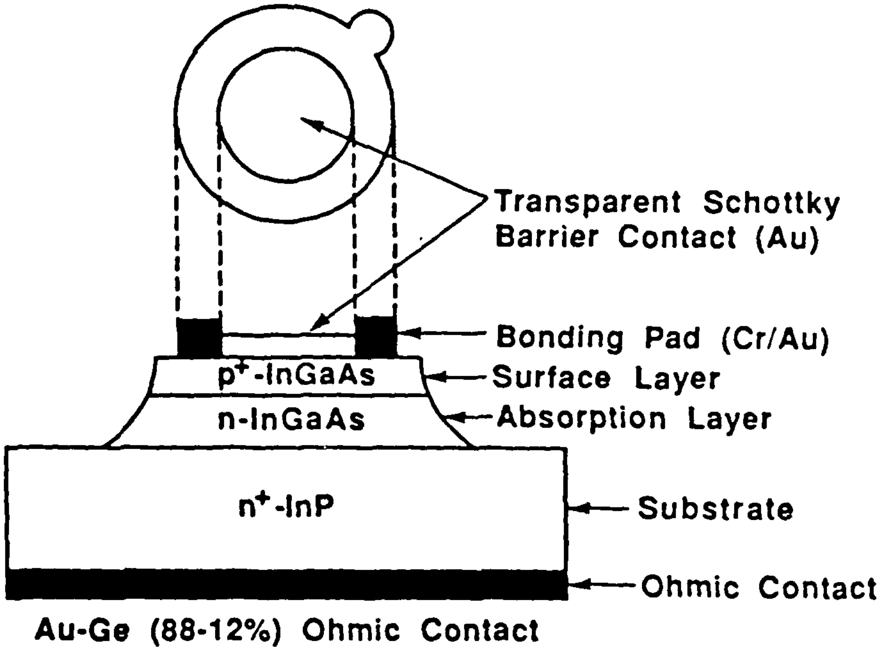
Transparent Schottky Barrier Contact (Au)
Bonding Pad (Cr/Au)
p+-InGaAs
Surface Layer
n-InGaAs
Absorption Layer
n+-InP
Substrate
Ohmic Contact
Au-Ge (88-12%) Ohmic Contact

Fig. 4.2. Structure of p^+-n-InGaAs/n^+-InP Schottky Barrier Photodiode.

4.4. Experimental Results and Discussion

4.4.1. Current-Voltage (I-V) Measurement

The current-voltage characteristics show that the breakdown voltages for our devices are mostly around 5-8 V. The dark current was measured by using HP 4140B pA meter controlled by HP 9845B computer. The current-voltage (I-V) characteristics of the Au/p^+-n-$In_{0.53}Ga_{0.47}As$/n^+-InP Schottky diode with a p-InGaAs layer of 1,500 Å thick show a large reverse leakage current. However, the leakage current is greatly reduced in a Schottky diode with a p^+-InGaAs layer of 300 Å as was shown in Fig.3.12. The results show that the reverse leakage current depends strongly on the thickness of the p^+-InGaAs surface layer. The reverse leakage current density is given by 5.0×10^{-3} A/cm^2 at $V_R = 1$ V.

4.4.2. Capacitance-Voltage (C-V) Measurement

The junction capacitance of the photodiode was measured accurately by using HP 4280A C-Meter/C-V Plotter. The result shows that the total capacitance is $C_j = 0.2$-0.3 pF at $V_R = 5$ V for the Au/p^+-n-$In_{0.53}Ga_{0.47}As$/n^+-InP Schottky diode with the contact area of 3.0×10^{-6} cm^2. This shows that our photodiodes were well designed for high speed operation.

4.4.3. A.C. Admittance Measurement

The frequency-dependent a.c. admittance measurement [77] is commonly used to determine the circuit elements of a Schottky barrier diode; series resistance (R_s), shunt resistance (R_p), and junction capacitance (C_j). From a plot of the Im{Y(W)} vs. Re{Y(W)}, the series resistance of the diode can be determined.

$$Y(w) = \frac{R_s + R_p/[1+(wR_pC_j)^2]}{\{R_s + R_p/[1+(wR_pC_j)^2]\}^2 + \{wR_p{}^2C_j/[1+(wR_pC_j)^2]\}^2}$$

$$+ j\,\frac{wR_p{}^2C_j/[1+(wR_pC_j)^2]}{\{R_s + R_p/[1+(wR_pC_j)^2]\}^2 + \{wR_p{}^2C_j/[1+(wR_pC_j)^2]\}^2} \qquad (4.14)$$

In the low frequency limit (w->0), $Re\{Y(w)\} = 1/(R_s + R_p)$ and in the high frequency limit (w->oo), $Re\{Y(w)\} = 1/R_s$. By measuring the frequency dependent conductance and susceptance component of a Schottky barrier diode in the frequency range of 20 to 575 MHz using a HP 4191A RF impedance analyzer, the series resistance and shunt resistance of the diode can be determined. The junction capacitance can be calculated from the measured values; $Z_1 = R_s + R_p/[1+(wR_pC_j)^2]$ or $Z_2 = wR_p{}^2C_j/[1+(wR_pC_j)^2]$ for a given frequency. This allows accurate determination of the R_s, R_p, and C_j over a wide range of frequency. From the plot of Im{Y(W)} vs. Re{Y(W)} is shown in Fig. 4.3., the series resistance was found to be 11.8 ohm for p^+-n-$In_{0.53}Ga_{0.47}As$ Schottky barrier photodiode.

4.4.4. Spectral Response Measurement

The spectral response was measured by using a Jarrell-Ash 82-410 quarter-meter Monochromator. The input optical power was measured by using a Laser Precision RL-3610 power meter with CTX-532 Chopper and RKP-360 detector probe. The power meter responds only to that radiation which is interrupted by the chopper. Therefore, the effects of background signals and ambient temperature variations can be eliminated. The responsivity of the photodetector is determined by the average photocurrent divided by the average incident optical power. Without AR coating, a quantum efficiency of 40.5 % between 1.3 to 1.65 um was obtained for the Au/p^+-n-InGaAs/n^+-InP Schottky photodiode.

4.4.5. Response Speed Measurement

The response speed was directly measured by impulse response technique using a sampling scope in time domain. This method requires an optical source generating ultrashort pulses preferably shorter than the impulse response of the photodiode. The impulse response of a photodiode to a laser pulse of 110 ps FWHM (70 ps risetime) with a 10 KHz-pulse repetition rate at a wavelength of 820

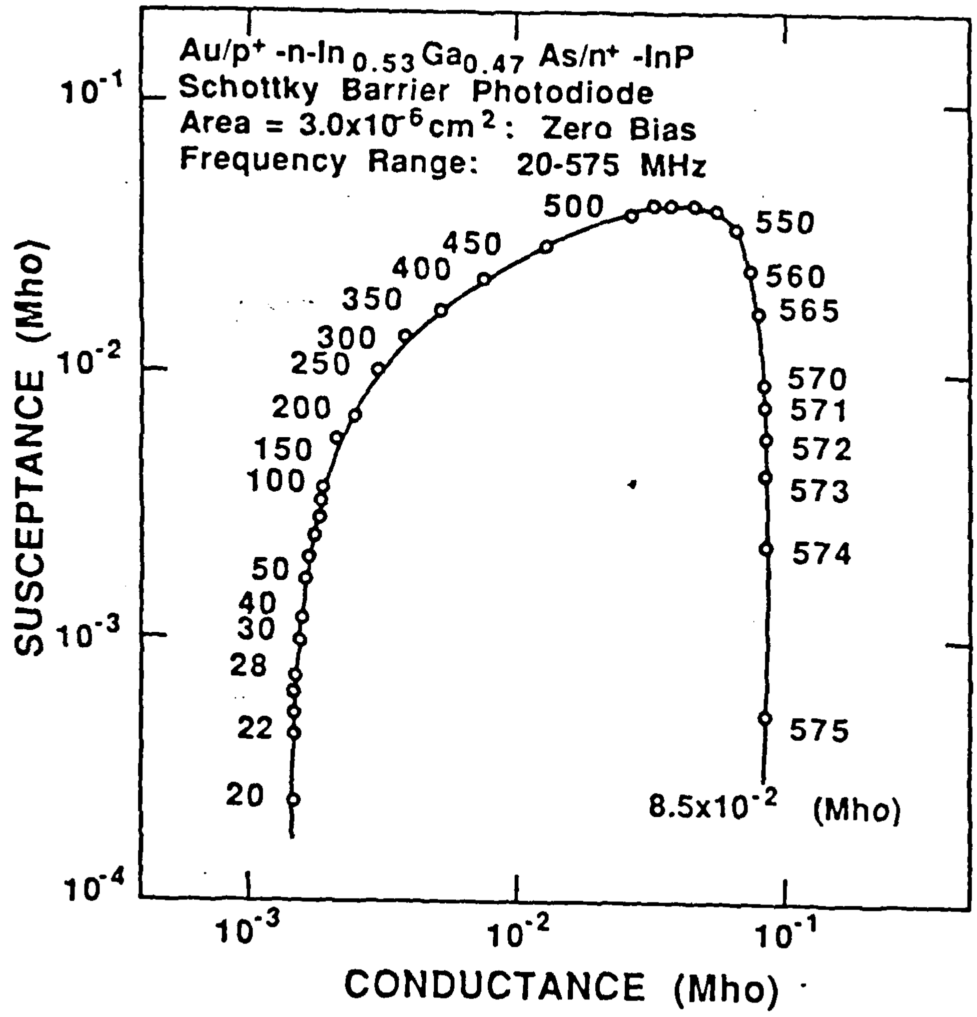

Fig. 4.3. A.C. Admittance of p^+-n-InGaAs/n^+-InP Schottky Barrier Photodiode.

nm was measured by a Tektronix 7S-12 sampling scope with an S-4 sampling head of risetime of 25 ps (55 ps FWHM). The sampling scope introduces considerable instrumental broadening to produce a pulse of a risetime of 25 ps (55 ps FWHM). The schematic diagram for the impulse response measurement system is shown in Fig. 4.4. The response is mainly limited by the finite width of the laser pulse and the rise time of the sampling scope. The result shows that our photodetector has a risetime of 180 ps and 0.9 ns FWHM as is shown in Fig.4.5. The measured RC time constant is around 0.56 ps. Therefore, further improvement in the packaging of the detector is needed in order to obtain a true response speed. Table 4.1. lists the physical parameters of InGaAs material. Table 4.2. and Table 4.3. summarize the design parameters and the test results of the p^+-n-InGaAs/n^+-InP Schottky barrier photodiodes.

Table 4.1. Physical Parameters for $In_{0.53}Ga_{0.47}As$

Energy-Gap	E_g = 0.75 eV at 300 ° K
Dielectric Constant	ϵ_s = 12.0
Mobility	u_n = 1.0×10^4 cm^2/Vsec u_p = 2.0×10^2 cm^2/Vsec
Diffusion Constant	D_n = 260 cm^2/sec D_p = 5.2 cm^2/sec
Diffusion Length	L_n = 2.28 um (p-InGaAs) L_p = 0.32 um (n-InGaAs)
Effective Mass	m_n^* = 0.041 m_o m_{pl}^* = 0.050 m_o m_{ph}^* = 0.490 m_o m_p = 0.500 m_o
Intrinsic Carrier Concentration	n_i = 7.1×10^{11} cm^{-3}
Effective Density of States	N_C = 2.09×10^{17} cm^{-3} N_V = 8.90×10^{18} cm^{-3}
Effective Richardson Constant	A^* = 4.92 $Acm^{-2}K^{-2}$ (n-InGaAs) A^* = 61.9 A $cm^{-2}K^{-2}$ (p-InGaAs)

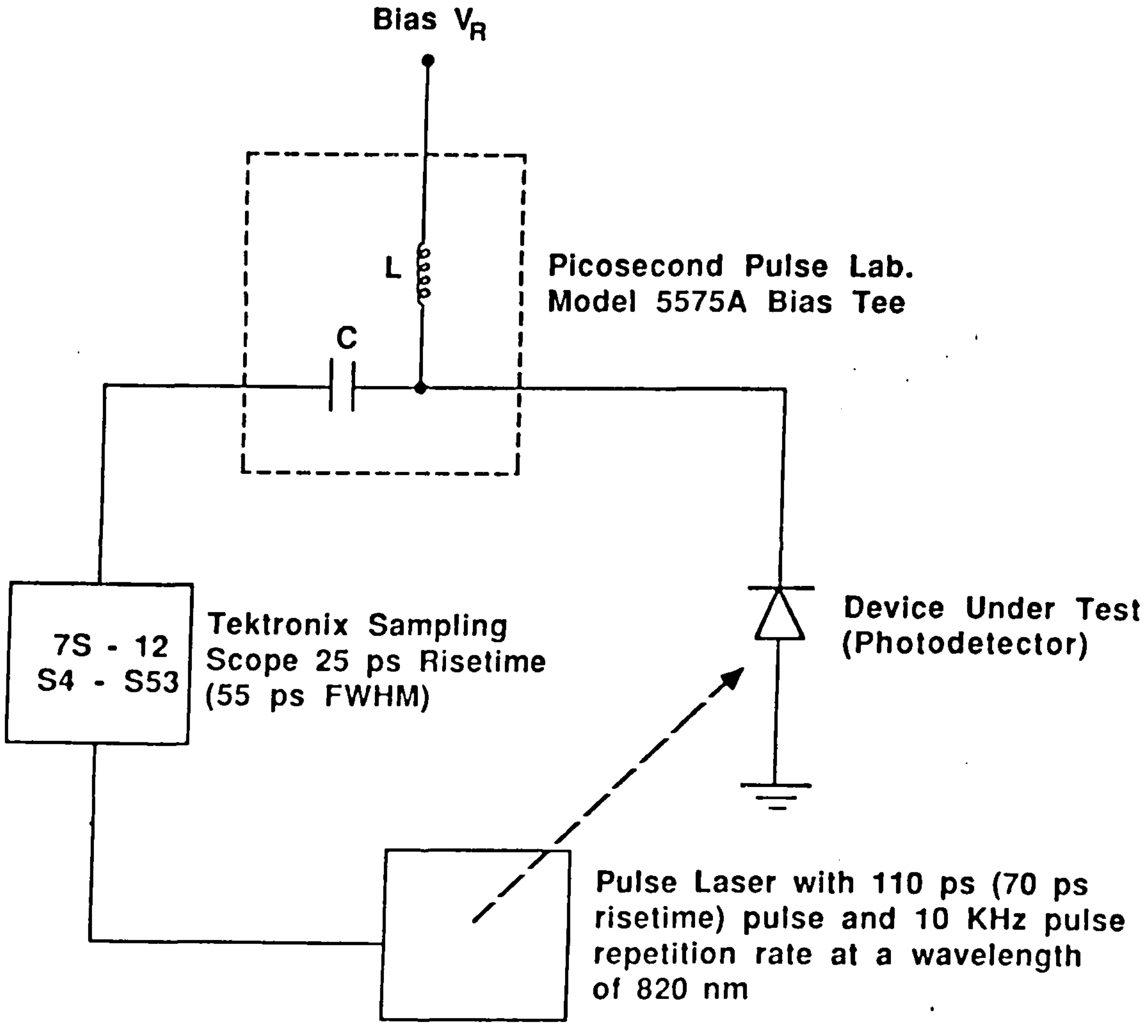
Bias V_R
L
C
Picosecond Pulse Lab.
Model 5575A Bias Tee
7S - 12
S4 - S53
Tektronix Sampling
Scope 25 ps Risetime
(55 ps FWHM)
Device Under Test
(Photodetector)
Pulse Laser with 110 ps (70 ps
risetime) pulse and 10 KHz pulse
repetition rate at a wavelength
of 820 nm

Fig. 4.4. Schematic Diagram for Impulse Response Measurement System.

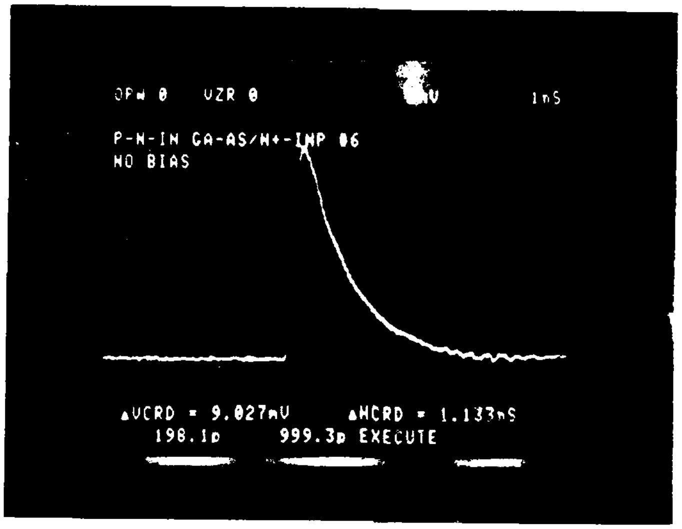

Fig. 4.5. Impulse Response of p^+-n-InGaAs/n^+-InP Schottky Barrier Photodiode.

Table 4.2. Parameters for p^+-n-$In_{0.53}Ga_{0.47}As/n^+$-InP High-Speed Schottky barrier Photodiode

Schottky Contact	Au (100 Å)
Bonding Pad	Cr/Au (60 Å/1,000 Å)
p^+-$In_{0.53}Ga_{0.47}As$ Surface Layer	0.03 - 0.15 um 5.5×10^{16} - 9.0×10^{17} cm^{-3}
n-$In_{0.53}Ga_{0.47}As$ Epilayer	1.5 - 2.0 um 3.0×10^{15} cm^{-3}
Growing Technique	MBE
Substrate	Sn doped n^+-InP 3.0×10^{18} cm^{-3}
Ohmic Contact on n-InP	Au-Ge (88-12 %), 1,500 Å
Alloy	400 °C for 30 sec
Microstrip Line	
Cr/Au Thickness	100-200 A / 0002"
Output Impedance	50 ohm
Stripline Width	0.02425"
W/H Ratio	0.97
Effective Stripline Width	0.02478"

Table 4.3. Results for p^+-n-$In_{0.53}Ga_{0.47}As/n^+$-InP High-Speed Schottky Barrier Photodiode

Device Structure	p^+-n-InGaAs
Diameter (um)	20 - 50
Photodiode Area (cm^2)	$2x10^{-5}$-$3x10^{-6}$
Epilayer Doping (cm^{-3}) Thickness (um)	$3.0x10^{15}$ 1.5 - 2.0
Dark Current Density (A/cm^2) at $V_R = 5$ (V)	$5.0x10^{-3}$
Capacitance (pF) at $V_R = 5$ (V)	0.2 - 0.3
Series Resistance (ohm)	11.8
Quantum Efficiency (%)	40.5
Bandwidth (GHz)	12.9
RC time constant (ps)	1.77
Risetime (ps)	185

4.5. Summary and Conclusions

We report a novel metal/p^+-n-InGaAs/n^+-InP Schottky barrier photodetector capable of detecting up to 13 GHz modulating optical signals at 1.30-1.65 um infrared regime. The results show that the intrinsic response speed for our photodetectors with an active area ($3x10^{-6}$ cm^2) of 20 um in diameter was estimated to be 13 GHz for a Au/p^+-n-$In_{0.53}Ga_{0.47}As/n^+$-InP Schottky barrier photodiode based on the RC time calculated from the measured values of the total capacitance (0.1-0.2 pF) and series resistance (5.3-11.8 ohm). The true response speed can be further improved by reducing the stray capacitance through improving our packaging technique.

CHAPTER FIVE

DEVELOPMENT OF A HIGH-SPEED Au/p-$In_{0.53}Ga_{0.47}As/p^+$-InP SCHOTTKY BARRIER PHOTODETECTOR FOR 1.30-1.65 um PHOTODETECTION

5.1. Introduction

A high-speed photodetector operating in the infrared regime, especially close to the dispersion minimum of optical fibers is of great interest for lightwave communications. Until now, the photodetectors have been fabricated mainly on GaAs using a Schottky barrier structure for 0.80 - 0.90 um and on $In_{0.53}Ga_{0.47}As$ using a p-i-n structure for 1.30 - 1.65 um. More recently we have reported a Au/p-$In_{0.53}Ga_{0.47}As/p^+$-InP Schottky barrier photodetector [19,20], which is capable of demodulating the modulated optical signals at 1.30 - 1.55 um. Schottky barrier contacts on n-$In_{0.53}Ga_{0.47}As$ yield very low barrier height (Φ_{Bn} = 0.2-0.3 eV), which makes Schottky contacts too leaky to be useful for photodetector applications. On the other hand, Schottky barrier contact on a moderately doped p-$In_{0.53}Ga_{0.47}As$ epilayer is expected to produce good barrier height when suitable metals and surface preparation are used. Schottky barrier structure on p-InGaAs has been demonstrated recently by Emeis et al. [18], however, their structure seems too complex even though it has an advantage of being suitable for monolithic integration.

In this chapter, we report the fabrication of a long wavelength high-speed Au/p-$In_{0.53}Ga_{0.47}As/p^+$-InP Schottky barrier photodetector for 1.30-1.65 um infrared detection. This photodiode has been fabricated on p-$In_{0.53}Ga_{0.47}As$ epilayer using a mesa Schottky barrier structure on p^+-InP substrate. The photodiode has a reponsivity of 0.43 A/W at 1.3 um and a risetime of 85 ps. The measured RC time constant for the photodiode with a 50-ohm load resistance is found to be 34.7 ps.

5.2. Theoretical Analysis

The main considerations in the design of photodetectors are response speed and responsivity. For high response speed, the photodetector requires a narrow depletion region for short transit time and a small area and wide depletion region for low junction capacitance. Therefore, the thickness of a depletion layer should be optimized.

5.2.1. Quantum Efficiency

The total photocurrent density consists of two main components coming from the depletion region and the quasi-neutral base region. The photocurrent density due to the photogenerated excess carriers in the depletion layer for an incident monochromatic light is given by:

$$J_d = qaT\Phi\{1-\exp(-aW)\} \qquad (5.1)$$

The photocurrent density due to the electrons collected in the quasi-neutral base region is given by [76,77]:

$$J_n = [qa\Phi TL_n/(a^2L_n{}^2-1)]e^{-aW}\{aL_n - [\cosh(H'/L_n) - e^{-aH'}]/\sinh(H'/L_n)\} \qquad (5.2)$$

The total photocurrent density is obtained from Eq.(5.1) and Eq.(5.2).

$$J_{ph} = q\Phi T[1 - e^{-aW}] + [qa\Phi TL_n/(a^2L_n{}^2-1)]e^{-aW}\{aL_n - [(\cosh(H'/L_n) - e^{-aH'}]/\sinh(H'/L_n)\} \qquad (5.3)$$

where a is the absorption coefficient, Φ is the incident photon flux density, T is the transmission coefficient in the metal film, H (=H'+ W) is the thickness of the epilayer, and W is the depletion layer width. The quantum efficiency can be obtained from Eq.(5.3), which is given by:

$$\eta = T\{1+e^{-aW}/(a^2L_n^2-1)[1-aL_n(\cosh(H'/L_n)-e^{-aH'})/\sinh(H'/L_n)]\} \quad (5.4)$$

Note that Eq.(5.4) can be reduced to Garter's expression [74] of the quantum efficiency when the device thickness is larger than the diffusion length, i.e., $H' \gg L_n$. For a single layer antireflection coating, the thickness of the dielectric film can be obtained from the well-known quarter wavelength formula given by [75,76]:

$$d_1 = (\lambda_o/4\, n_1)\tan^{-1}[2n_1k_s/(n_1^2-n_s^2-k_s^2)] \quad (5.5)$$

where λ_o is wavelength of incident light at peak intensity, n_1 is index of refraction of the dielectric film, and n_s is complex index of refraction of the semiconductor.

5.2.2. Response Speed

The response speed of a photodetector is determined primarily by the transit (drift) time in the depletion region, the diffusion time in the quasi-neutral base region, and the RC time constant required to discharge the junction capacitance (C_j) through a combination of internal and external resistances. The total risetime of a photodiode, which is defined as the time of response from 10 % to 90 % of a pulse height, is essentially equal to the largest of the three. To a good approximation, the total risetime can be expressed by:

$$t_r = (t_{tr}^2 + t_{diff}^2 + t_{RC}^2)^{1/2} \quad (5.6)$$

The carrier transit (drift) time across the depletion region is given by $t_{tr} = W/2.8\, v_s$, where v_s is the saturation drift velocity of the carriers. For high mobility materials, the transit time is limited by the saturated drift velocity. The carriers generated within the highly doped contact region or the quasi-neutral region will result in a time delay of the carriers reaching the drift region. The frequency response for diffusion time is given by t_{diff} =

$W_n^2/(2.43\ D_p)$. The RC time constant is given by $t_{RC} = (R_s + R_L)C_j$. The shunt resistance (R_i) is generally very high but is included to account for the relatively low leakage resistance of the photodiode. The series resistance (R_s) is composed of the lead resistance, the spreading resistance in the base material, and the sheet resistance of the thin epilayer. The sheet resistance term is the most important. This resistance is distributed, depending on the contact geometry, and is frequency dependent. Thus, the cutoff frequency is given by

$$f_c = 0.35/t_r \tag{5.7}$$

5.2.3. Dark Current

For high mobility low doped (less than 10^{17} cm^{-3}) semiconductors the dark current density can be described by thermionic-emission theory.

$$J = A^{*}T^{2}\exp(-q\Phi_{Bn}/kT)[\exp(qV/nkT) - 1] \tag{5.8}$$

$$= J_s[\exp(qV/nkT) - 1] \tag{5.9}$$

The quantum-mechanical tunneling through the barrier may modify the ordinary thermionic-emission process. The current-voltage relation suitable for thermionic-field emission due to tunneling of excited carriers, which do not have sufficient energy for thermionic-emission, can be expressed by [69]:

$$J = J_s\{\exp(qV/kT) - \exp[(n^{-1} - 1)qV/kT]\} \tag{5.10}$$

When n equals unity Eq.(5.10) is reduced to Eq.(5.9). For $n > 2$, the Schottky contact conducts better under reverse bias because tunneling is the dominant mechanism. At zero bias the depletion region of the Schottky barrier is in thermal equilibrium and the rate of electron-hole pair generation is balanced by the rate of recombination. In the presence of an applied voltage, there will be a net generation or recombination of carriers depending on the polarity of the applied bias. The generation-recombination current J_{g-r} through the midgap traps in the depletion region is given by:

$$J_{g-r} = J_{ro}[\exp(qV/2kT) - 1] \tag{5.11}$$

where $J_{ro} = qn_iW/2t_o$ and $t_o = (t_nt_p)^{1/2}$ is the minority carrier lifetime in the depletion region. This current is added to the thermionic-emission current and may cause deviation from ideal behavior (i.e., n = 1) in Schottky barrier diodes. The recombination current is important in high barrier, in low lifetime material, at low temperature, and at low forward bias voltage.

5.3. Device Fabrication

A high-speed Au/p-$In_{0.53}Ga_{0.47}As$/p^+-InP mesa Schottky barrier photodiode has been fabricated using a lift-off process. The photodiode structure is shown in Fig.5.1. The p-$In_{0.53}Ga_{0.47}As$ epilayer was grown on p^+-InP substrate by liquid phase epitaxy (LPE) technique. The thickness of p-$In_{0.53}Ga_{0.47}As$ epilayer is 2.0 um with a dopant density of $1.0\text{-}5.0\times10^{15}$ cm^{-3}. A 100 Å gold film was deposited onto the p-$In_{0.53}Ga_{0.47}As$ epilayer with a deposition rate of 2 Å/sec at a pressure of 5.0×10^{-7} Torr for a transparent Schottky contact and Cr/Au (60/1,000 Å) was deposited for the bonding pad. For ohmic contact to p^+-InP, Mn/Au (100/900 Å) was deposited sequentially and alloyed at 460 °C for 30 sec in H_2-N_2 (5-95 %) forming gas ambient. For mesa etch, $H_2SO_4:H_2O_2:H_2 = 3:1:1$ was used for the $In_{0.53}Ga_{0.47}As$ with an etch rate of 0.1 um/sec at T = 300 K. For characterization, the photodiode was mounted on a 50-ohm microstrip transmission line fabricated on the Cr-Au metallized alumina (Al_2O_3) through an OSSM subminiature coaxial connector. The high-speed packaging, on which the photodiode is mounted is shown in Fig.5.2.

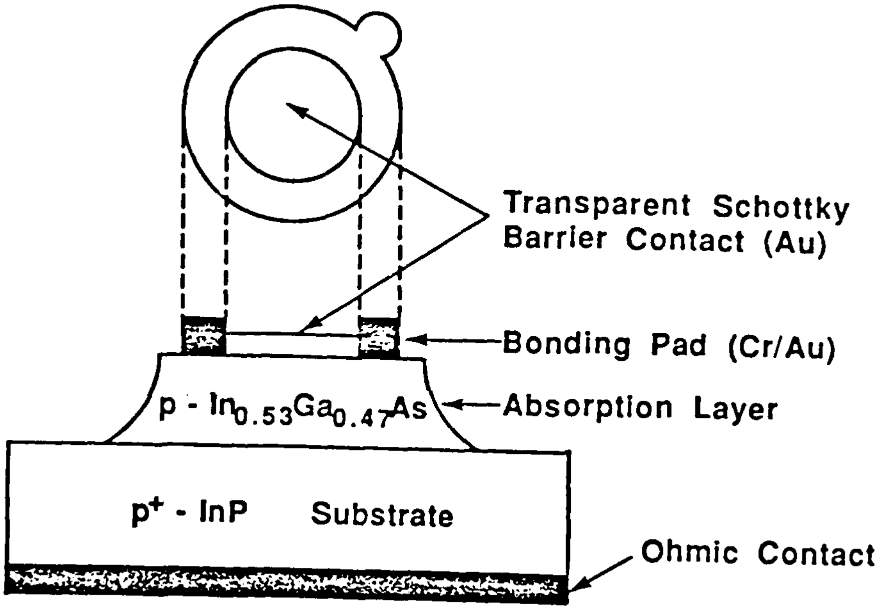
Transparent Schottky Barrier Contact (Au)
Bonding Pad (Cr/Au)
p - $In_{0.53}Ga_{0.47}As$
Absorption Layer
p^+ - InP Substrate
Ohmic Contact

Ohmic Contact: Mn (100 Å)/Au (900 Å)

Fig. 5.1. Structure of p-InGaAs/p^+-InP Schottky Barrier Photodiode.

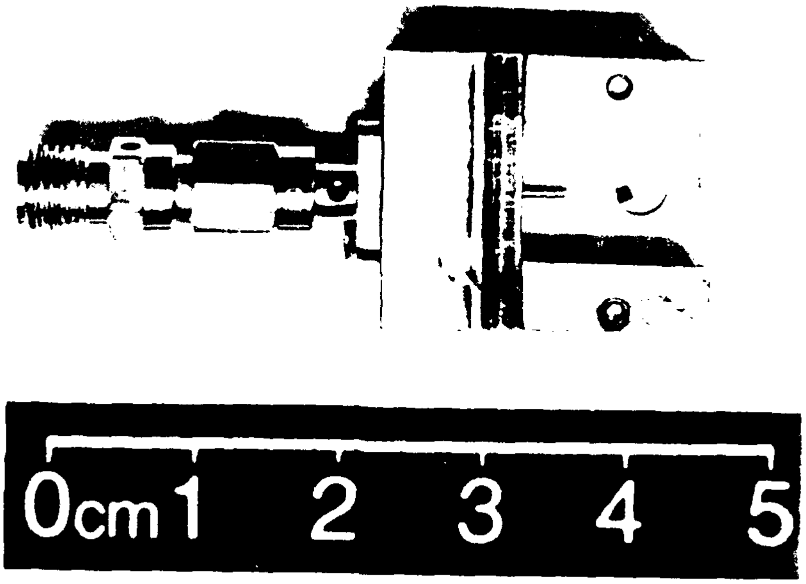

Fig. 5.2. Microwave Package for our Photodetectors used in this research project.

5.4. Experimental Results and Discussion

5.4.1. Current-Voltage (I-V) Measurement

The current-voltage characteristics in Fig.5.3. show that the breakdown voltages for our devices are mostly around 5-8 V. The dark current was measured by using HP 4140B pA meter controlled by HP 9845B computer. Figure 5.4. and 5.5. show the forward-biased and the reverse-biased current-voltage characteristics of a Au/p-InGaAs/p^+-InP Schottky barrier photodiode.

5.4.2. Capacitance-Voltage (C-V) Measurement

The junction capacitance of the photodiode was measured by using HP 4280A C-Meter/C-V Plotter. The result shows that the total capacitance is C_j = 0.10–0.20 pF at V_R = 5 V for the Au/p-$In_{0.53}Ga_{0.47}As$/p^+-InP Schottky diode with the contact area of 3.0×10^{-6} cm^2. Based on $(1/C^2)$ vs. V_R curve shown in Fig.5.6, the Schottky barrier height was around 0.58 eV.

5.4.3. A.C. Admittance Measurement

From a plot of the Im{Y(W)} vs. Re{Y(W)}, the series resistance of the diode can be determined.

$$Y(w) = \frac{R_s + R_p/[1+(wR_pC_j)^2]}{\{R_s + R_p/[1+(wR_pC_j)^2]\}^2 + \{wR_p^2C_j/[1+(wR_pC_j)^2]\}^2}$$

$$+ j \frac{wR_p^2C_j/[1+(wR_pC_j)^2]}{\{R_s + R_p/[1+(wR_pC_j)^2]\}^2 + \{wR_p^2C_j/[1+(wR_pC_j)^2]\}^2} \qquad (5.12)$$

In the low frequency limit (w->0), Re{Y(w)} = $1/(R_s + R_p)$ and in the high frequency limit (w->oo), Re{Y(w)} = $1/R_s$. By measuring the frequency dependent conductance and susceptance component of a Schottky barrier diode in the frequency range of 7 to 227 MHz by using a HP 4191A RF impedance analyzer, the series resistance and shunt resistance of the diode can be determined. The junction capacitance can be calculated from the measured values;

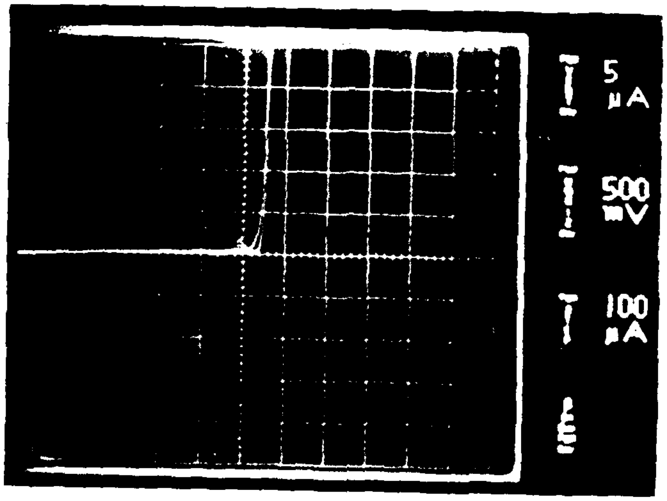

Fig. 5.3. Current-Voltage (I-V) Characteristics for Au/p-In$_{0.53}$Ga$_{0.47}$As/p^{+}-InP Schottky Barrier Photodiode.

Contact Area: 20 um diameter

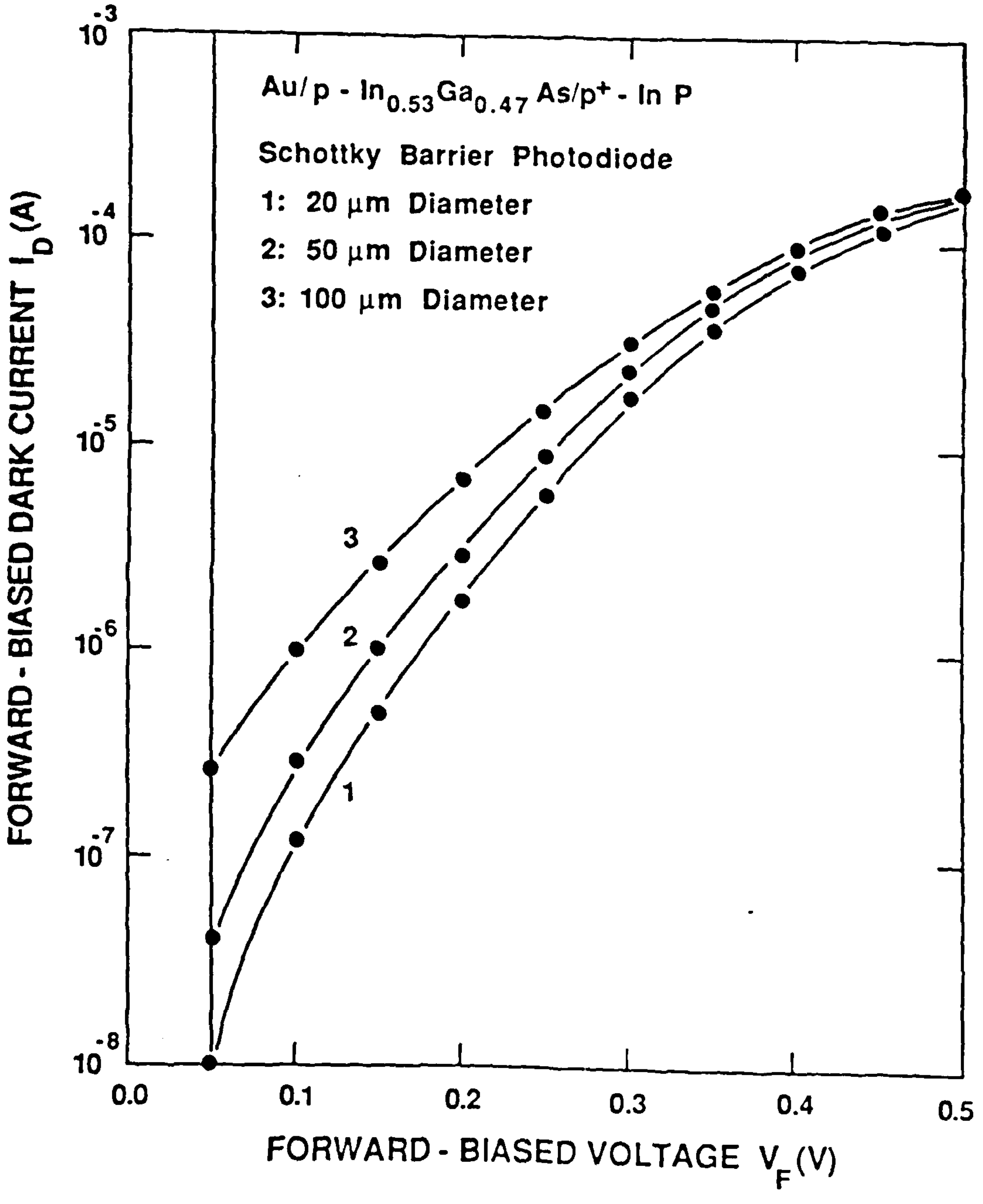

Fig. 5.4. Forward-biased Dark Current of p-InGaAs/p^+-InP Schottky Barrier Photodiode.

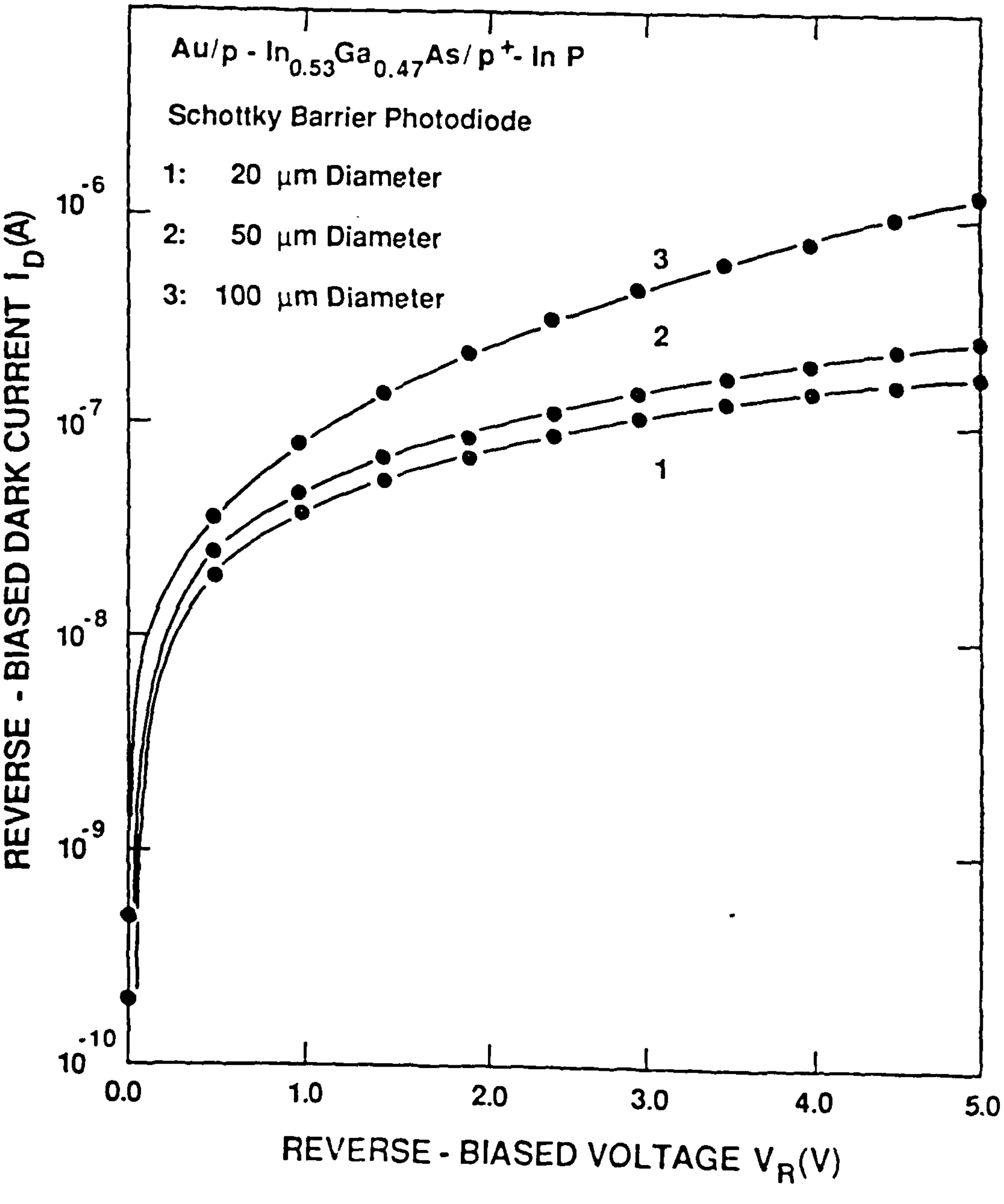

Fig. 5.5. Reverse-biased Dark Current of p-InGaAs/p$^+$-InP Schottky Barrier Photodiode.

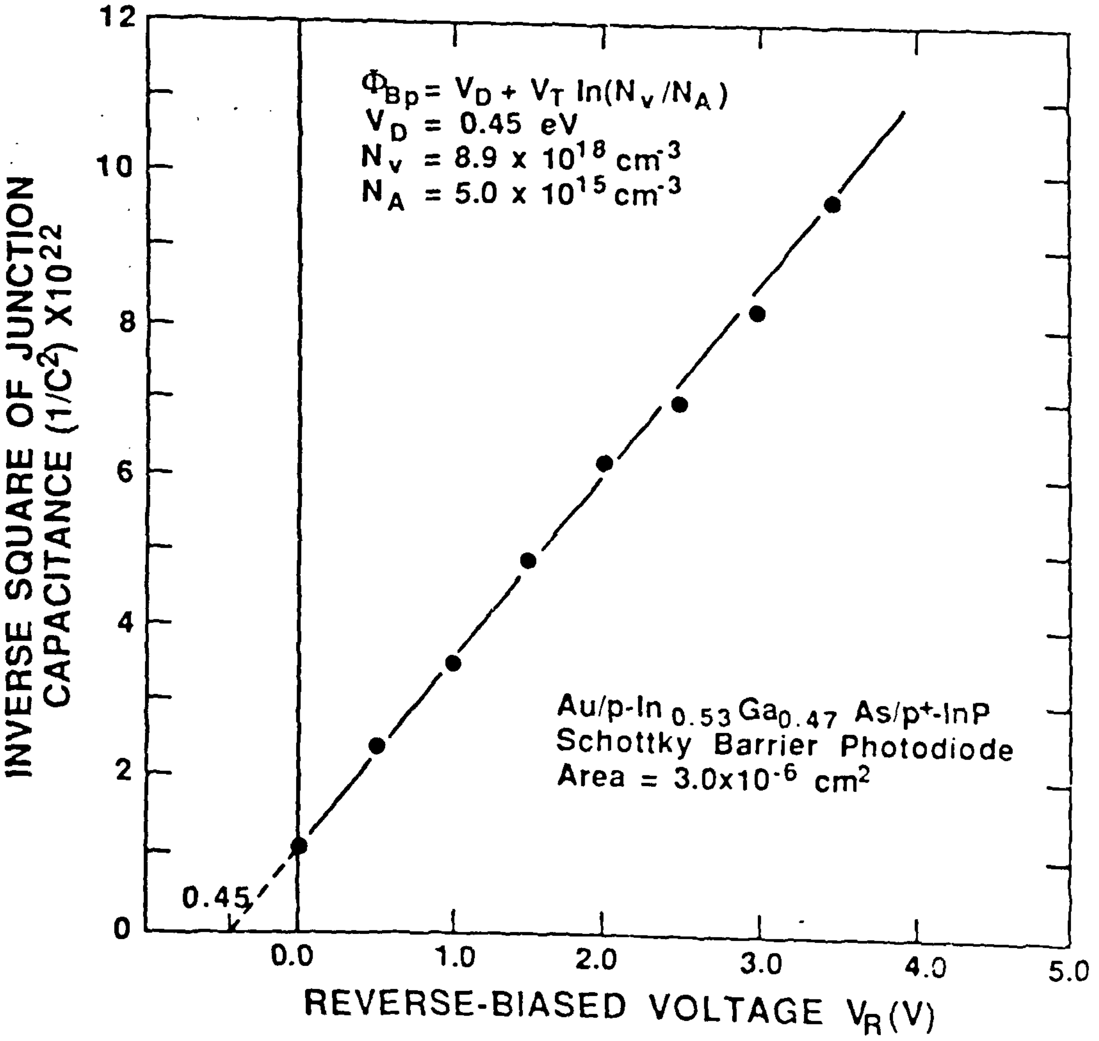

Fig. 5.6. Inverse Square of Capacitance of p-InGaAs/p$^+$-InP Schottky Barrier Photodiode.

$Z_1 = R_s + R_p/[1+(wR_pC_j)^2]$ or $Z_2 = wR_p^2C_j/[1+(wR_pC_j)^2]$ for a given frequency. This allows accurate determination of the R_s, R_p, and C_j over a wide range of frequency. The series resistance was found to be 5.3 ohm for p-$In_{0.53}Ga_{0.47}As$ Schottky barrier photodiode from the plot of Im{Y(W)} vs. Re{Y(W)} in Fig. 5.7.

5.4.4. Spectral Response Measurement

The spectral response was measured by using a Jarrell-Ash 82-410 quarter-meter Monochromator. The input optical power was measured by using a Laser Precision RL-3610 power meter with CTX-532 Chopper and RKP-36C detector probe. The power meter responds only to that radiation which is interrupted by the chopper. Therefore, the effects of background signals and ambient temperature variations can be eliminated. The schematic diagram for the spectral response measurement system is shown in Fig. 5.8.

The responsivity of the photodetector is determined by the average photocurrent divided by the average incident optical power. Without anti-reflection coating, the photodiode has a responsivity of 0.43 A/W and a quantum efficiency of 40.[illegible] % at 1.3 µm. The quantum efficiency for Au/p-InGaAs/p^+-InP Schottky barrier photodiode is shown in Fig.5.9.

5.4.5. Response Speed Measurement

The response speed was directly measured by impulse response technique using a sampling scope in time domain. This method requires an optical source generating ultrashort pulses preferably shorter than the impulse response of the photodiode. The impulse response of a photodiode to a laser pulse of 110 ps FWHM (70 ps risetime) with a 10 KHz-pulse repetition rate at a wavelength of 820 nm was measured by a Tektronix 7S-12 sampling scope with an S-4 sampling head of risetime of 25 ps (55 ps FWHM). The response is mainly limited by the finite width of the laser pulse and the risetime of the sampling scope. The impulse response is shown in Fig.5.10. and 5.11. The response speed is mainly limited

AD-A180 594 DEVELOPMENT OF A HIGH SPEED INGAAS/INP SCHOTTKY BARRIER 2/2
PHOTODETECTOR FOR..(U) FLORIDA UNIV GAINESVILLE S S LI
JUL 87 RADC-TR-87-83 F30602-81-C-0202

UNCLASSIFIED F/G 20/6.1 NL

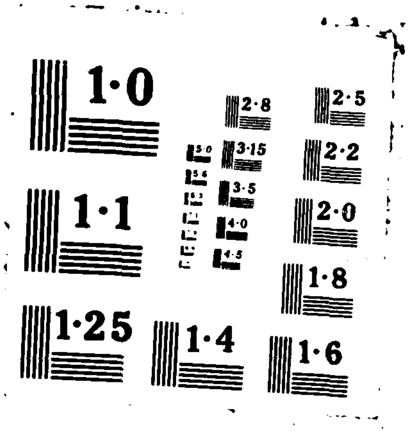
1·0
2·8
2·5
3·2
3·6
4·0
2·2
2·0
1·1
1·8
1·25
1·4
1·6

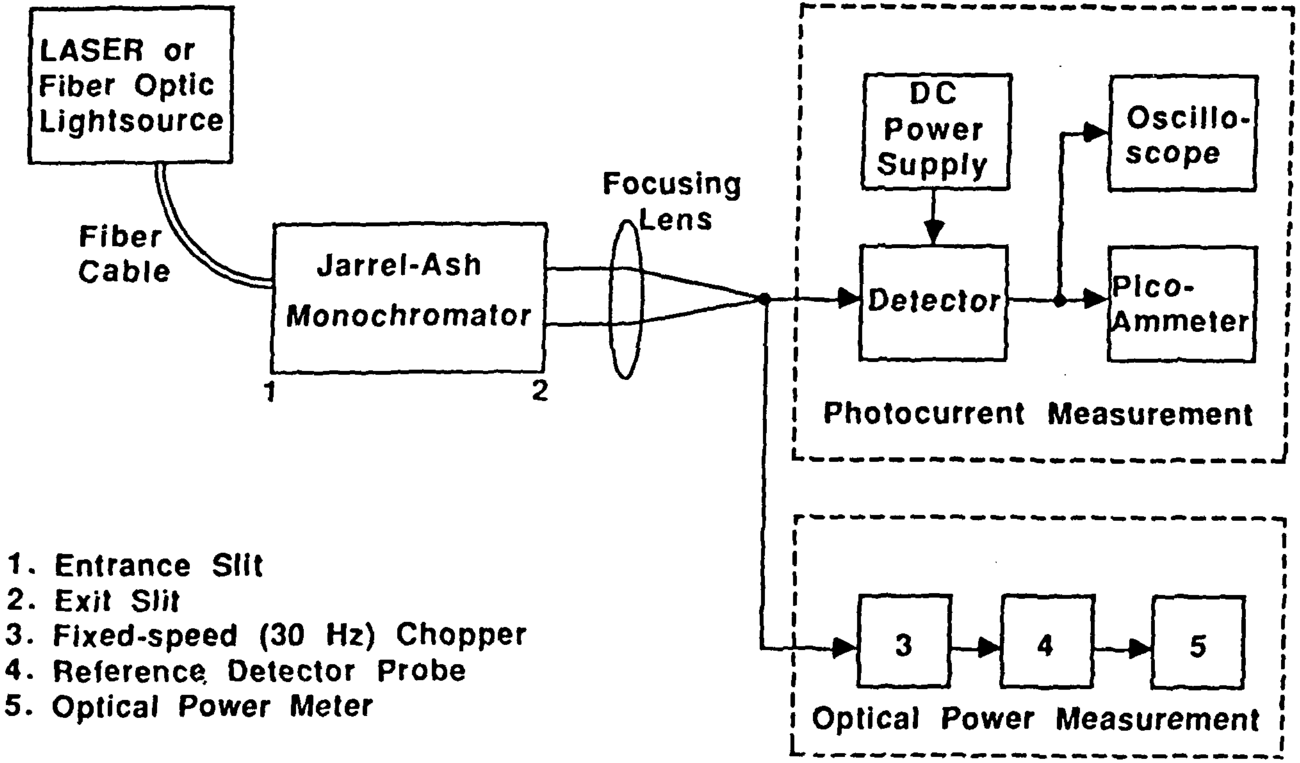
LASER or Fiber Optic Lightsource
Fiber Cable
Jarrel-Ash Monochromator
1
2
Focusing Lens
DC Power Supply
Detector
Oscillo-scope
Pico-Ammeter
Photocurrent Measurement
3
4
5
Optical Power Measurement
1. Entrance Slit
2. Exit Slit
3. Fixed-speed (30 Hz) Chopper
4. Reference Detector Probe
5. Optical Power Meter

Fig. 5.8. Schematic Diagram for Spectral Response Measurement System.

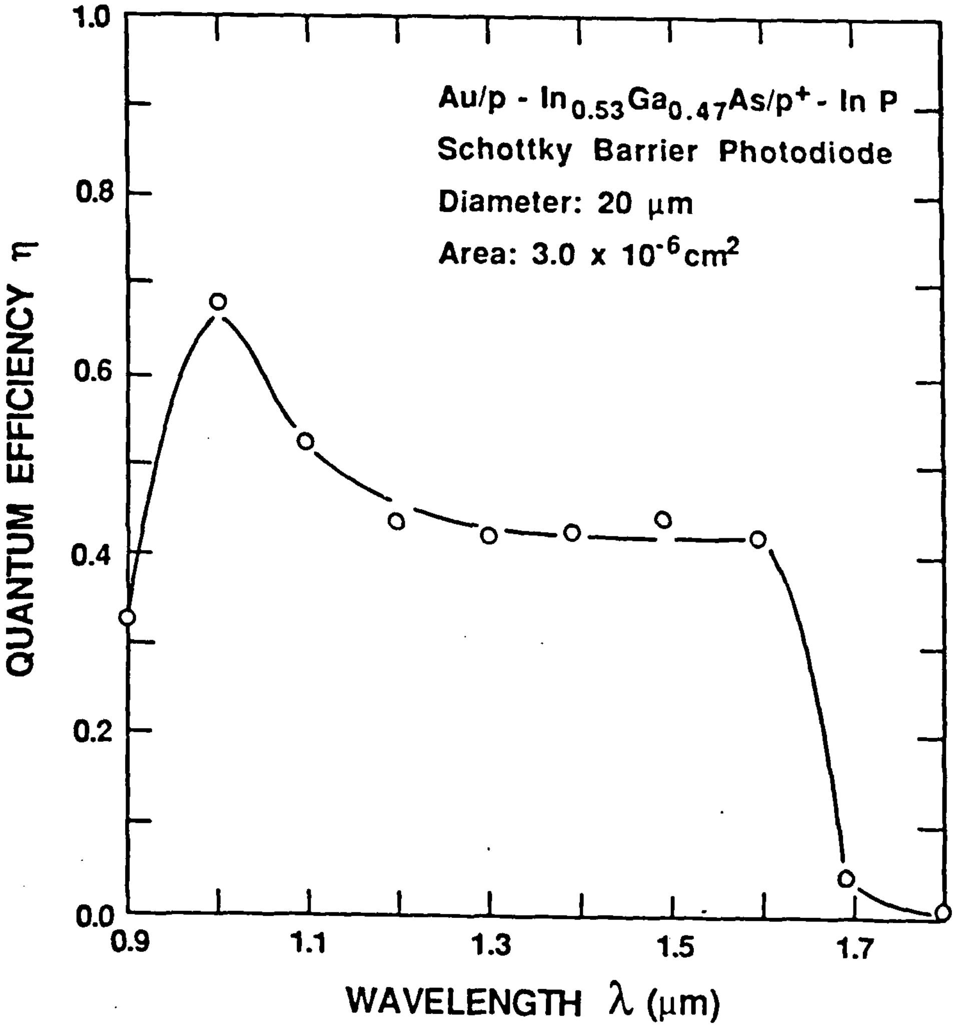

Fig. 5.9. Quantum Efficiency of p-InGaAs/p^+-InP Schottky Barrier Photodiode.

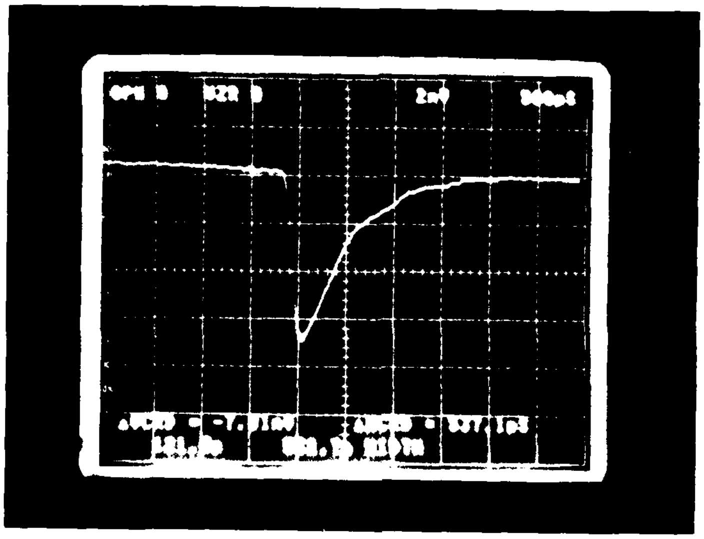

Fig. 5.10. Impulse Response of p-InGaAs/p$^+$-InP Schottky Barrier Photodiode.

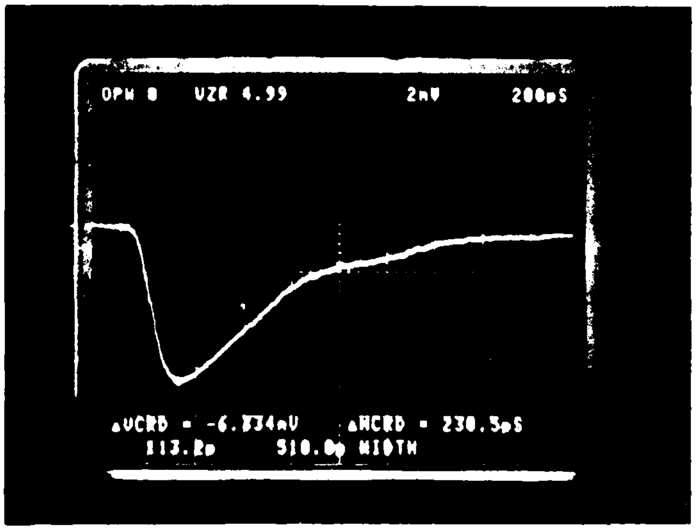

Fig. 5.11. Impulse Response of p-InGaAs/p^+-InP Schottky Barrier Photodiode.

by the finite width of the laser pulse and the risetime of the sampling scope.

The impulse response for the Au/p-$In_{0.53}Ga_{0.47}As/p^+$-InP Schottky barrier photodiode is thus given by the risetime of 85 ps and FWHM of 490 ps. This long tail might be due to (1) a time delay resulting from the carrier diffusion in the undepleted epilayer, (2) a long pulse (i.e., 110 ps) of laser as an optical source, (3) the use of a pulse laser with a wavelength of 0.82 um instead of 1.3 um, and (4) package parasitics. However, the measured RC time constant for a photodiode is $t_{RC} = 2\pi(R_s + R_L)C = 34.7$ ps, which corresponds to the cutoff frequency of 28.8 GHz. Therefore, the impulse response measurement with a shorter pulse laser and further improvement in the package of the photodetector are necessary to obtain a true response speed for our photodiodes. The design parameters and the experimental results of the photodetectors are summarized in Table 5.1. and Table 5.2., respectively.

Table 5.1. Parameters for Au/p-InGaAs/p^+-InP Schottky Barrier Photodiode

Device Structure	p-InGaAs/p^+-InP
Schottky Contact	Au (100 Å)
Contact Diameter	20-50 um
Photodiode Area	2×10^{-5}-3×10^{-6} (cm^2)
Bonding Pad	Cr/Au (60/1,000 Å)
Epitaxial Layer	p-$In_{0.53}Ga_{0.47}As$ 1.5 - 2.0 um 1.0 - 5.0×10^{15} cm^{-3}
Growing Technique	LPE
Substrate	Zn doped p^+-InP 2.0×10^{18} cm^{-3}
Ohmic Contact	Mn/Au (100/900 Å)
Alloy	460 °C for 30 sec

Table 5.2. Results for Au/p-InGaAs/p$^+$-InP Schottky Barrier Photodiode

Device Structure	p-InGaAs/p$^+$-InP
Diameter (um)	20-50
Photodiode Area (cm^2)	2x10^{-5}-3x10^{-6}
Epilayer Doping (cm^{-3}) Thickness (um)	1.0-5.0x10^{15} 1.5 - 2.0
Dark Current Density (A/cm^2) at V_R = 1 (V)	2.5x10^{-3}
Capacitance (pF) at V_R = 5 (V)	0.1 - 0.2
Series Resistance (ohm)	5.3
Barrier Height	0.58
Quantum Efficiency (%)	40.8
Responsivity (A/W)	0.43
Risetime (ps)	85
RC Time Constant (ps)	34.7
Bandwidth (GHz)	28.8

5.5 Summary and Conclusions

A new high-speed long wavelength Au/p-$In_{0.53}Ga_{0.47}As$/p$^+$-InP Schottky barrier photodetector has been fabricated and characterized in this study. The results show that the intrinsic response speed for our photodetectors with an active area of 3x10^{-6} cm^2 was estimated to be 28.8 GHz based on the measured RC time constant (C = 0.15 pF and R_s = 5.3 ohm). Therefore, the response speed of the photodiode can be further improved by reducing the Schottky contact area for low junction capacitance and by optimizing the thickness and dopant density of the InGaAs epilayer to achieve shorter transit time and lower junction capacitance, and by minimizing the photodetector package parasitics.

CHAPTER SIX
SUMMARY, CONCLUSIONS, AND RECOMMENDATION

6.1. Summary and Conclusions

The objective of this research project is to develop a high-speed long wavelength (1.30-1.55 um) photodetector capable of demodulating optical signals greater than 20 GHz for millimeter-wave optical fiber links. For this purpose, a novel high-speed $In_{0.53}Ga_{0.47}As$ Schottky barrier photodiode using Au/p^+-n-InGaAs /n^+-InP and Au/p-InGaAs/p^+-InP structure has been successfully developed in this research project. The Schottky barrier photodiode structure with a thin transparent metal film was employed because of its many advantages including simplicity of fabrication, reliability, low temperature process.

The test results of our photodetectors have shown that a Au/p-InGaAs/p^+-InP Schottky barrier photodiode is very promising for high-frequency and high-speed detector applications. However, a p^+-n-InGaAs Schottky barrier photodiode needs more study to obtain good reproducibility of the barrier height enhancement. The results show that our Au/p-InGaAs/p^+-InP Schottky barrier photodiodes have a responsivity of 0.43 A/W and a quantum efficiency of 40.5 % at 1.3 um without anti-reflection coating. The impulse response measurement for the Au/p-$In_{0.53}Ga_{0.47}As/p^+$-InP Schottky barrier photodiode shows a risetime of 85 ps and an FWHM of 490 ps.

The response speed is mainly limited by the finite width of the laser pulse and the risetime of the sampling scope. The observed long tail in the impulse response measurement might be due to (1) a time delay resulting from the carrier diffusion in the undepleted epilayer, (2) a long pulse (i.e., 110 ps) of laser itself as an optical source, and (3) packaging parasitics. The RC time constant for our p-InGaAs/p^+-InP Schottky barrier photodetectors with an active area of $3x10^{-6}$ cm^2 is found to be 34.7 ps based on the measured values (i.e.,

$C = 0.15$ pF and $R_s = 5.3$ ohm), which implies that the intrinsic response speed for the photodetector is 28.8 GHz. Therefore, the response speed of our photodetectors can be further improved by optimizing the device parameters and minimizing the packaging parasitics. We plan to focus our efforts on two main tasks which include fabrication of the InGaAs photodetectors on the semi-insulating InP substrate and optimal design of the photodetector package to minimize the parasitics.

6.2. Recommendations for Follow-up Research

6.2.1. Packaging Optimization

Packaging optimization and interconnections are most important tasks for high frequency devices because most reliability constraints are related to these problems. The interconnection capacitance between a discrete photodetector and amplifier contributes to an important fraction of the total receiver capacitance. To improve high-speed packaging technique, the microwave packaging using coplanar waveguide (CPW) transmission line needs to be developed, which is expected to greatly reduce degradation of response speed due to the packaging parasitics. CPW has an important advantage over microstrip transmission line in that the signal conductors and the ground plane conductor share the same surface of the dielectric substrate [78,79]. This waveguiding system offers convenient incorporation of lumped devices and short circuits, which is more difficult in microstrip line. This means circuit connections to ground can be made simply with short, low parasitic bond wire connections.

6.2.2. Development of High-speed $In_{0.53}Ga_{0.47}As$ Schottky Barrier Photodetector on Semi-insulating InP Substrate for Monolithic Integration.

The use of the semi-insulating substrate is important for high frequency applications because the parasitic capacitances associated with discrete devices and devices to ground plane can be minimized. The photodetectors on the semi-insulating substrate are suitable for the monolithic optoelectronic integration. The monolithic optoelectronic integration [80,81] may have advantages of a reduction in cost, an increase in functionality, and an improvement in performance and reliability. Significant improvements in speed, sensitivity, and noise can be obtained via monolithic integration by reducing the package parasitics associated with discrete devices and test fixture. This might be due to the elimination of bond wire connections, the use of semi-insulating substrates where the bond pad is located on, and the improved package and test fixture. In order to reduce a surface leakage current the mesa structure of which the surface is covered with a dielectric passivation layer is necessary for the proposed photodiode. The Schottky barrier contact with an interdigitated structure will be desirable to increase a quantum efficiency.

6.2.3.Monolithic Integration of An Optical Receiver Module

With the advent of optical fiber communications the monolithic integration of optoelectronic devices and complex circuits on a single substrate provides the promise of improved performance and reliability, increased functionality, economy of size and scale, and the resulting proliferation of the computer industry. The improvement in sensitivity obtained by the integrated p-i-n/FET becomes more significant for high bit rates, and the p-i-n/FET may be an alternative to an avalanche photodiode (APD) as a means of increasing receiver performance at very high bit rates. The optical receiver modules [82-84] have a potential of improving receiver performance over that which can be obtained using a hybrid photodetector/preamplifier. Therefore, a monolithically integrated optical receiver which typically consists of a photodetector, detector biasing circuit, and at least one stage of voltage gain is a promising detector candidate for optical fiber communications.

CHAPTER SEVEN
REFERENCES

1. C. H. Lee, Picosecond Optoelectronic Devices, Academic Press,1984.

2. W. T. Tsang,Lightwave Communication Technology: Photodetectors, Semiconductors and Semimetals, Vol. 22-D, Academic Press, 1985.

3. S. Y. Wang, " Ultra High Speed Photodetectors," IEEE IEDM, pp. 712, 1984:

4. G. E. Stillman et al., " InGaAsP Photodiodes, " IEEE Elec. Dev., Vol.30, No.4, pp.364, 1983.

5. J.Muller, " Photodiodes for Optical Communication," Adv. in Elec. and Elec. Phy., edited by L.Marton and C. Marton, Vol.55, pp.189, 1981.

6. S. Y. Wang, D.M. Bloom, and D.M. Collins," Ultrahigh Speed photodetector" Proc. SPIE, Vol.439, pp.178, 1983.

7. H. Blauvelt, G. Thurmond, J. Parsons, D. Lewis, and H. Yen, " Fabrication and Characterization of GaAs Schottky Barrier Photodetectors for Microwave Fiber Optic Links, " Appl. Phys. Lett., 45(3), pp.195, 1984.

8. J. H. Kim andS. S. Li, " High Speed Photodetectors Development for Millimeter Wave Fiber Optic Links," Final Technical Report, US Air Force RADC/DCLW, Contract No. F30602-84-C-0137, 1985.

9. Jae H.Kim, Sheng S. Li, and J. J. Pan, "Picosecond Response High-Speed GaAs Schottky Barrier Photodetector for Microwave Optical Fiber Links," SPIE Proc., Vol.716, 1986.

10. N. Bar-Chaim, K.Y.Lau, I. Ury, and A. Yariv, " High-Speed GaAlAs/GaAs p-i-n Photodiode on a Semi-insulating GaAs Substrate ," Appl. Phys. Lett., 43(3), pp.261, 1983.

11. W. Lenth, A. Chu, L. J. Mahoney, R. W. McClelland, R.W. Mountain, and D. J. Silversmith, " Planar GaAs p-i-n Photodiode with Picosecond Time Response," Appl. Phys. Lett., 46(2), pp.191, 1985.

12. K. Li, E. Rezek, and H.D. Law, "InGaAs PIN Photodiode Fabricated on Semi-insulating InP Substrate for Monolithic Integration," Electronics Lett., 20(5), pp.195, 1984.

13. G. E. Stillman et al., " Long-Wavelength (1.3-1.6 um) Detectors for Fiber Optical Communications, " IEEE Elec. Dev., Vol. ED-29, N0.9, pp.1355, 1982.

14. T. P.Pearsall et al., " A GaInAs/InP Hetero-Photodiode with Reduced Dark Current, " IEEE Quan. Elec., Vol.17, No.2, pp.255, 1981.

15. T. P. Lee etal., " InGaAs/InP p-i-n Photodiodes for Lightwave Communications at the 0.95-1.65 um Wavelength, " IEEE Quan. Elec., Vol.17, N0.2, pp.232, 1981.

16. S.R. Forrest et al., " Low Dark-Current, High-Efficiency Planar InGaAs/InP P-I-N Photodiodes, " IEEE EDL., Vol.2, No.11, pp.283, 1981.

17. R. F. Leheny et al., " Characterization of InGaAs Photodiodes Exhibiting Low Dark Current and Low Junction Capacitance, " IEEE Quan. Elec., Vol.17, No.2, pp.227, 1981.

18. N. Emeis, H. Schumacher, and H. Beneking, "High-Speed GaInAs Schottky Photodetector," Electronics Lett., 21(5), pp.180, 1985.

19. Jae H. Kim and Sheng S. Li, " Development of A High-Speed Au/$In_{0.53}Ga_{0.47}As$ /InP Schottky Barrier Photodiode for 1.3-1.65 um Photodetection," High Speed Electronics, 18th International Conference on the Physics of Semiconductor, Stockholm, Sweden, 1986.

20. J. H. Kim, S. S. Li, L. Figueroa, E. Rezek, and R. Wagner, " A High-Speed p-$In_{0.53}Ga_{0.47}As/p^{+}$-InP Schottky Barrier Photodiode for Infrared Photodetection," Proc. of Optics and Quantum Electronics, Dec. 1986.

21. J. H. Kim, S. S. Li, L. Figueroa, and P.K. Bhattacharya, " Development of High-Speed Long Wavelength p^{+}-n-InGaAs/InP Schottky Barrier Photodiode ," will be submitted to IEEE Elec. Dev. Lett., Jan. 1987.

22. F.Capasso, " Multilayer Avalanche Photodiodes and Solid-State Photomultipliers, " Laser Focus/Electro-Optics, July 1984.

23. F. Capasso, W.T. Tsang, A.L. Hutchinson, and G.F. Williams," Enhancement of Electron Impact Ionization in a Superlattice: A New Avalanche Photodiode with a Large Ionization Rate Ratio," Appl. Phys. Lett., 40(1), pp.38, Jan. 1982.

24. F. Capasso, W. T. Tsang, and G.F. Williams, " Staircase Solid-State Photomultipliers and Avalanche Photodiodes with Enhanced Ionization Rates Ratio, " IEEE Electron Devices, Vol. ED-30, No.4, pp. 381, April 1983.

25. K. Mohammed, F. Capasso, J. Allam, A.Y. Cho, and A.L. Hutchinson, " New High-Speed Long Wavelength $Al_{0.48}In_{0.52}As/Ga_{0.47}In_{0.53}As$ Multiquantum Well Avalanche Photodiodes," Appl. Phys. Lett., 47(6), pp.597, Sep. 1985.

26. C.W.Slayman and L. Figueroa, " Frequency and Pulse Response of a Novel High Speed Interdigital Surface Photoconductor (IDPC)," IEEE Electron Device Letters, Vol. EDL-2, N0.5, May 1981.

27. L.Figueroa and C.W. Slayman, " A Novel Heterostructure Interdigital Photodetector (HIP) with Picosecond Optical Response," IEEE Electron Device Letters, Vol. EDL-2, No.8, Aug. 1981.

28. C.Y. Chen and G.C. Chi, "Low-noise $Ga_{0.53}In_{0.47}As$ Photoconductive Detectors using Fe Compensation," Appl. Phys. Lett., 45(10), pp.1083, 1984.

29. M.V. Raoand P. K. Bhattacharya," High-Gain $In_{0.53}Ga_{0.47}As$:Fe Photoconductive Detectors, " Elec. Lett., Vol.20, No.20, pp.812, 1984.

30. H. Beneking, " Gain and Bandwidth of Fast Near-Infrared Photodetectors : A Comparison of Diodes, Phototransistors, and Photoconductive Devices," *IEEE Elec. Dev.*, Vol.29, No.9, pp.1420, 1982.

31. H. Beneking, " On the Response Behavior of Fast Photoconductive Optical Planar and Coaxial Semiconductor Detectors, " *IEEE Elec.Dev.*, Vol.29, No.9, pp.1431, 1982.

32. H.J. Klein et al., " High-Speed GaInAs Photoconductive Detector for Picosecond Light Pulses, " *Elec. Lett.*, Vol.17, No.12, pp.421, 1981.

33. G.C Shahidi, E.P. Ippen, and J. Melngailis, " Submicron-gap High Mobility Silicon Picosecond Photodetectors, " *Appl. Phys. Lett.*, 46(8), pp.719, 1985.

34. T. H. Windhorn, L. W. Cook, and G. E. Stillman, " Electron Drift Velocities in InGaAs at Very High Electric Fields, " *IEEE IEDM*, pp.641, 1981.

35. T.P. Pearsall, *GaInAsP Alloy Semiconductor*, Wiley, 1982.

36. T. P. Pearsall, " $Ga_{0.47}In_{0.53}As$: A Ternary Semiconductor for Photodetector Appplications, " *IEEE Quan. Electron.*, Vol.16, No.7, pp.709, 1980.

37. K. Kajiyama et al., " Schottky Barrier Height of n-$In_xGa_{1-x}As$ Diodes, " *Appl. Phys. Lett.*, 23(8), pp.458, 1973.

38. J.L. Veteran, " Schottky Barrier Measurements on p-Type $In_{0.53}Ga_{0.47}As$, " *Thin Solid Films*, Vol.97, pp.187, 1982.

39. J. Selders, N. Emeis, and H. Beneking, "Schottky Barriers on p-Type GaInAs," *IEEE Trans. Electron Devices*, Vol.32, No.3, pp. 605, 1985.

40. H. Kraulte et al., " Contacts on GaInAs, " *IEEE Electron Device*, Vol.32, No.6, pp.1119, 1985.

41. N.D.Arora and J.R.Hauser," Antireflection Layers for GaAs Solar Cells, " *J. Appl. Phys.*, 53(12), pp.8839, 1982.

42. G. Lucovsky and R.B. Emmons, " High Frequency Photodiodes, " *Appl. Optics*, Vol.4, No.6, pp.697, 1965.

43. E.H. Rhoderick,*Metal-Semiconductor Contacts*, Clarendon Press, Oxford, 1978.

44. H.K. Henisch, *Semiconductor Contacts: An approach to ideas and models*, Clarendon Press, Oxford, 1984.

45. B.L. Sharma, *Metal-Semiconductor Schottky Barrier Junctions and Their Applications*, Plenum Press, New York, 1984.

46. T.T. Ha,*Solid-State Microwave Amplifier Design*, pp. 51, Wiley, 1981.

47. H.A. Wheeler, " Transmission-Line Properties of a Strip on a Dielectric Sheet on a Plane, " *IEEE MTT*, Vol.25, No.8, pp.631, 1977.

48. E.J.Denlinger," Losses of Microstrip Lines," IEEE MTT, Vol.28, No.6, pp.513, 1980.

49. E.T. Simon, " Calculator Program Simplifies Microstrip Lines Computations," Microwaves & RF, pp.103, 1984.

50. S. Y. Wang, D.M. Bloom, and D.M. Collins, " 20 GHz Bandwidth GaAs Photodiode, " Appl. Phys. Lett., 42(2), pp.190, 1983.

51. D.H. Auston, " Impulse Response of Photoconductors in Transmission Lines, " IEEE Quan. Electron., Vol.19, No.4, pp.639, 1983.

52. S.Y. Wang, D.M. Bloom, and P.S. Cross, " Electro-Optic Sampling With Picosecond Resolution, " Electron. Lett., Vol.19, No.15, pp.574, 1983.

53. J.A. Valdmanis, G. Mouron, and C.W. Gabel, " Subpicosecond Electrical Sampling, " IEEE Quan. Electron., Vol.19, No.4, pp.664, 1983.

54. B.H. Kolner, D.M. Bloom, and P.S. Cross, " Electro-Optic Sampling with Picosecond Resolution, " Electron. Lett., Vol.19, No.15, pp.574, 1983.

55. A. Yariv, Introduction to Optical Electronics, 2nd., Holt, Rinehart and Winston, pp.305, 1976.

56. C.W. Wilmsen, Physics and Chemistry of III-V Compound Semiconductor Interfaces, Plenum Press, New York, 1985.

57. D.V. Morgan and J. Frey, " Increasing the Effective Barrier Height of Schottky Contacts to n-$In_xGa_{1-x}As$, " Elec. Lett., 14, pp.737, 1978.

58. D.V. Morgan and J. Frey, " Comments on the Modifications of Schottky Barrier Height by Interfacial Oxides, " Phys. Stat. Sol., a, 51, K-29, 1979.

59. S.S. Li, " Theoretical Analysis of a Novel MPN GaAs Schottky Barrier Solar Cell, " Solid-State Electron., Vol.21, pp.435, 1978; Japan Journal of Appl. Phys., 17(1), pp.291, 1977.

60. C.Y. Chen, A.Y. Cho et al., " Characteristics of an $In_{0.53}Ga_{0.47}As$ Very Shallow Junction Gates Structure Grown by Molecular Beam Epitaxy, " IEEE Electron Device Lett., 3(1), pp.15, 1982.

61. C.Y. Chen, A.Y. Cho et al., " Quasi-Schottky Barrier Diode on n-$Ga_{0.47}In_{0.53}As$ using a Fully Depleted p+ $Ga_{0.47}In_{0.53}As$ Layer grown by Molecular Beam Epitaxy, " Appl. Phys. Letts., 40(5), pp.401, 1982.

62. J.H. Kim, S.S. Li, L. Figueroa, W.P. Hong, and P.K. Bhattacharya, "Barrier-enhanced Schottky Contact on n-$In_{0.53}Ga_{0.47}As$ Epilayer MBE-Grown on n^+-InP Substrate," will be submitted to IEEE Elec. Dev. Lett., Jan. 1987.

63. P.M. Capani, " Low Resistance Alloyed Ohmic Contacts to $Al_{0.48}In_{0.52}As/n^+$-$Ga_{0.47}In_{0.53}As$, " Electron Lett., 20(11), pp.446, 1984.

64. K.H. Hsieh et al., " GaInAs, AlInAs Schottky Barrier Diodes and GaInAs/AlInAs Heterojunction Diode as Internal Photoemission Detectors, " IEEE IEDM, pp.729, 1984.

65. H. Morkoc et al., " Schottky Barriers and Ohmic Contacts on n-Type InP Based Compound Semiconductors for Microwave FET's, " IEEE Electron Device, Vol.28, No.1, pp.1, 1981.

66. V.L. Rideout, " A Review of the Theory and Technology for Ohmic Contacts to Group III-V Compound Semiconductors, " Solid-State Elec., Vol.18, pp.541, 1975.

67. B.L. Sharma, " Ohmic Contacts to III-V Compound Semiconductors, " Semiconductors and Semimetals, Vol.15, pp.1, Academic Press, 1981.

68. A. Piotrowska et al., " Ohmic Contacts to III-V Compound Semiconductors: A Review of Fabrication Techniques, " Solid-State Elec., Vol.26, No.3, pp.179, 1983.

69. G.Y. Robinson, " Schottky Diodes and Ohmic Contacts for the III-V Semiconductors," Physics and Chemistry of III-V Compound Semiconductor Interfaces, edited by C.W. Wilmsen, Plenum Press, New York, 1985.

70. W.G. Petro et al., " High Schottky Barriers on and Thermally Induced Process at the Au-GaAs (110) Interface, " J. Vac. Sci. Tech., Vol.21, No.2, pp.585, 1982.

71. A.D. Huelsman and C.G. Fonstad, " Fabrication and Characterization of Nonalloyed Cr/Au Ohmic Contacts to n- and p-Type $In_{0.53}Ga_{0.47}As$, " IEEE Elec. Dev., Vol.33, No.2, pp.294, 1986.

72. O. Wada, A. Majerfeld, and P.N. Robson, " InP Schottky Contacts with Increased Barrier Height, " Solid-State Elec., Vol.25, No.5, pp.381, 1982.

73. E. Kuphal, " Low Resistance Ohmic Contacts to n- and p-InP, " Solid-State Elec., Vol. 24, No.1, pp.69, 1981.

74. W.W. Gartner, " Depletion-Layer Photoeffects in Semiconductor, " Phys. Rev., Vol.116, No.1, pp. 84, 1959.

75. Sheng S. Li, " Optoelectronics," Semiconductor Physical Electronics, Lecture Note in The University of Florida, 1986, which will be published in Plenum Press, New York, 1987.

76. H.J.Hovel, Solar Cell, Semiconductors and Semimetals, Vol.11, Academic Press, 1975.

77. J. Engemann, " A.C. Admittance Studies of Schottky Diodes Using A Vector-Analyzer Systems, " Solid-State Electron., Vol.24, pp. 467, 1981.

78. T.C. Edwards, Foundations for Microstrip Circuit Design, Wiley, 1981.

79. K.C. Gupta, R. Garg, and I.J. Bahl, Microstrip Lines and Slotlines, Artech House, 1986.

80. N. Bar-Chaim, S. Margalit, A. Yariv, and I. Ury, " GaAs Integrated Optoelectronics, " IEEE Elec. Dev., Vol.29, No.9, pp.1372, 1982.

81. S.R. Forrest," Monolithic Optoelectronic Integration: A New Component Technology for Lightwave Communications," IEEE Electron Devices, Vol. 32, N0.12, pp. 2640, Dec. 1985.

82. M. Brain and T.P. Lee, " Optical Receivers for Lightwave Communication Systems,"IEEE Electron Devices, Vol. 32, No.12, pp. 2673, Dec. 1985.

83. K. Kasahara et al., " Monolithic Integrated $In_{0.53}Ga_{0.47}As$-PIN/InP-MISFET Photoreceiver," IEEE IEDM, pp.475, Dec. 1983.

84. J. Cheng et al., " Monolithically Integrated $In_{0.53}Ga_{0.47}As$/InP Direct-Coupled Junction Field-Effect Transistor Amplifier," IEEE Electron Device Letters, Vol. 7, No.4. April 1986.

85. P. Chattopadhyay and A.N. daw, " On the Barrier Height of a Metal-Semiconductor Contact with a Thin Interface Layer, " Solid-State Elec., Vo.28, No.8, pp.831, 1985.

86. C. Y. Wu, " Interfacial Layer Theory of the Schottky Barrier Diodes," J. Appl. Phys., 51(7), pp.3786, July 1980.

87. S. M. Sze, Physics of Semiconductor Devices, 2nd edition, Wiley, 1981.

88. N. Susa et al., " Planar Type Vapor Phase Epitaxial InGaAs Photodiode, " IEEE EDL, 1(4), pp.55, 1980.

89. V. Diadiuk et al., " Surface Passivation Techniques For InP and InGaAsP p-n Junction Structures, " IEEE EDL, 1(9), pp.177, 1980.

90. R. Yeats and K.V. Dessonneck, " Polyimide Passivation of $In_{0.53}Ga_{0.47}As$, InP, and InGaAs/InP p-n Junction Structures, " Appl. Phys. Letts., 44(1), pp.145, 1984.

CHAPTER EIGHT
LIST OF PUBLICATIONS

1. J.H. Kim and S.S. Li, " Development of A High-Speed Au/$In_{0.53}Ga_{0.47}As$/InP Schottky Barrier Photodiode for 1.3-1.5 um photodetection" High-Speed Electronics, 18th International Conference on Physics of Semiconductor, Stockholm, Sweden, Aug. 1986.

2. J.H. Kim, S.S. Li, and J.J. Pan, " Picosecond Response High-Speed GaAs Schottky Barrier Photodetector for Microwave Optical Fiber Links," SPIE Proc., Vol.716, Sep. 1986.

3. Jae H. Kim, Sheng S. Li, and Luis Figueroa, " High-speed $In_xGa_{1-x}As$ Schottky Barrier Photodiode for Infrared Photodetection," presented at the International Conference on Lasers'86, Orlando, FL., Nov.3-7, 1986 and published in Proc. of Optics and Quantum Electronics, Dec. 1986.

4. Sheng S. Li and Jae H. Kim, " High Speed Photodetectors Development for Millimeter-Wave Fiber Optic Links," Final Technical Report submitted to US Air Force RADC/DCLW, Contract No. F30602-84-C-0137, Oct. 1985.

5. Jae H. Kim, Sheng S. Li, Luis Figueroa, E. Rezek, and R. Wagner, " Picosecond Au/p-$In_{0.53}Ga_{0.47}As/p^+$-InP Schottky Barrier Photodetector for 1.30 - 1.50 um photodetection," will be submitted to IEEE Elec. Dev. Lett., Dec. 1986.

6. J.H. Kim, S.S. Li, L. Figueroa, W.P. Hong, and P.K. Bhattacharya, "Barrier-enhanced Schottky Contact on n-$In_{0.53}Ga_{0.47}As$ Epilayer MBE-Grown on n^+-InP Substrate, " will be submitted to IEEE Elec. Dev. Lett., Jan. 1987.

7. J.H. Kim, S.S. Li, L. Figueroa, and P.K. Bhattacharya, " Development of High-Speed Long Wavelength p^+-n-InGaAs/InP Schottky Barrier Photodiode ," will be submitted to IEEE Elec. Dev. Lett., Jan. 1987.

APPENDIX A. Fabrication Procedures of InGaAs Schottky Barrier Photodiode

STEP	PROGRESS	DETAILED DESCRIPTION
1	Clean and degrease wafer	- TCE for 5 min. with ultrasonic agitation - ACETONE for 5 min. with ultrasonic agitation - METHANOL for 5 min. with ultrasonic agitation
2	Metallization for Ohmic Contact on Substrate 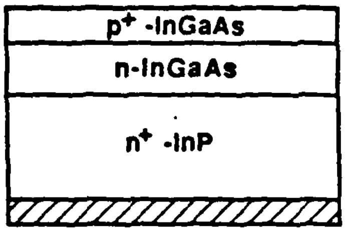	- Deposit Au-Ge (88-12%) metal alloy for contact to n^+-InP substrate at a deposit rate of 2 Å/sec and a pressure of 5.0×10^{-7} Torr. - Deposit Au-Zn (84-16%) metal alloy or Mn/Au sequentially (100 Å/900 Å) for ohmic contact to p^+-InP substrate at a rate of 2 Å/sec and a pressure of 5.0×10^{-7} Torr. - Alloy Au-Ge ohmic contact at 400°C for 30 sec and Mn/Au ohmic contact at 460°C for 30 sec
3	Deposit photoresist 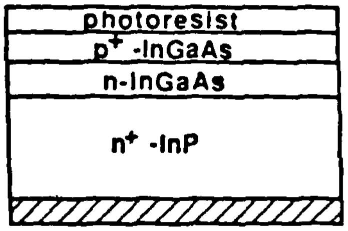	- Prebake at 150°C for 20 min, cool down 1 min - Spin on positive PR at 4,500 rpm for 30 sec (Shipley AZ-1470 positive PR) - Softbake at 90°C for 15 min, align, and expose for 8-10 sec for positive PR - Develop with Shipley developer for positive PR (MF-351:D.I. Water = 1:5)
4	Open Window for Schottky Barrier Contact 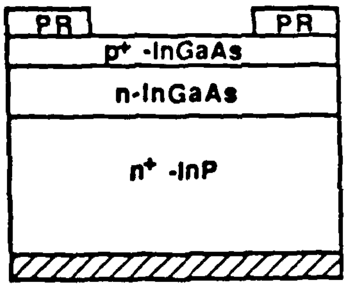	- Develop with Shipley developer for positive PR (MF-351:D.I. Water = 1.5), then pattern such that the areas in which metal is desired are not covered with photoresist
5	Metallization 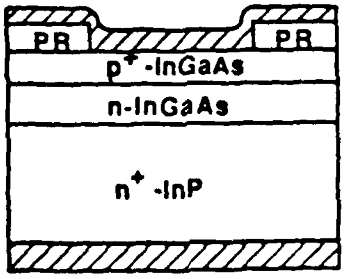	- Clean wafer with TCE, Acetone, Methanol under ultrasonic agitation rinse with D.I. Water, and etch just prior to metallization. - Deposit metal with E-beam evaporation at a pressure of less than 10^{-6} Torr.

6 Lift-Off

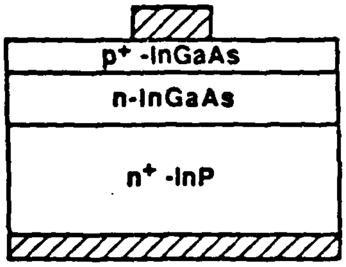

- Lift-off the unwanted metal with photoresist having the metal contact in the desired area by stripping.

---

7 Strip Photoresist

- Strip the Photoresist in acetone, which does not attack the metal film, with ultrasonic agitation. Then the unwanted metal comes off with the photoresist having the metal contact in the desired area.

---

8 Deposit photoresist

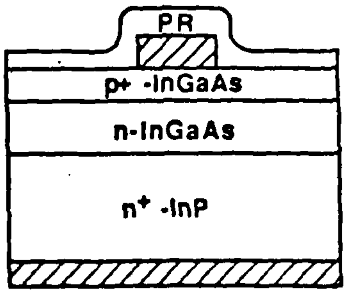

- Prebake at 150°C for 20 min., cool down 1 min.
- Spin on positive PR at 4,500 rpm for 30 sec (Shipley AZ-1470 positive PR)
- Softbake at 90°C for 15 min., align, and expose for 8-10 sec for positive PR
- Develop with Shipley developer for positive PR (MF-351:D.I. Water=1:5)

---

9 Open Window for Bondpad

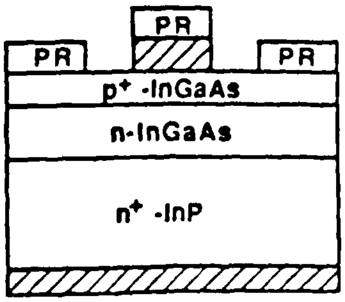

- Develop with Shipley developer for positive PR (MF-351:D.I. Water=1:5), then pattern such that the areas in which metal is desired are not covered with photoresist.

10 Metallization

- Clean wafer with TCE, Aceton, Methanol under ultrasonic agitation, rinse with D.I. water, and etch just prior to metallization.
- Deposit metal with E-beam evaporation at a pressure of less than 10^{-6}Torr

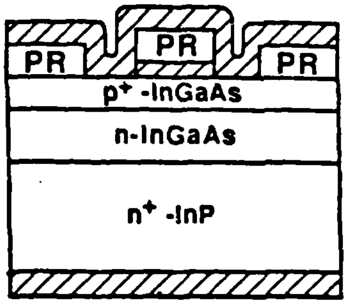
PR
PR
PR
p+ -InGaAs
n-InGaAs
n+ -InP

---

11 Lift-Off

- Lift-off the unwanted metal with photoresist having the metal contact in the desired area by stripping.

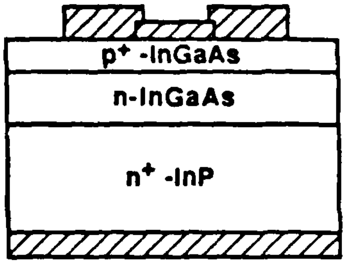
p+ -InGaAs
n-InGaAs
n+ -InP

---

12 Strip Photoresist

- Strip the photoresist in acetone, which does not attack the metal film, with ultrasonic agitation. Then the unwanted metal comes off with the photoresist having the metal contact in the desired area.

---

13 Mesa Etch

- $H_2SO_4:H_2O_2:H_2O = 3:1:1$ with a etch rate of 1.0 µm/10 sec at T = 300°K

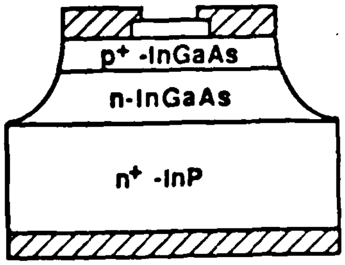
p+ -InGaAs
n-InGaAs
n+ -InP

APPENDIX B. Circuit Simulation for determining Response Speed

The SLICE simulation of the photodiode equivalent circuit model yields the frequency response for the InGaAs Schottky barrier photodiode. The 3-dB frequency of the proposed photodiodes is found to be at 12 GHz for a Au/p^+-n-InGaAs/n^+-InP structure in Fig.B.1 and 25 GHz for a Au/p-InGaAs/p^+-InP structure in Fig.B.2. These results are consistent with the estimated values by the measured RC time constant. Thus, the proposed InGaAs Schottky barrier photodiodes are capable of detecting the optical signals up to around 20 GHz range. The equivalent circuit of the photodiode is shown below. The measured value of the circuit elements are given as following:

C_d = 0.1 - 0.2 pF

L_b = 0.05 nH

R_L = 50 ohm

R_s = 5.3 -11.8 ohm

C_p = 0.04 pF

R_i = 100 Mohm

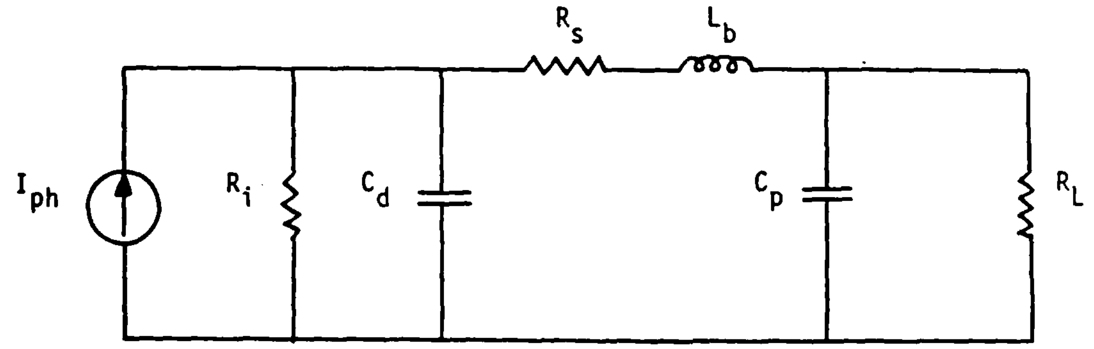

```
20*LOG10(V(3)):P

                 Y1      19.000E+00          27.000E+00          35.000E+00
                             .........................................
  1.000E+09   3.395E+01      .         .         .         .      1  .
  1.259E+09   3.393E+01      .         .         .         .      1  .
  1.585E+09   3.391E+01      .         .         .         .      1  .
  1.995E+09   3.386E+01      .         .         .         .      1  .
  2.512E+09   3.380E+01      .         .         .         .      1  .
  3.162E+09   3.369E+01      .         .         .         .      1  .
  3.981E+09   3.353E+01      .         .         .         .     1   .
  5.012E+09   3.329E+01      .         .         .         .     1   .
  6.310E+09   3.293E+01      .         .         .         .    1    .
  7.943E+09   3.242E+01      .         .         .         .   1     .
  1.000E+10   3.172E+01      .         .         .         . 1       .
  1.259E+10   3.078E+01      .         .         .        1.         .
  1.585E+10   2.962E+01      .         .         .      1  .         .
  1.995E+10   2.824E+01      .         .         .  1      .         .
  2.512E+10   2.666E+01      .         .        1.         .         .
  3.162E+10   2.492E+01      .         .    1    .         .         .
  3.981E+10   2.305E+01      .         1         .         .         .
  5.012E+10   2.106E+01      .    1    .         .         .         .
                             .........................................
```

Fig. B.1. Cutoff Frequency of p^+-n-InGaAs/n^+-InP Schottky Barrier Photodiode.

```
20*LOG10(V(3)):P

              Y1       26.000E+00          30.000E+00          34.000E+00
                           .........................................
 1.000E+09  3.397E+01      .         .         .         .         1
 1.259E+09  3.397E+01      .         .         .         .         1
 1.585E+09  3.396E+01      .         .         .         .         1
 1.995E+09  3.395E+01      .         .         .         .         1
 2.512E+09  3.394E+01      .         .         .         .         1
 3.162E+09  3.391E+01      .         .         .         .         1
 3.981E+09  3.387E+01      .         .         .         .        1.
 5.012E+09  3.381E+01      .         .         .         .        1.
 6.310E+09  3.371E+01      .         .         .         .        1.
 7.943E+09  3.356E+01      .         .         .         .       1 .
 1.000E+10  3.333E+01      .         .         .         .      1  .
 1.259E+10  3.299E+01      .         .         .         .    1    .
 1.585E+10  3.250E+01      .         .         .         . 1       .
 1.995E+10  3.180E+01      .         .         .        1.         .
 2.512E+10  3.088E+01      .         .         .   1     .         .
 3.162E+10  2.970E+01      .         .        1.         .         .
 3.981E+10  2.826E+01      .         .1        .         .         .
 5.012E+10  2.657E+01      .  1      .         .         .         .
                           .........................................
```

Fig. B.2. Cutoff Frequency of p-InGaAs/p^+-InP Schottky Barrier Photodiode.

APPENDIX C. General Model for Schottky Barrier Height

The barrier height of metal-semiconductor system is determined by both the metal work function and the interface traps. The general expression of the barrier height can be obtained on the basis of the following assumptions: (1) The metal and the semiconductor are assumed to be separated by a thin insulating interfacial layer of atomic dimensions which is transparent to electrons and can withstand potential across it, (2) the interface traps per unit area per electron volt at the interface are properties of the semiconductor surface and are independent of the metal.

Designating the oxide charge $Q_{ox} = -qN_{ox}$ in the region of oxide close to the oxide-semiconductor interface, the charge neutrality condition of the system can be written as

$$Q_M + Q_{sc} + Q_{it} + Q_{ox} = 0 \qquad \text{(C.1)}$$

$$Q_{ox} = Q_f + Q_m + Q_{ot} \qquad \text{(C.2)}$$

where Q_M is surface charge on metal, Q_{sc} space charge in the depletion layer of semiconductor, Q_{it} interface trap charge, Q_{ox} oxide charge, Q_f is oxide fixed charge, Q_m mobile ionic charge, and Q_{ot} oxide trapped charge.

$$Q_{sc} = \{2qC_sN_D(\Phi_{Bn} - V_n + \Delta\Phi - (kT/q)\}^{1/2} \qquad \text{(C.3)}$$

$$Q_{it} = -qD_{it}\{\exp((Eg - q\Phi_o - q\Phi_{Bn})/Es) - \exp((Eg - q\Phi_o - q\Phi_{fn})/Es)\} \qquad \text{(C.4)}$$

$$Q_M = -[\{2qC_sN_D(\Phi_{Bn} - V_n)\}^{1/2} - qD_{it}Es\{\exp((Eg - q\Phi_o - q\Phi_{Bn})/Es) - \exp((Eg - q\Phi_o - q\Phi_{fn})/Es)\} + qN_f] \qquad \text{(C.5)}$$

$$D_{it}(E) = D_{it}\{\exp[(E - q\Phi_o)/Es] + \exp[-(E - q\Phi_o)/Es]\} \qquad \text{(C.6)}$$

The potential drop across the interfacial layer can be obtained by the application of Gauss's law.

$$\Delta = -\left(dQ_M/\epsilon_i\right) \tag{C.7}$$

where ϵ_i is the permittivity of the interfacial layer and d is its thickness. Again Eq.(C.7) can be expressed as

$$\Delta = \Phi_m - X - \Phi_{Bn} \tag{C.8}$$

Introducing the quantities,

$$C_1 = 2qC_sN_Dd^2/\epsilon_i^{\,2} \tag{C.9}$$

$$C_2 = \epsilon_i/(\epsilon_i + q^2dD_{it}) \tag{C.10}$$

then the barrier height can be expressed as [18]

$$\begin{aligned}\Phi_{Bn} = \; & [C_2(\Phi_m - X) + (1-C_2)\Phi_{fn} - (1-C_2)N_{ox}/qD_{it} - \Delta\Phi] + [C_2{}^2C_1/2 \\ & - C_2{}^{3/2}\{C_1(\Phi_m - X) + (1-C_2)\Phi_{fn}C_1/C_2 - (1-C_2)N_{ox}C_1/qD_{it}C_2 \\ & - C_1(V_n + (kT/q))/C_2 + C_2C_1{}^2/4\}^{1/2}]\end{aligned} \tag{C.11}$$

For $N_D < 10^{18}$ cm^{-3}, the terms within the second bracket can be neglected, and Eq.(C.11) can be reduced to the following expression.

$$\Phi_{Bn} = C_2(\Phi_m - X) + (1-C_2)\Phi_{fn} - (1-C_2)N_{ox}/qD_{it} - \Delta\Phi \tag{C.12}$$

where Φ_o represents the position of the neutral level for the interface traps from the top of the valence band. Here ϵ_i is the permittivity $(=\epsilon_o\epsilon_r)$ and d is the thickness of the interfacial layer. D_{it} is the density of the interface traps per unit area per electron volt. The two limiting cases considered previously can be obtained from Eq.(C.12).

The two limiting cases can be obtained as follows:

(1) Mott Limit ($D_{it} \rightarrow 0$, $C_2 \rightarrow 1$, and $\Phi_{fn} \rightarrow V_n$)

$$\Phi_{Bn} = (\Phi_m - X) - \Delta\Phi \tag{C.13}$$

which is the barrier height for an ideal Schottky barrier contact where surface state effects are neglected. Note that this expression is identical to the ideal Schottky barrier except for the barrier lowering term.

(2) Bardeen Limit ($D_{it} \rightarrow \infty$, $C_2 \rightarrow 0$, and $\Phi_{fn} \rightarrow E_g/q - \Phi_o$)

$$\Phi_{Bn} = (E_g/q - \Phi_o) - \Delta\Phi \tag{C.14}$$

The Fermi level at the interface is pinned by the interface traps at the value $q\Phi_o$ above the valence band. The barrier height is independent of the metal work function and determined entirely by the surface properties of the semiconductor.

APPENDIX D. Schottky Barrier Height Enhancement

The Schottky barrier height enhancement can be obtained by depositing a very thin p^+-InGaAs surface layer on an n-InGaAs epilayer. The effective barrier height is increased by band bending due to the space charge in the p^+-InGaAs surface layer provided the dopant density and the thickness of the surface layer are selected to an optimum value and the surface layer is fully depleted at thermal equilibrium. We consider an abrupt p-n structure with a p-region width of W_p which is considered variable as long as the p-region is not too large, this region will be totally depleted at thermal equilibrium. It should be noted that if the p-region becomes sufficiently large, the structure becomes a p-type Schottky barrier with a p-n junction in series and then the p-region is approximately neutral.

Let W_n be the width over the depletion region which extends into the n-InGaAs epilayer and let $x = 0$ at the metal contact. In the depletion approximation, the Poisson's equations are given by:

$$d^2\Phi/dx^2 = qN_A/\epsilon_o\epsilon_r \qquad \text{for} \quad 0 < x < W_p \tag{D.1}$$

$$d^2\Phi/dx^2 = -qN_D/\epsilon_o\epsilon_r \qquad \text{for} \quad W_p < x < W_p + W_n \tag{D.2}$$

The boundary conditions are given by:

$$\Phi(0) = 0 \text{ and } \Phi(W_p + W_n) = \Phi_m - \Phi_n - V \tag{D.3}$$

$$\Phi(x) \text{ and } d\Phi(x)/dx \text{ are continuous at } x = W_p \tag{D.4}$$

$$d\Phi(x)/dx = q(N_DW_n - N_AW_p)/\epsilon_o\epsilon_r \quad \text{at } x = 0 \quad \text{and}$$

$$d\Phi(x)/dx = 0 \qquad \text{at } x = W_p + W_n \tag{D.5}$$

The solutions for $\Phi(x)$ are given by:

$$\Phi(x) = (qN_A/\epsilon_o\epsilon_r)[(1/2)x^2 - xW_p] + (qN_A/\epsilon_o\epsilon_r)xW_n \quad \text{for } 0 < x < W_p \tag{D.6}$$

$$\Phi(x) = -(qN_D/\epsilon_o\epsilon_r)[(1/2)x^2 - x(W_p + W_n)]$$

$$- q(N_A + N_D)W_p^2/2\epsilon_o\epsilon_r \qquad \text{for } W_p < x < W_p + W_n \tag{D.7}$$

The width of the n region follows from the boundary condition Eq.(D.4).

$$\Phi_m - \Phi_n - V = qN_D(W_p + W_n)^2/2\epsilon_o\epsilon_r - q(N_A + N_D)W_p^2/2\epsilon_o\epsilon_r \tag{D.8}$$

If $N_DW_n < N_AW_p$, the potential energy maximum is located inside the p+ region. The potential energy will be $q\Phi_{Bn}$ at $x = 0$ and reach a maximum value at $x = x_m$, which can be obtained from the condition:

$$d\Phi(x)/dx = 0 \text{ at } x = x_m, \tag{D.9}$$

which gives

$$x_m = (1/N_A)(N_AW_p - N_DW_n) \text{ and } E_m = (q/\epsilon_o\epsilon_r)(N_AW_p - N_DW_n) \tag{D.10}$$

The enhancement of the barrier height for a metal-p-n quasi-Schottky barrier diode, $\Delta\Phi_{Bn}$ due to the p surface layer is obtained by substituting x_m into Eq.(D.6).

$$\Delta\Phi_{Bn} = (q/2\epsilon_o\epsilon_r N_A)(N_A W_p - N_D W_n)^2 \qquad (D.11)$$

$$= qN_A x_m{}^2/2\epsilon_o\epsilon_r \qquad (D.12)$$

The effective barrier height Φ'_{Bn} occurs at $x = x_m$ and is given by

$$\Phi'_{Bn} = \Phi_{Bn} + E_m x_m - qN_A x_m{}^2/2\epsilon_o\epsilon_r \qquad (D.13)$$

For $N_A >> N_D$ and $N_A W_p >> N_D W_n$ Eq.(D.13) will be simplified

$$\Phi'_{Bn} = \Phi_{Bn} + qN_A W_p{}^2/2\epsilon_o\epsilon_r \qquad (B.14)$$

It can be shown that Eq.(D-14) holds only for $\Delta\Phi_{Bn} >> V_D N_D/N_A$. Note that N_A and N_D denote the dopant density of the p^+- and n-InGaAs layer, respectively. W_p is the thickness of the p^+-layer, and V_D is the built-in potential of the p^+-n junction. The thickness and dopant density of the InGaAs layers are determined subject to the condition given above. The effective barrier height will increase as the product $N_A W_p$ increases. The barrier height for such a photodetector can be tailored to its optimum value via properly selected thickness and dopant density of the surface layer. The depletion layer width in the n-epilayer can be calculated from Eq.(D.8) and is given by:

$$W_n = -W_p + [\ W_p{}^2 + (N_A/N_D)W_p{}^2 + 2\epsilon_o\epsilon_r(\Phi_m - \Phi_n - V)/qN_D\ ]^{1/2} \qquad (D.15)$$

$$\Phi_n = X_s + (kT/q)\ln(N_c/N_D) \qquad (D.16)$$

The effective barrier height Φ'_{Bn} of a Schottky barrier diode can be calculated from the following expression:

$$\Phi'_{Bn}{}^{I-V} = (kT/q)\ln(A^{*}T^{2}/J_{s}) \qquad (D.17)$$

$$\Phi'_{Bn}{}^{C-V} = V_{D} + (kT/q)\ln(N_{V}/N_{A}) \qquad (D.18)$$

$$\Phi'_{Bn}{}^{I-T} = -kT\ln(J/A^{*}T^{2}) \qquad (D.19)$$

$$\Phi'_{Bn}{}^{I-E} = h\nu - kT(J/A^{*}T^{2}) \qquad (D.20)$$

where A^{*} (= $4\pi qm^{*}k^{2}/h^{3}$) is effective Richardson constant for thermionic-emission, neglecting the effects of optical phonon scattering, quantum mechanical reflection, and tunneling of carriers at the metal-semiconductor interface and J_{s} is the reverse saturation current density.

APPENDIX E. Schottky Barrier and Ohmic Contact Formation

1. The starting material is p-$In_{0.53}Ga_{0.47}As$ or n-$In_{0.53}Ga_{0.47}As$ material grown on InP substrate. Clean and degrease wafer with TCE, aceton, methanol, and D.I. water followed by blowing dry with N_2.
2. Deposit metal by e-beam evaporation at a pressure of less than 10^{-6} Torr. The Au-Ge or Au-Ge/Ni alloy can be used for ohmic contact to n-type III-V compound semiconductors. The Au-Ge ohmic contact is usually formed by evaporating a eutectic composition of Au-Ge (88-12 %) alloy (1500 Å) followed by a thin layer of Ni (400 Å). For p-type ohmic contact, a Au-Mg or Au-Zn (90-10 %) alloy (1500 Å) corresponding to the stoichiometric composition of Au_3Zn can be used. The adhesion to InP with Au-Zn alloy is much better than with Zn and Au sequentially deposited. For Au-Zn alloy, it is better to evaporate micro-foil Cr (50 Å) first for good adhesion, and then evaporate Au-Zn (1500 Å) and Au (500 Å) sequentially.
3. Alloy the contact in H_2-N_2 forming gas ambient at 450°C for 2 min (p-type) and 400°C for 2 min (n-type). For heat-treatment above the Au-Ge eutectic temperature (T_{eu} = 360°C), ohmic contact behavior is observed and uniform

alloyed contact surface is formed due to the presence of Ni at the semiconductor interface. The most commonly used method of heat treatment of metal-semiconductor systems is alloying furnace in H_2-N_2 forming gas. Note that during the process of contact alloying the dopant diffuses into the semiconductor and produces a modified region of high doping concentration at the metal-semiconductor interface resulting in low resistance contact formation.

4. Clean and degrease wafer with TCE, aceton, methanol, and D.I. water followed by blowing dry with N_2.
5. Prebake wafer at 150°C for 20 min, cool it down for 1 min, and spin on positive photoresist (Shipley AZ-1470) at 4,500 rpm for 40 sec. The wafers should always be blown dry with N_2 just before spinning on the photoresist to remove any dust particles that may be on the surface. After spinning, any excess photoresist on the back of the wafer must be cleaned off with a stopper.
6. Softbake wafer at 95°C for 15 min, align, and expose with UV light for 15-20 sec to a contact mask. Then develop with a Shipley developer (MF 351:D.I. water = 1:5) for 40 sec.
7. Perform sputter-etching or chemical etching before metal deposition. Chemical etching can be done by dipping the InGaAs wafer in etch ($NH_4OH:H_2O_2:H_2O$ = 20:7:975) and stop solution ($NH_4OH:H_2O$ = 10:150) or BHF ($HF:H_2O$ = 1:5) solution for 30 sec to remove native oxides from surface of the contact area. The surface should be prepared with the minimum amount of oxide and contamination to leave it smooth and stoichiometric.
8. Deposit a Schottky metal (e.g., Al, Au, or Ti) by e-beam evaporation at a pressure of less than 10^{-6} Torr and anneal wafer at 320°C in a N_2 forming gas ambient for 2-15 min.

APPENDIX F. Lift-Off Photolithography

1. Clean and degrease wafer with TCE, aceton, methanol, and D.I. water followed by blowing dry with N_2.
2. Prebake wafer at 150°C for 20 min, cool it down for 1 min, and spin on a positive photoresist (Shipley AZ-1470) at 4,500 rpm for 40 sec. Softbake wafer at 95°C for 15 min, align, and expose with UV light to a contact mask for 15-20 sec. Then develop with a Shipley developer (MF-351:D.I. water = 1:5) for a positive photoresist. After developing the pattern a hardbake is not necessary for the lift-off process.
3. Spin on a positive photoresist before metalization, pattern such that the areas in which metal is desired are not covered with photoresist, and deposit Schottky metal by e-beam evaporation.
4. Strip the photoresist in acetone, which does not attack the metal film, with ultrasonic agitation. Then the unwanted metal comes off with the photoresist having the metal contact in the desired area. The success of the lift-off technique requires the use of a relatively thick photoresist film so that the deposited metal film is very thin or even discontinuous at the sides of the step

APPENDIX G. Chemical Etch

Mesa Etch

1. For $In_{0.53}Ga_{0.47}As$ material, the mesa etch solution (1) $H_2SO_4:H_2O_2:H_2O=3:1:1$ with etch rate 1.0 um/10 sec at T = 300°K for InGaAs (2) 1.0 -1.5 % Bromine-Methanol ($Br\text{-}CH_3OH$) etch (3) $H_3PO_4:H_2O_2:H_2O=1:1:8$
2. For InP, HCl can be used for mesa etch with etch rate 10 um/min.
3. After etching rinse in H_2O for at least 15 sec to remove any residual etch.

Gold Etch

1. Dip into $KI:I_2:H_2O=4:1:4$ at 40°C.

2. Rinse with D.I. water for 5 minutes.

Chromium Etch

1. Dip into potassium ferricyanide=1:3 with D.I. water at 40°C.

2. Rinse with D.I. water for 5 minutes.

Note: Chromium etch contains cyanide and should not be mixed with acids.

APPENDIX H. Surface Passivation

1. The surface passivation can be obtained using Dupont PI 2555 (semiconductor grade) polyimide diluted 1:1 with N-Methylpyrrolidone (NMP) solvent.
2. Prebake wafer at 200°C for 30 min in N_2 forming gas and immediately spin on the polyimide at 3,000 rpm for 30 sec.
3. Prebake wafer at 120°C for 30 min, cool it down for 1 min, and spin on positive Photoresist (e.g., Shipley Az-1415 or 3000) at 4,500 rpm for 30 sec to pattern the polyimide.
4. Softbake wafer at 95°C for 15 min, align, and expose for 25 sec. Polyimide is soluble in alkaline solution such as positive photoresist developer, and thus the polyimide can be patterned at the same time the photoresist is developed.
5. Plasma etch the wafer in an O_2 plasma for 1 min using an RF power of 200 W before the photoresist is removed. This removes organic residue and produces a sharper profile in the polyimide.
6. After plasma etching strip the photoresist using Acetone and cure the polyimide at 250°C for 1 hour.

MISSION
of
Rome Air Development Center

RADC plans and executes research, development, test and selected acquisition programs in support of Command, Control, Communications and Intelligence (C^3I) activities. Technical and engineering support within areas of competence is provided to ESD Program Offices (POs) and other ESD elements to perform effective acquisition of C^3I systems. The areas of technical competence include communications, command and control, battle management, information processing, surveillance sensors, intelligence data collection and handling, solid state sciences, electromagnetics, and propagation, and electronic, maintainability, and compatibility.

END
FILMED
MARCH, 1988
DTIC